# Final report

Date: 20th January 2021

**Project title:** Characterising the biological effects of particulate matter (PM) exposures in coal mining to protect and improve the health of workers

**Chief Investigator:** Associate Professor Jay Horvat & Prof Phil Hansbro

**Ref Number:** 20649

**Project end date:** 31st December 2020

**Report no:** 3rd report (Final report)

**Project aim:**

- To assess the biological effects of exposure to inhalable coal mining dust fractions on the lungs using acute (short term), chronic (long term) exposure in *in-vivo* (mouse) models and *in-vitro* (human cell) models

**Outcomes:**

- To inform the potential health impacts of exposure to different types of dust exposures in coal mining operations to better identify those dusts that pose the greatest risk to workers.

**Overview:** $PM_{10}$ and below fractions of six different well-characterised dust samples (Dust A – F) were sourced from different stages of different types of mining operations (open cut and longwall mining) to include the initial, through to the final, stages of production. Physicochemical analyses of these six different samples demonstrate that these dusts vary dramatically in terms of chemical constituents, including metals (especially iron) and silica. The effects of short-term and long-term exposure to all six dust samples was investigated using murine models. Mice were intranasally challenged with $PM_{10}$ sourced from the six different coal mining operations/sites for 5 days/week up to 2 (acute exposure) and 12 (chronic exposure) weeks at different concentrations that modeled exposure concentrations of $1mg/m^3$, $3mg/m^3$ and $10mg/m^3$ of $PM_{10}$ per hour for 8 hours/per day (corrected for human: mouse weights). The effects of exposure on lung disease were determined by assessing lung function, airway inflammation, inflammatory gene expression and histology. We also assessed the effects of dust exposure in human epithelial cells grown at the air-liquid interface. The effects of exposure to dust on susceptibility to influenza A and bacterial lung infections (*Haemophilus*

*influenzae*) were also assessed in mice and human airway epithelial cell cultures as shown in Fig 1.

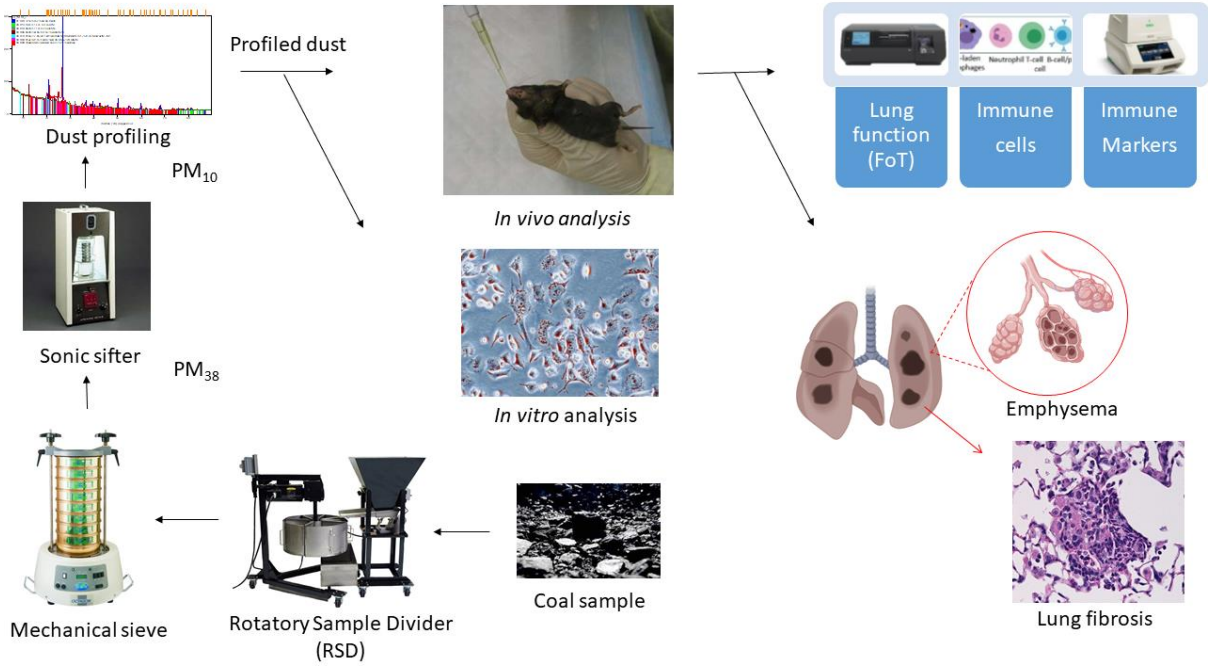


**Figure 1**: Graphical illustration of the overview of the study.

**Results:** Interestingly, we show that all the dust samples tested induced increased airway hyper-responsiveness (AHR) in response to methacholine following 2 weeks of exposure. Importantly, the magnitude of response differed dramatically between the different concentrations and between the different samples. Similar effects on AHR were observed following chronic (12 week) exposure, although the magnitude of AHR induced was not as high as observed at 2 weeks. Importantly, a number of the samples tested induced a significant reduction in gas-exchange (decreased diffusion factor for carbon monoxide [$DF_{CO}$]) of lungs of mice within 2 weeks of exposure, even at the lower concentrations of exposure (1mg/m$^3$ equivalent). All dust exposures resulted in decreased gas diffusion by 12 weeks and this was associated with key histological features of coal workers pneumoconiosis (CWP, i.e. emphysema and coal macules/fibrotic nodules) even at the lowest levels of dust exposure (1mg/m$^3$), with the magnitude of histological changes observed worse for some dust sample exposures compared to others. Interestingly, only some of the samples tested induced an increase in pro-inflammatory responses, with several of the exposures associated with decreased inflammatory/immune factor responses (including decereased macrophage phagocytosis) following both short-term and long-term exposures. Interestingly, and in support of our *in vivo* findings, we did not observe an increase in pro-inflammatory factor release by human epithelial cells grown at the air liquid interface that were exposed to three of the dust samples tested. We also showed evidence that exposure to certain types of dust may increase susceptibility to influenza A-induced disease (especially worsened lung function), although the analyses associated with these infection-induced studies are currently being finalised.

**Conclusions:** We show evidence that the chemical composition of dust generated at different stages of mining operations may play a critical role in determining disease outcomes in coal dust exposure-associated illnesses. Importantly, we show that even relatively low levels of exposure (1mg/m$^3$) may be sufficient to induce key features of lung disease within relatively short time periods. The effects of dust exposure may not be associated with profound increases

in airways inflammatory responses, indeed immune responses appear to be largely blunted in the lungs following exposure. This suggests that other methods for measuring the effects of harmful exposures (e.g. lung function parameters measured using FoT, gas diffusion [CO, NO]) may represent more appropriate means for assessing early onset disease.

**Ongoing analyses:** As a result of restrictions with lab access and issues sourcing some materials due to COVID19, we experienced some difficulties completing three of the dust exposure models with enough time to analyse all the data in time for this final report. Whilst this report contains all the lung function and inflammatory cell data for both the acute and chronic dust exposures for all six dust samples (A – F), we are currently finalising histological and/or inflammatory cytokine analyses for three samples (D, E and F). We are also finalising analyses from the influenza A infections in both mouse *in vivo* and human *in vitro* models. We estimate that these ongoing analyses will be completed by March 2021, with the data prepared for submission for publication in the middle of 2021. We would like the opportunity to provide a presentation of our data to Dr David Meredith and the Coal Services Health and Safety Trust Board to discuss the findings further.

## 1. Dust Collection and characterization

### 1.1 Dust Collection

Randomized sampling method was used in the collection of coal samples from six different mining operations of which samples Dust A, Dust B, and Dust C represents the final stage (final product), whereas Dust D, Dust E, and Dust F represent the initial stages of mining operations as shown in Table 1.

**Table 1:** Showing the dust types and locations

| Mining operation | Dust sample | Location/type |
|---|---|---|
| **Final stage** | Dust A | Thermal plant/Thermal coal |
| | Dust B | Industrial/metallurgical coal |
| | Dust C | Industrial/PCI coal |
| **Initial stage** | Dust D | Mining/longwall |
| | Dust E | Mining/Overburden |
| | Dust F | Mining/ROM coal |

Each coal sample was passed through a rotatory sample divider (RSD) to obtain a representative sample. Further, each representative coal sample was passed through a series of mechanical sieves with a pore size ranging from 5cm to 38µm with intermediate drying in nitrogen supplemented ovens operated at 40ºC to remove excess moisture.

To obtain the $PM_{10}$ fractions, the 38µm samples were passed through Advantech L3P sonic sifter equipped with custom made precision electroformed mesh sieve with a pore size of 10µm according to manufacturer guidelines.

The collected $PM_{38}$ and $PM_{10}$ samples were stored in airtight containers and stored in RT. Due to the low yield of $PM_{10}$, the $PM_{38}$ samples were used for physicochemical analysis, whereas PM10 samples were used *in vivo* and *in vitro* studies.

Australian standard protocols AS 4264-2009 (coal sampling); AS 3638-1993 (sieving); AS 1038.1-2001 (moisture content; oven drying) with minor modifications were used in the collection and processing of the coal samples.

### 1.2 Dust characterization

To obtain the chemical profile of each dust sample, the following analytical techniques were performed:

#### 1.2.1 CNS analysis

**Table 2:** Showing the percentage of Carbon (C), Nitrogen (N) and Sulfur content of the six coal dust samples (<PM38) collected from mining and workplaces

| | Carbon (%) | Nitrogen (%) | Sulfur (%) |
|---|---|---|---|
| **Dust A** | 64.30 | 1.37 | 0.986 |
| **Dust B** | 80.07 | 1.68 | 2.46 |
| **Dust C** | 75.10 | 1.57 | 1.47 |
| **Dust D** | 79.85 | 1.91 | 4.44 |
| **Dust E** | 10.46 | 0.27 | 0.2 |
| **Dust F** | 40.48 | 0.87 | 2.23 |

- The total carbon, nitrogen, and sulfur analysis carried out using the total combustion method showed that the total carbon percentage is much higher in the dust obtained from the final stages (Dust A, B & C) compared to the dust from initial mining operations (Dust E & F), except Dust D (longwall coal dust), which was found to have high carbon (79.85%), nitrogen (1.91%) and sulfur (4.44%) levels.

### 1.2.2 X-ray fluorescence (XRF) analysis

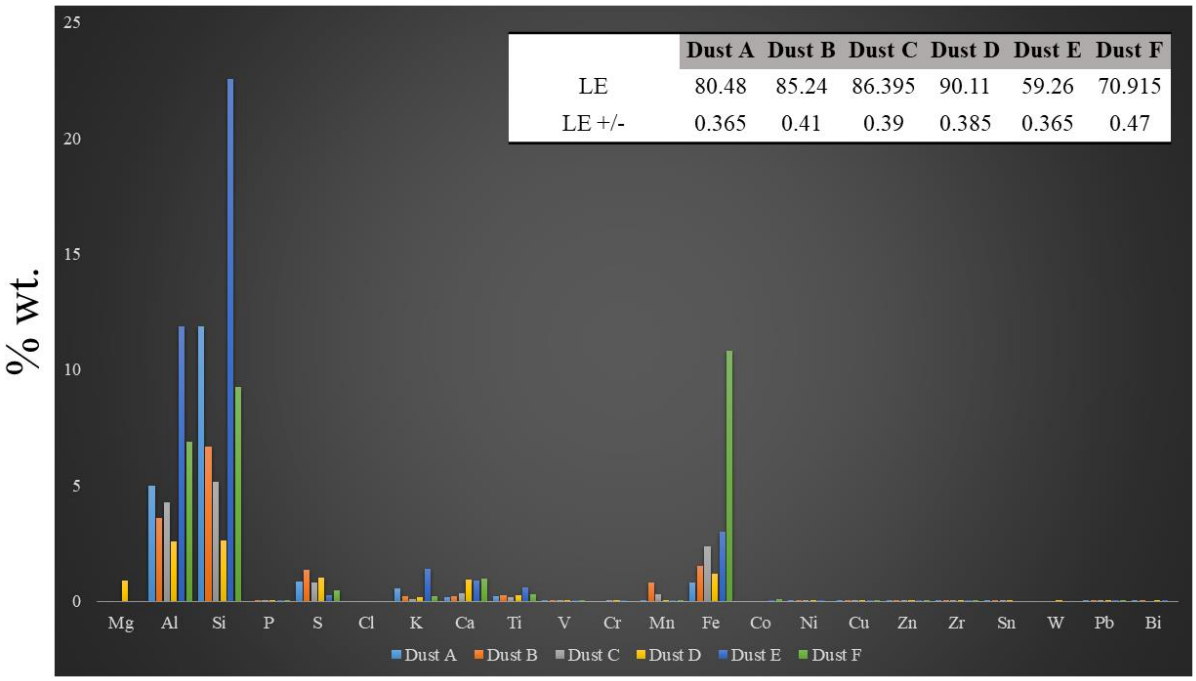


**Figure 2:** Bar graph showing elemental composition (%) of the six different coal dust samples

- The elemental analysis (%) using X-ray fluorescence shows that all six dust samples vary in elemental composition. The abundant elements were found to be Al, Si, S, K, Ca, Ti and Fe. Among the tested samples, Dust E was found to have the highest silica content followed by Dust F, which was rich in Fe and Si.

### 1.2.3 ICP-OES - Inductively coupled plasma optical emission spectrometry analysis

**Table 3:** Quantitative analysis of macro elemental composition (mg/kg) of dust samples

| Sample | Al | Ca | Fe | K | Mg | Mn | Na | P | S |
|---|---|---|---|---|---|---|---|---|---|
| **Dust A** | 6626.63 | 1929.58 | 2376.69 | 1373.92 | 457.24 | 83.93 | 1286.11 | 94.06 | 1326.04 |
| **Dust B** | 3295.49 | 1563.37 | 6838.28 | 1012.24 | 489.19 | 6294.89 | 1227.36 | 115.17 | 917.59 |
| **Dust C** | 2866.33 | 1947.51 | 9948.83 | 697.65 | 937.44 | 1718.52 | 2088.27 | 111.37 | 1356.52 |
| **Dust D** | 4522.57 | 5831.12 | 5284.34 | 866.40 | 1213.87 | 74.11 | 1885.40 | 542.99 | 2701.94 |
| **Dust E** | 3658.59 | 10773.47 | 23943.80 | 1163.27 | 3520.49 | 377.91 | 1176.54 | 565.13 | 228.72 |
| **Dust F** | 4297.57 | 8338.78 | 126792.20 | 768.28 | 2862.48 | 415.42 | 1008.05 | 407.60 | 3633.30 |

- The quantitative analysis using ICP-OES shows that all the six dust samples vary in macro elemental composition i.e. Al, Ca, Fe, K, Mg, Mn, Na, P and S. Interestingly, the Dust E & F showed the highest concentration of iron (Fe) i.e. 23943.8 & 126792.2mg/kg, well-known to disrupt lung integrity and function when accumulated at higher concentrations.

### 1.2.4 ICP-MS - Inductively Coupled Plasma Mass Spectrometry analysis

**Table 4:** Quantitative analysis of trace elemental composition (µg/g) of dust samples

| Element | Dust A | Dust B | Dust C | Dust D | Dust E | Dust F |
|---|---|---|---|---|---|---|
| **Be** | 0.723 | 0.973 | 0.258 | 0.613 | 0.879 | 1.315 |
| **V** | 15.848 | 10.523 | 12.400 | 11.143 | 20.336 | 11.347 |
| **Cr** | 1.132 | 8.545 | 6.892 | 0.842 | 2.967 | 6.513 |
| **Mn** | 78.018 | 5951.294 | 1706.875 | 62.020 | 336.804 | 412.682 |
| **Fe** | 2414.749 | 7228.218 | 10567.948 | 4825.842 | 23171.773 | 127483.337 |
| **Co** | 1.738 | 2.379 | 1.956 | 2.739 | 8.461 | 1.456 |
| **Ni** | 1.117 | 12.723 | 7.704 | 35.025 | 3.097 | 5.355 |
| **Cu** | 8.393 | 60.939 | 66.959 | 54.876 | 23.356 | 70.168 |
| **Zn** | 18.109 | 34.852 | 53.164 | 27.148 | 64.812 | 64.723 |
| **As** | 1.653 | 2.164 | 1.374 | 1.913 | 6.172 | 3.270 |
| **Se** | 3.067 | 5.262 | 3.060 | 2.644 | 5.805 | 5.084 |
| **Sr** | 37.419 | 30.167 | 35.663 | 1120.138 | 98.437 | 57.222 |
| **Mo** | 0.973 | 2.108 | 0.669 | 0.415 | 1.476 | 0.196 |
| **Cd** | 0.091 | 0.182 | 0.175 | 0.474 | 0.110 | 0.181 |
| **Sb** | 0.261 | 0.496 | 0.251 | 0.184 | 0.403 | 0.451 |
| **Ba** | 52.961 | 495.694 | 153.840 | 339.063 | 170.039 | 115.858 |
| **Pb** | 9.717 | 140.062 | 46.025 | 8.360 | 11.773 | 22.989 |

- Quantitative analysis of trace elements using ICP-MS shows the presence of heavy metals like Cr, As, Mo, Cd and Pb in all the screened dust samples. Where Dust B, C & F showed highest levels of Cr i.e. 8.5, 6.8 & 6.5 ppm. Also, high levels of As and Pb i.e. 6.1 &140 ppm were observed in Dust E and F.

### 1.2.5 XRD - X-ray Diffraction analysis

**Table 5 (a-f)**: Showing the mineral composition and phase identification of the dust samples

a

**Dust A**

| Ref. code | Compound name | Score |
|---|---|---|
| 96-154-1966 | Al2 (Si2 O5) (OH)4 | 96 |
| 96-153-0003 | Al PO4 | 60 |
| 96-500-0036 | Quartz | 48 |
| 96-231-1020 | FeO. 974 O | 32 |
| 96-400-1395 | Calcium Catena Polyphosphate | 89 |

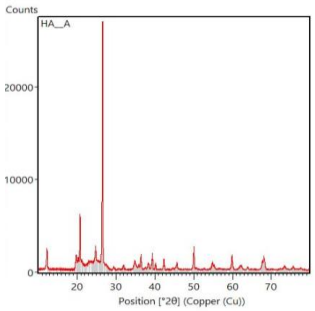


b

**Dust B**

| Ref. code | Compound name | Score |
|---|---|---|
| 96-900-5020 | Quartz | 51 |
| 96-900-0140 | Hematite | 48 |
| 96-154-1966 | Al2 (Si2 O5) (O H)4 | 93 |
| 96-400-1395 | Calcium Catena Polyphosphate | 88 |
| 96-900-3525 | Dolomite | 55 |
| 96-900-1635 | Albite | 86 |

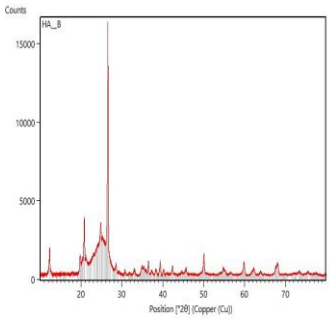


c

**Dust C**

| Ref. code | Compound name | Score |
|---|---|---|
| 96-153-0003 | Al PO4 | 55 |
| 96-900-4934 | Dolomite | 48 |
| 96-810-3727 | SiO2 | 44 |
| 96-900-0140 | Hematite | 43 |
| 96-154-1966 | Al2 (Si2 O5) (OH)4 | 88 |
| 96-210-3120 | Calcium carbonate | 59 |

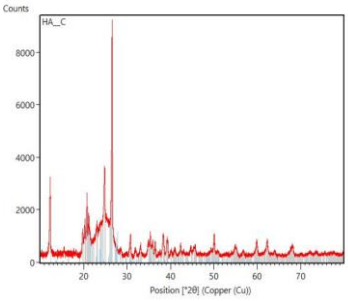

d

**Dust D**

| Ref. code | Compound name | Score |
|---|---|---|
| 96-900-5020 | Quartz | 42 |
| 96-231-0665 | Al PO4 | 50 |
| 96-900-0140 | Hematite | 40 |
| 96-154-1966 | Al2 (Si2 O5) (O H)4 | 93 |
| 96-900-0774 | Chloritoid | 82 |
| 96-210-7236 | Ca (Al2 Si2 O8) | 76 |
| 96-900-0709 | Albite | 81 |
| 96-901-6527 | Aragonite | 56 |

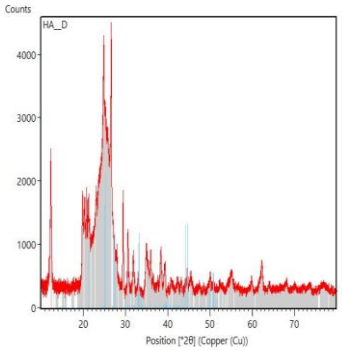


e

**Dust E**

| Ref. code | Compound name | Score |
|---|---|---|
| 96-230-0130 | aplha-magnesium sulfate | 97 |
| 96-900-9667 | Quartz | 74 |
| 96-231-0665 | Al P O 4 | 87 |
| 96-210-6265 | Fe (SO3) | 96 |
| 96-151-1680 | NaO. 364 MnO2 (H2 O) 0.544 | 91 |
| 96-900-0860 | Anorthoclase | 92 |
| 96-900-5443 | Chloritoid | 88 |
| 96-900-9664 | Albite | 97 |

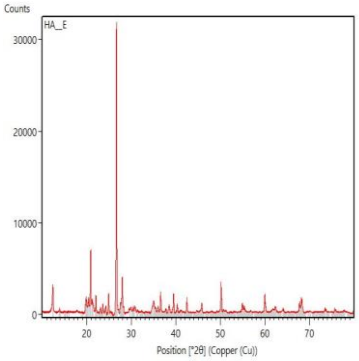


f

**Dust F**

| Ref. code | Compound name | Score |
|---|---|---|
| 96-230-0130 | aplha-magnesium sulfate | 33 |
| 96-900-5019 | Quartz | 32 |
| 96-231-0665 | Al P O 4 | 29 |
| 96-901-5066 | Hematite | 25 |
| 96-153-1680 | NaO. 364 MnO2 (H2 O) 0.544 | 40 |
| 96-900-5443 | Chloritoid | 48 |

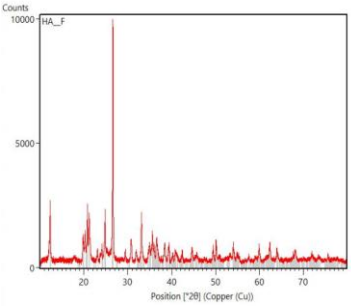


- The XRD analysis of the six dust samples shows different phases, however, the Al-Si composite was found to be common among all the samples. In addition, quartz, hematite and calcium carbonate phases were also observed.

### 1.2.6 ATR FT-IR analysis

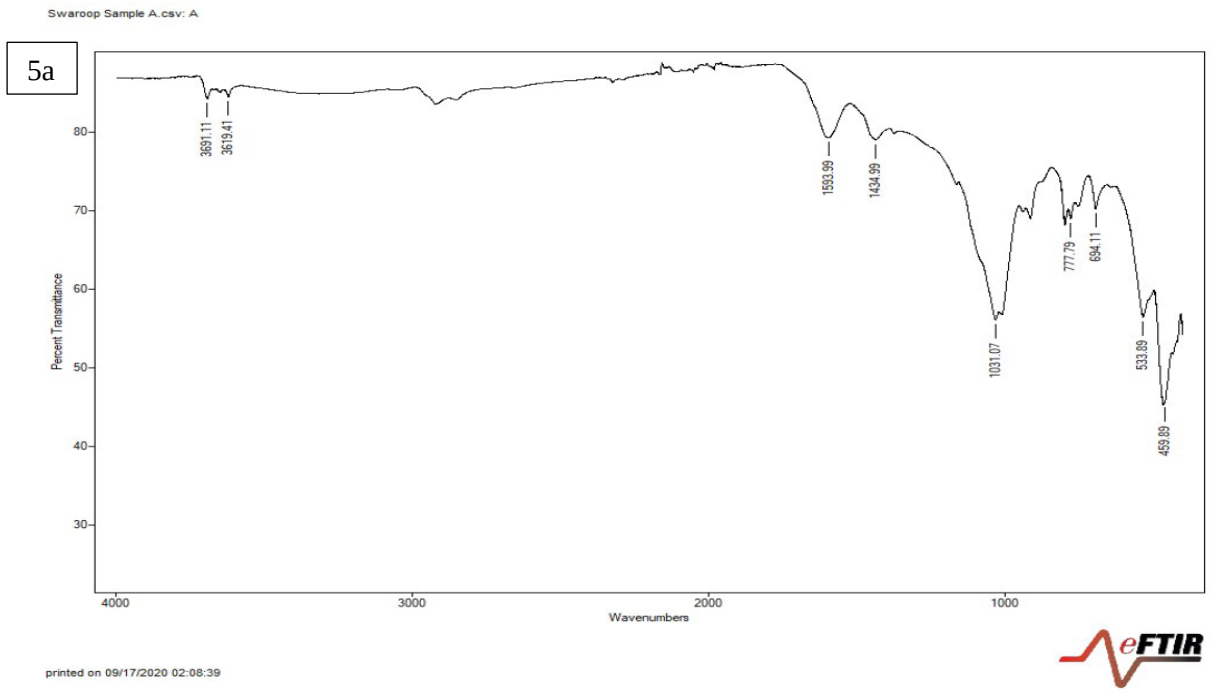


**Table 6a**

| Dust A | |
|---|---|
| **Range ($Cm^{-1}$)** | **Groups** |
| **3691, 3619** | -OH or -CH group (symmetric and asymmetric) (-CH2 and CH3) |
| **1593** | Aromatic C=C stretching |
| **1434** | O-C-O Stretching |
| **1031** | Si-O symmetrical stretching vibrations |
| **777.7** | C-H, CH=CH2 |
| **694** | Si-O symmetrical bending vibrations |
| **533** | asymmetrical bending vibrations of SiO4 |
| **459** | Si-O-Si (asymmetrical bending vibrations) |

5 b

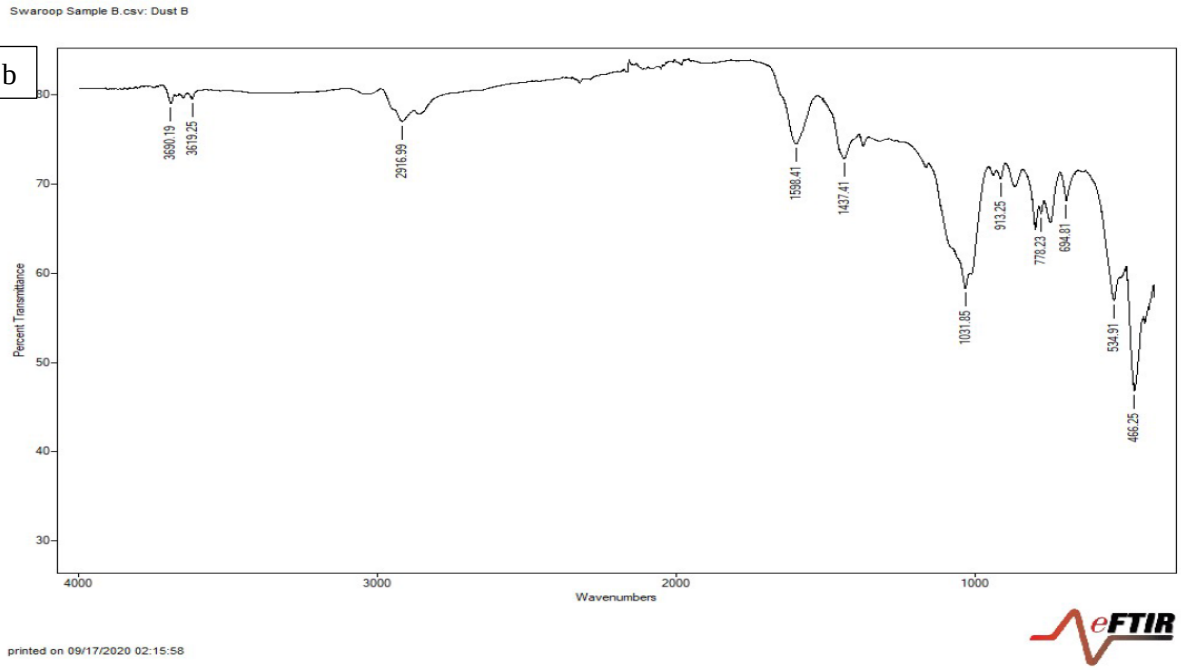


**Table 6b**

| | **Dust B** |
|---|---|
| 3690, 3619 | -OH or -CH group (symmetric and asymmetric) (-CH2 and CH3) |
| 1598 | Aromatic C=C stretching |
| 1437 | O-C-O Stretching |
| 1031 | Si-O stretching |
| 913 | Al-OH bending vibration |
| 778 | C-H, CH=CH2 |
| 694 | Si-O symmetrical bending vibrations |
| 535 | S-O-Al stretching |
| 466 | Si-O-Si bending |

5 c

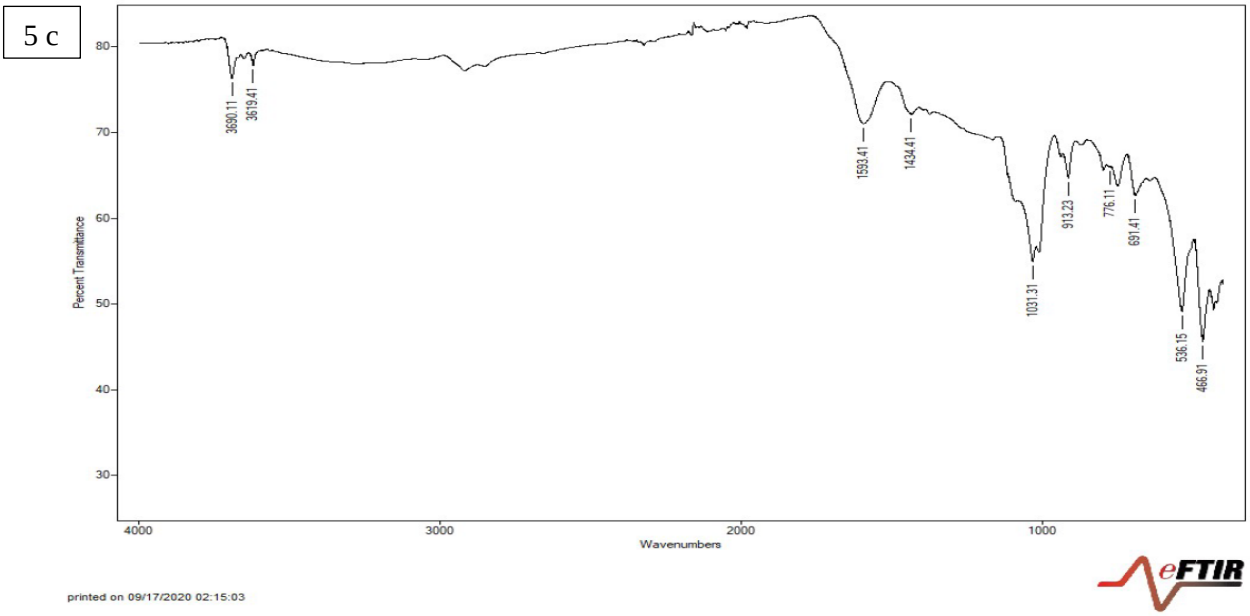

**Table 6c**

| Dust C | |
|---|---|
| **3690, 3619** | -OH or -CH group (symmetric and asymmetric) (-CH2 and CH3) |
| **1593** | Aromatic C=C stretching |
| **1434** | O-C-O Stretching |
| **1031** | Si-O stretching |
| **913** | Al-OH bending vibration |
| **776** | C-H, CH=CH2 |
| **694** | Si-O symmetrical bending vibrations |
| **536** | S-O-Al stretching |
| **466** | Si-O-Si bending |

5 d

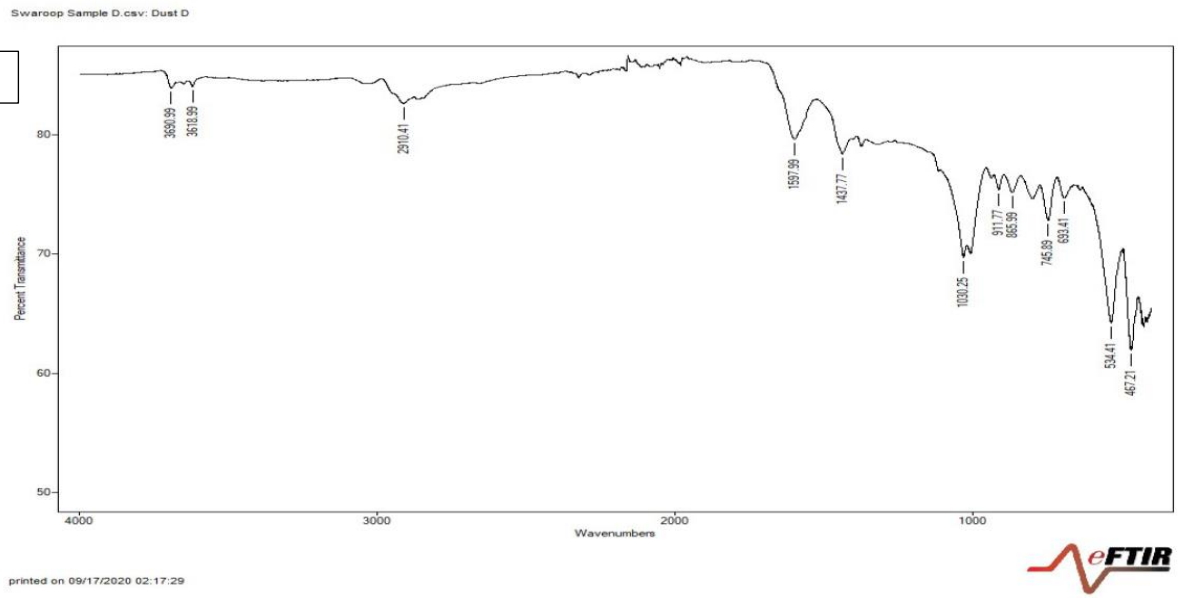


**Table 6d**

| Dust D | |
|---|---|
| **3690, 3618** | -OH or -CH group (symmetric and asymmetric) (-CH2 and CH3) |
| **2910** | C-H Stretching of [-(CH2)3CH3] |
| **1597** | C=C |
| **1437** | O-C-O Stretching |
| **1030** | Si-O symmetrical stretching vibrations |
| **911** | C-O-C, |
| **865.9** | a) $CO_3^{2-}$<br>b) Methly nitrite , C2H2, CO2, HCN |
| **775.8** | Methly nitrite , C2H2, CO2, HCN |
| **693.1** | Si-O symmetrical bending vibrations |
| **534.41** | S-O-Al stretching |
| **467.21** | Si-O-Si bending |

5 e

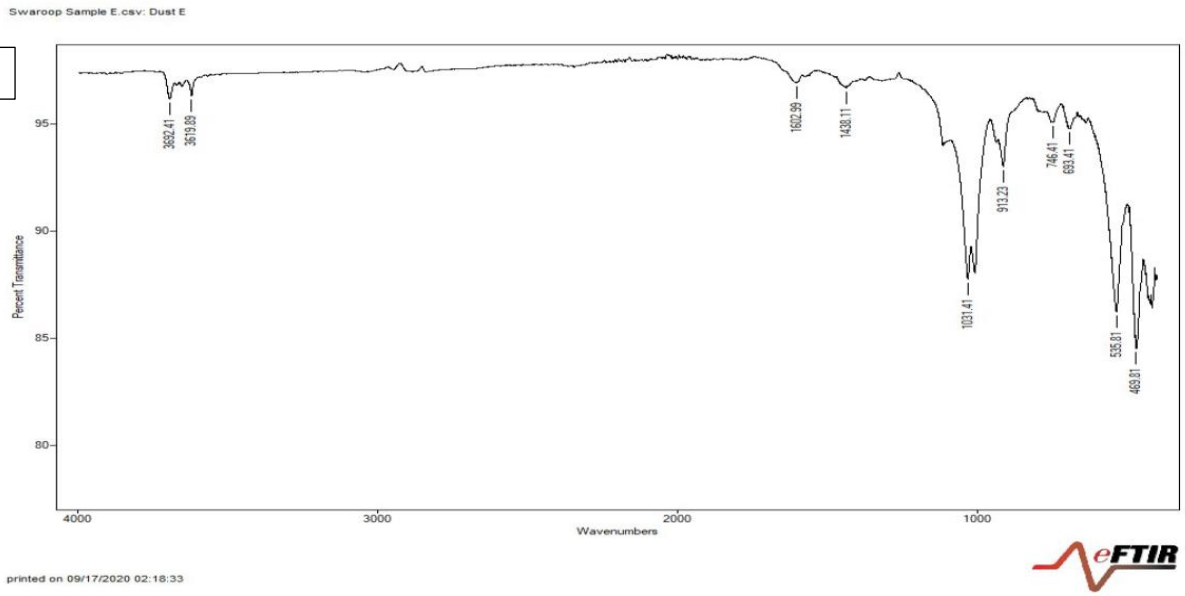


**Table 6e**

| | **Dust E** |
|---|---|
| **3692, 3619** | -OH or -CH group (symmetric and asymmetric) (-CH2 and CH3) |
| **1602.99** | C=N |
| **1438** | O-C-O Stretching |
| **1031** | Si-O symmetrical stretching vibrations |
| **913** | C-O-C, |
| **746** | C-H bending (alkene) |
| **693** | Si-O symmetrical bending vibrations |
| **535** | S-O-Al stretching |
| **469** | Si-O-Si bending |

5 f

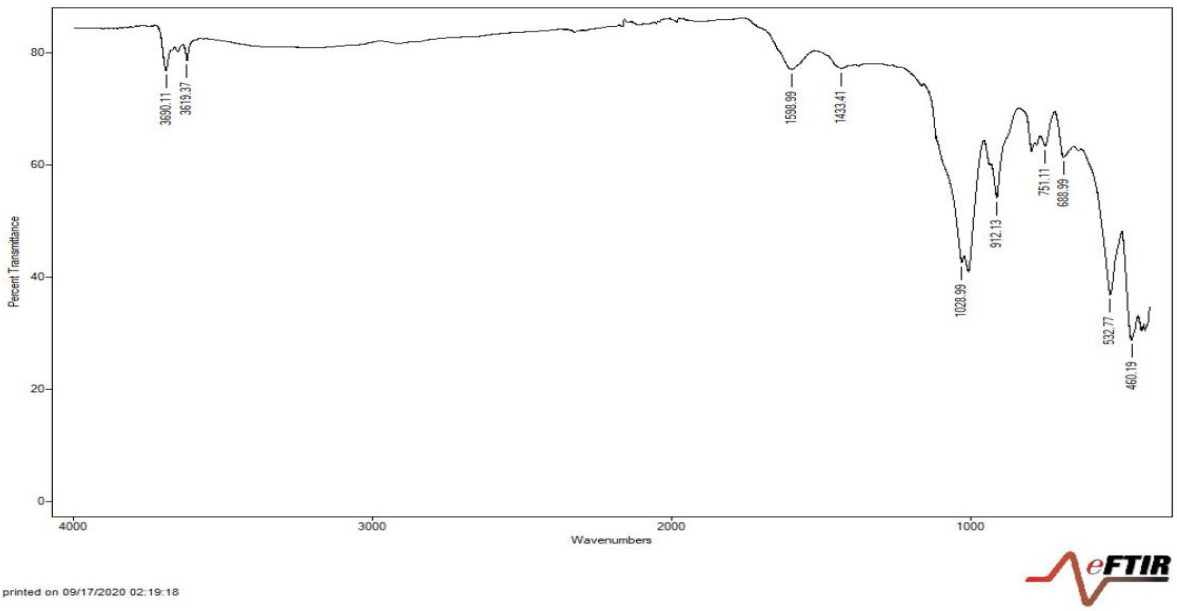

**Table 6f**

| Dust F | |
|---|---|
| **3690, 3619** | -OH or -CH group (symmetric and asymmetric) (-CH2 and CH3) |
| **1598.9** | C=N |
| **1433** | O-C-O Stretching |
| **1029.99** | Si-O symmetrical stretching vibrations |
| **912** | C-O-C, |
| **751** | C-H bending (alkene) |
| **688** | Si-O symmetrical bending vibrations |
| **532** | S-O-Al stretching |
| **460** | Si-O-Si bending |

**Figure 5 (a-f):** FT-IR spectrum showing the % transmittance of dust samples A-f

**Table 6 (a-f):** Illustrates the identified functional groups from the respective IR spectra shown in Fig 5 (a-f)

- Multiple functional groups were observed across different dust samples. FT-IR spectra of Dust A, B, C and D showed C=C aromatic stretch, indicating the presence of polyaromatic hydrocarbons (PAH's) or other aromatic contaminants. Further, the Si-O and Si-O-Al functional groups were observed across all the six dust samples.

### 1.2.7 Gas chromatography-mass spectrometry (GC-MS) – PAH analysis

**-Ongoing.**

## 2 Animal model

**Acute model:** The acute model was designed to study the short-term effects of coal dust PM on lungs. C57/BL6 female mice were opted for the study and were exposed to 3 different concentrations of coal PM (1mg/$m^3$, 3mg/$m^3$ & 10mg/$m^3$). All the animals were given a single dose of PM through intranasal for 5 days/week for 2 weeks, which is equivalent to what an average miner breaths during their 8 hours of shift for 5 days/week. Further, the mice were monitored, treated and culled according to approved guidelines and protocols by Animal Care and Ethics Comity (ACEC) of The University of Newcastle on the protocol A-2017-738.

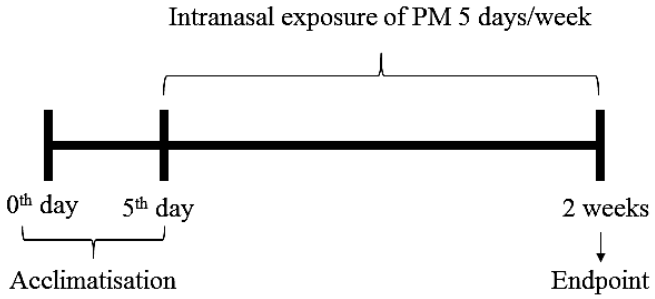


**Figure 6:** Shows the schematic representation of the acute model (2wk)

**Chronic model:** The chronic model was designed to understand the long-term effects of breathing coal PM on lungs. To do so, we have exposed the mice to similar concentrations to that of the acute model, however, the exposure time, i.e. 2 weeks was increased to 12 weeks the mice were culled according to approved guidelines and protocols by Animal Care and Ethics Comity (ACEC) of The University of Newcastle on the designated protocol number A-2017-738.

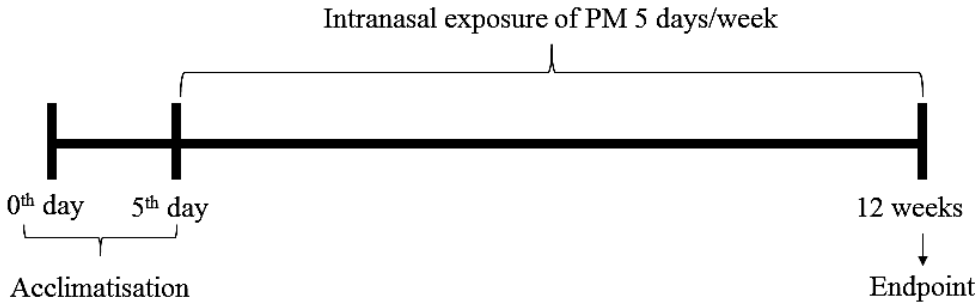


**Figure 7 :** Shows the schematic representation of Chronic model

**2.1** Diffusion of Carbon monoxide (DFco) - Acute (2wk) exposure model

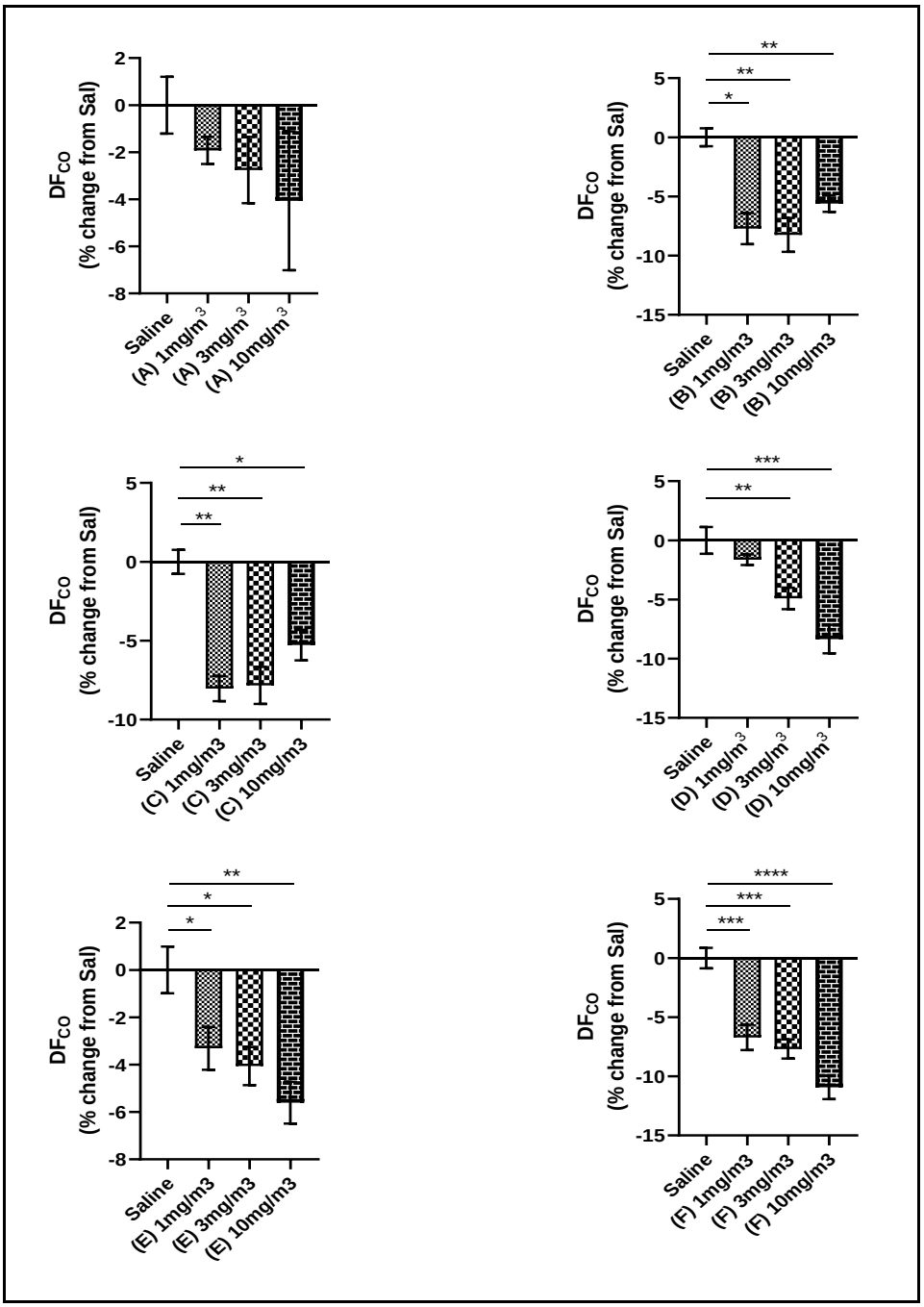


**Figure 8 :** Bar graph showing the gas exchange capability (CO diffusion) of mice exposed to dust (≤ $PM_{10}$) for 2weeks (Acute exposure). T-test; n=6; P < 0.05 *; P < 0.01 **; P < 0.001 ***; P < 0.0001 ****

- A dose-dependent response was observed across different dust types. The dust collected from the initial stages of mining (B&C) was found to effectively decrease the gas exchange capability at lower concentrations compared to 10mg/$m^3$. Whereas Dust A, D, E and F were able to affect the lungs at higher concentration. Dust F was found to have the worst effect (> 10% loss) among the tested samples, might be due to high Fe content.

**2.2** Diffusion of Carbon monoxide (DFco) - Chronic (12wk) exposure model

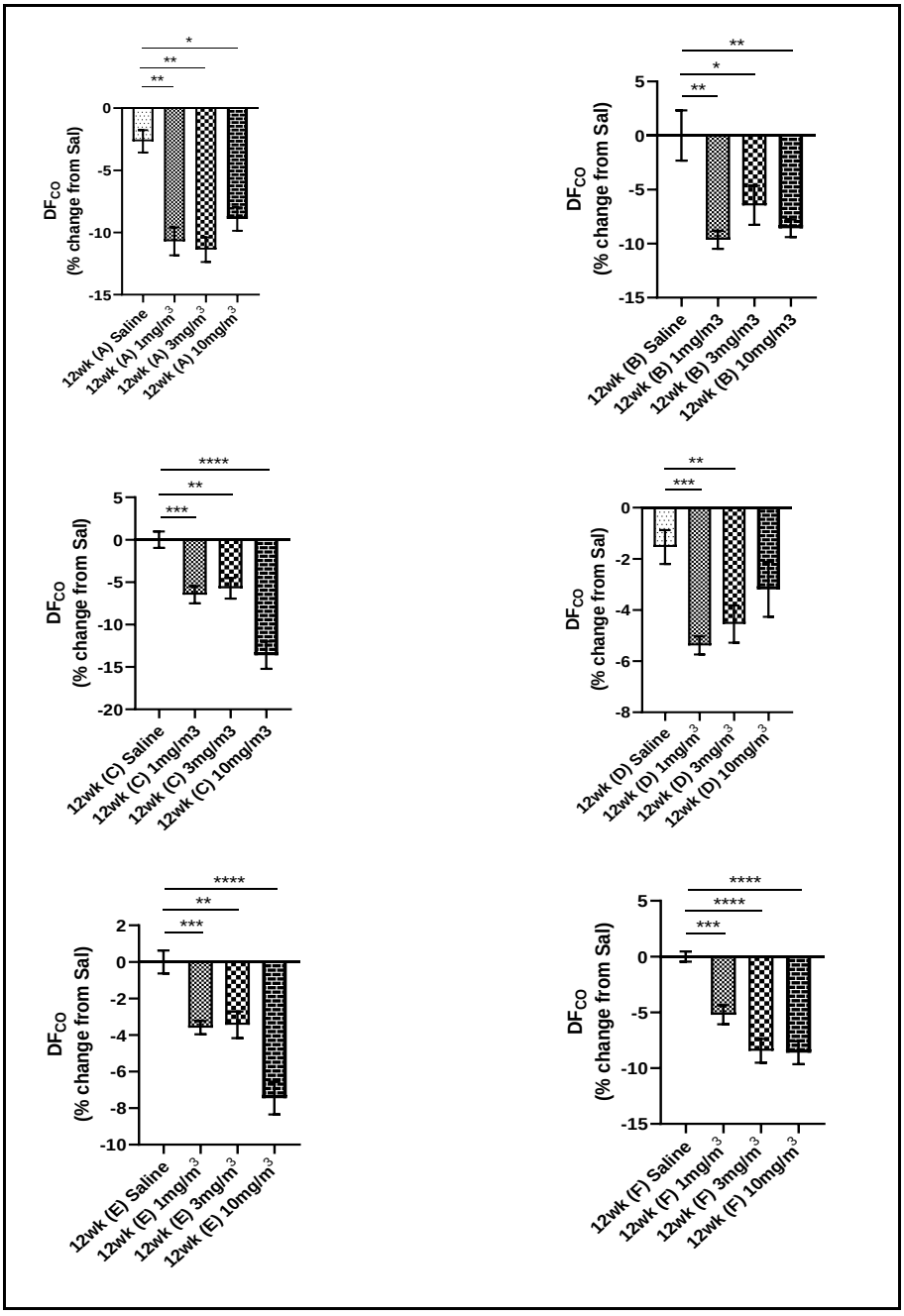


**Figure 9:** Bar graph showing the gas exchange capability (CO diffusion) of mice exposed to dust ($\leq PM_{10}$) for 12weeks (Chronic exposure). T-test; n=8; $P < 0.05$ *; $P < 0.01$ **; $P < 0.001$ ***; $P < 0.0001$ ****

- Interestingly, over chronic exposure, different dust types had different effects on lung function, irrespective of particle size. Dust A, B & D was found to reduce lung gas exchange capability at lower concentrations whereas C, E and F were effective at higher doses. Dust C was found to have the worst effect. Initial observations confirm that the damage caused by particulates over the short period is greater or saturated when compared to chronic exposures.

## 2.3 Central airways resistance at baseline (Rn) – Acute model

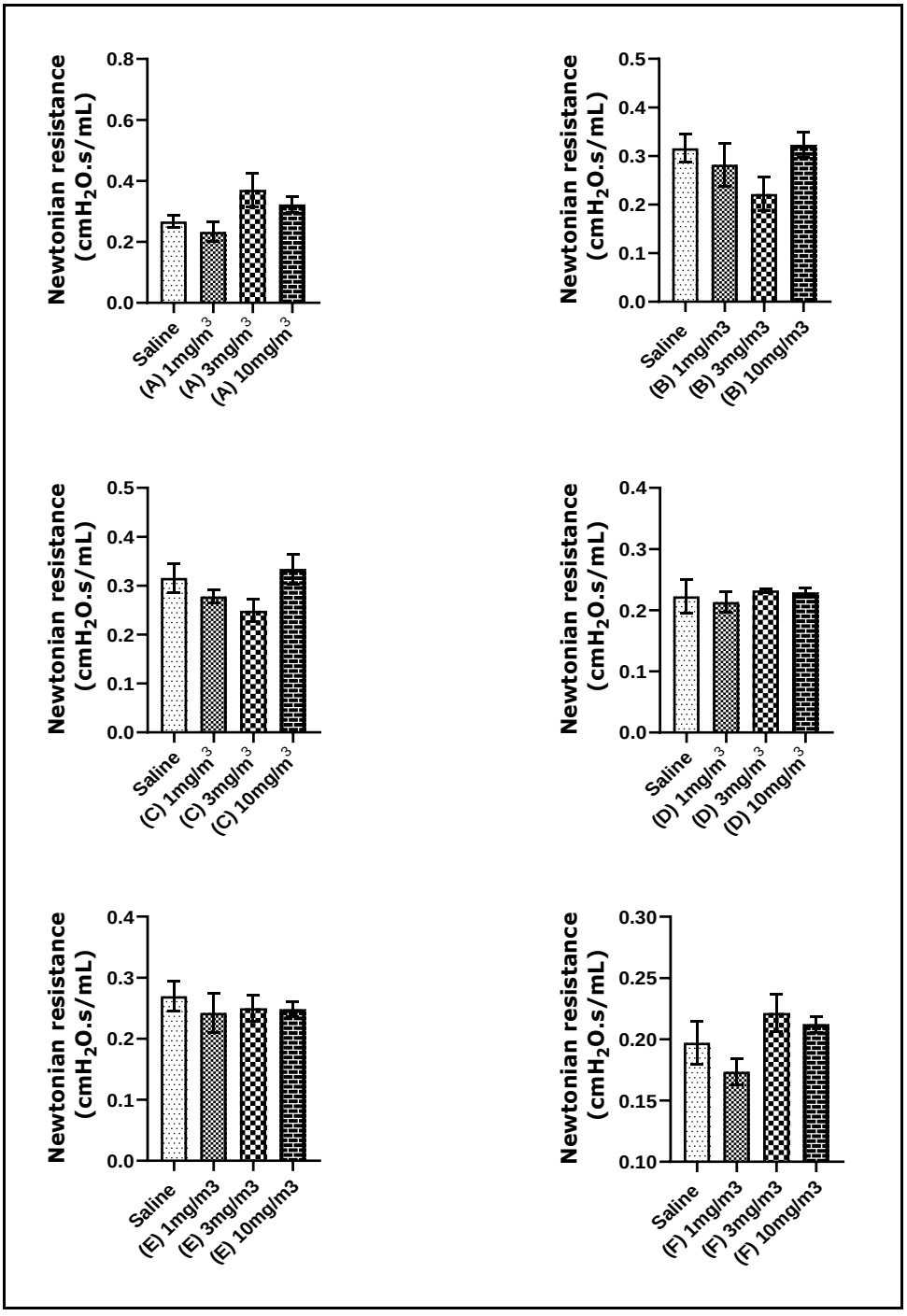


**Figure 10:** Bar graph showing the central airway resistance (baseline) of mice exposed to dust ($\leq PM_{10}$) for 2weeks. T-test; n=6; P < 0.05 *; P < 0.01 **; P < 0.001 ***; P < 0.0001 ****

- No statistically significant increase in central airways resistance at baseline was observed across different concentrations or samples upon 2wk of dust exposure

## 2.4 Transplumonary resistance at baseline (Rrs) – Acute model

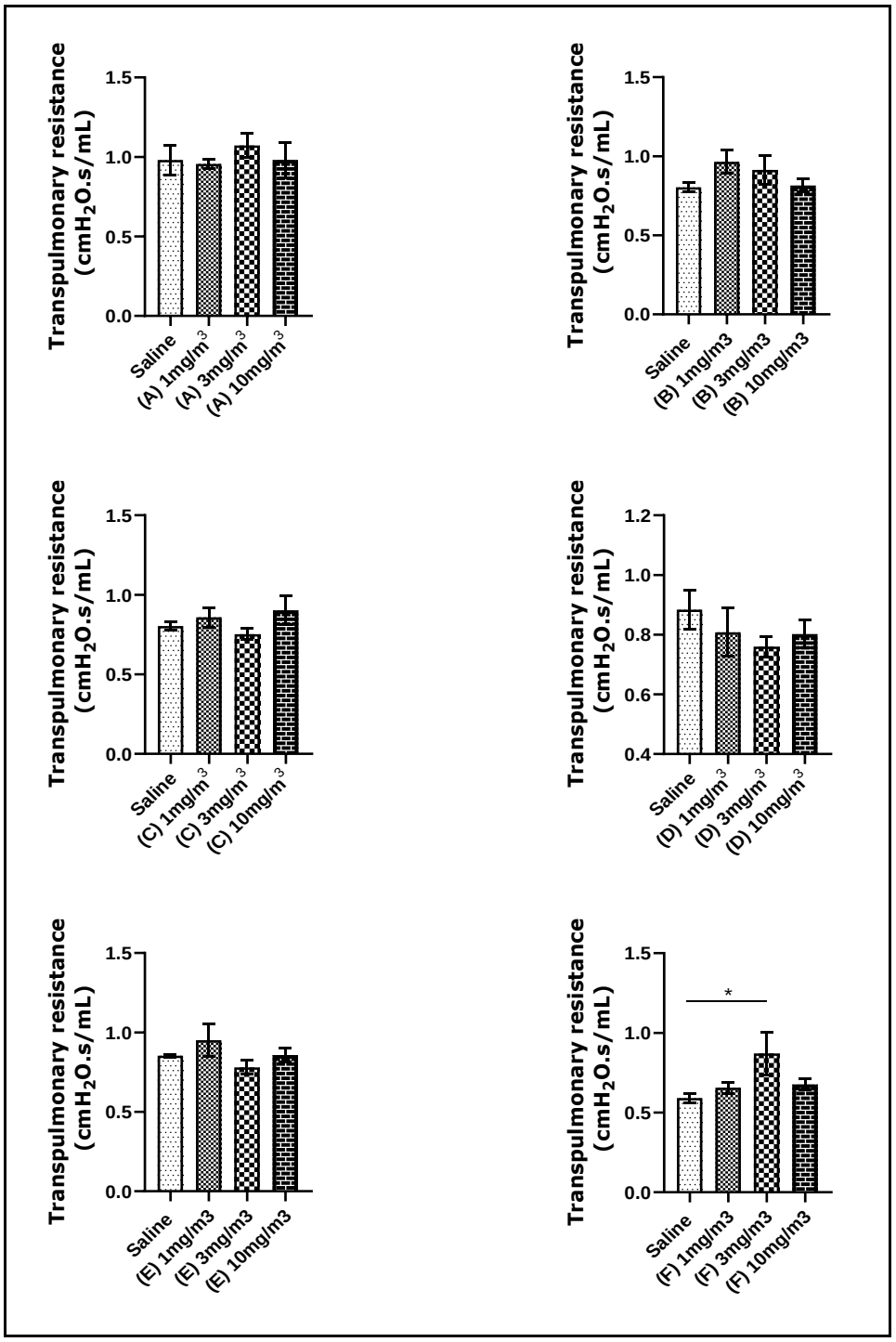


**Figure 11:** Bar graph showing the transpulmonary resistance (baseline) of mice exposed to dust ($\leq PM_{10}$) for 2weeks. T-test; n=6; $P < 0.05$ *; $P < 0.01$ **; $P < 0.001$ ***; $P < 0.0001$ ****

- Increase in transpulmonary resistance at baseline was observed with dust F at 3mg/m$^3$ concentration, a slight increase with 1mg and 10mg was observed, however, they are not statistically significant. Other samples did not affect at baseline.

## 2.5 Tissue damping at baseline (G) – Acute model

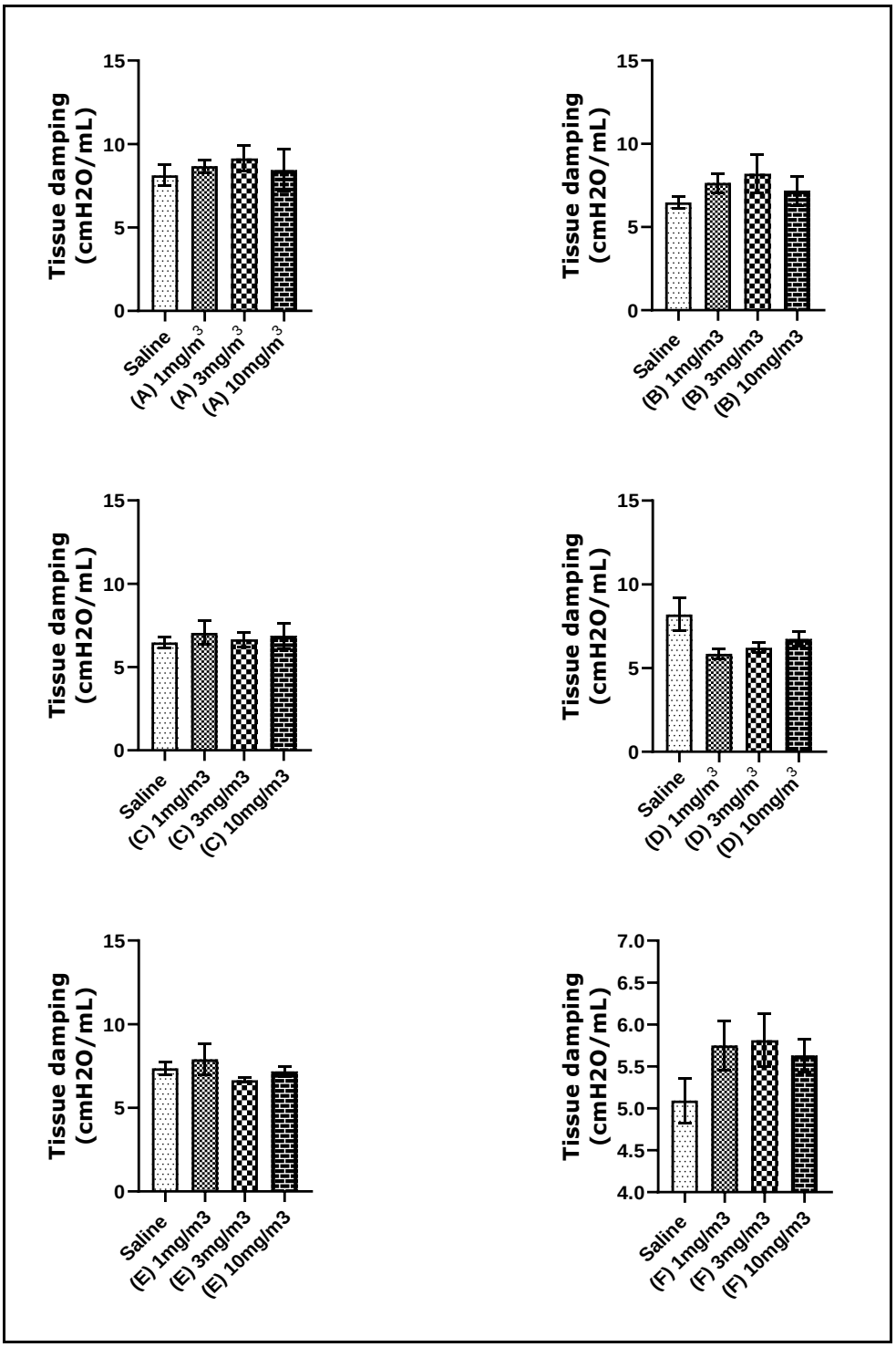


**Figure 12:** Bar graph showing the tissue damping (tissue resistance and reflects the energy dissipation in the alveoli) of mice exposed to dust (≤ $PM_{10}$) for 2weeks. T-test; n=6; P < 0.05 *; P < 0.01 **; P < 0.001 ***; P < 0.0001 ****

- No statistically significant increase in tissue damping at baseline was observed across different concentrations or samples upon 2wk of dust exposure

## 2.6 Tissue elastance at baseline (H) - Acute model

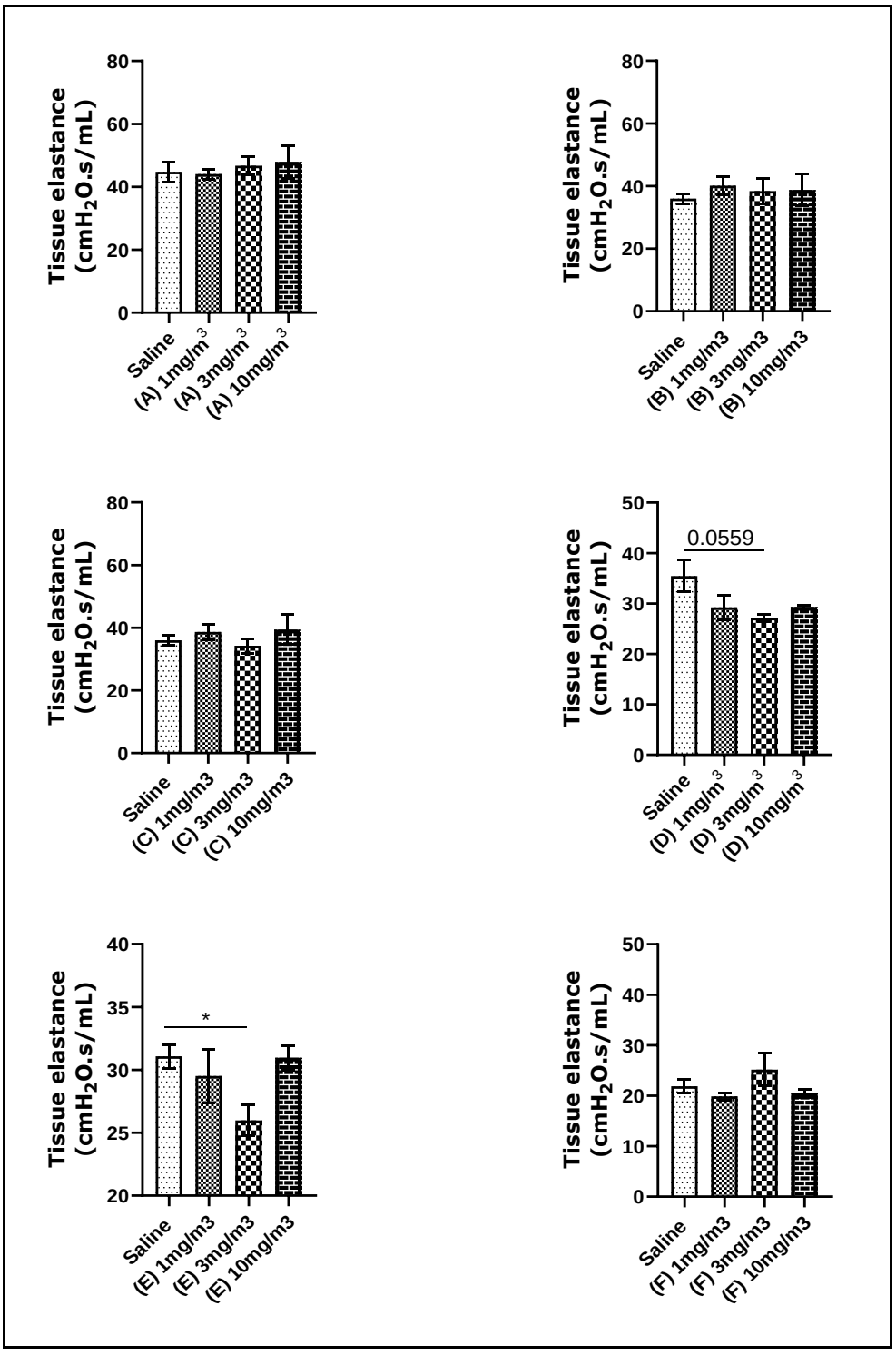


**Figure 13:** Bar graph showing the tissue elastance (tissue elastance and reflects the energy conservation in the alveoli) of mice exposed to dust (≤ $PM_{10}$) for 2weeks. T-test; n=6; P < 0.05 *; P < 0.01 **; P < 0.001 ***; P < 0.0001 ****

- Among the tested dust types and concentrations, Dust D showed a decreased trend of tissue elastance with all three concentrations, whereas Dust E 3mg/$m^3$ has shown a statistically significant decrease over all other doses.

## 2.7 Dynamic compliance (Crs) - Acute model

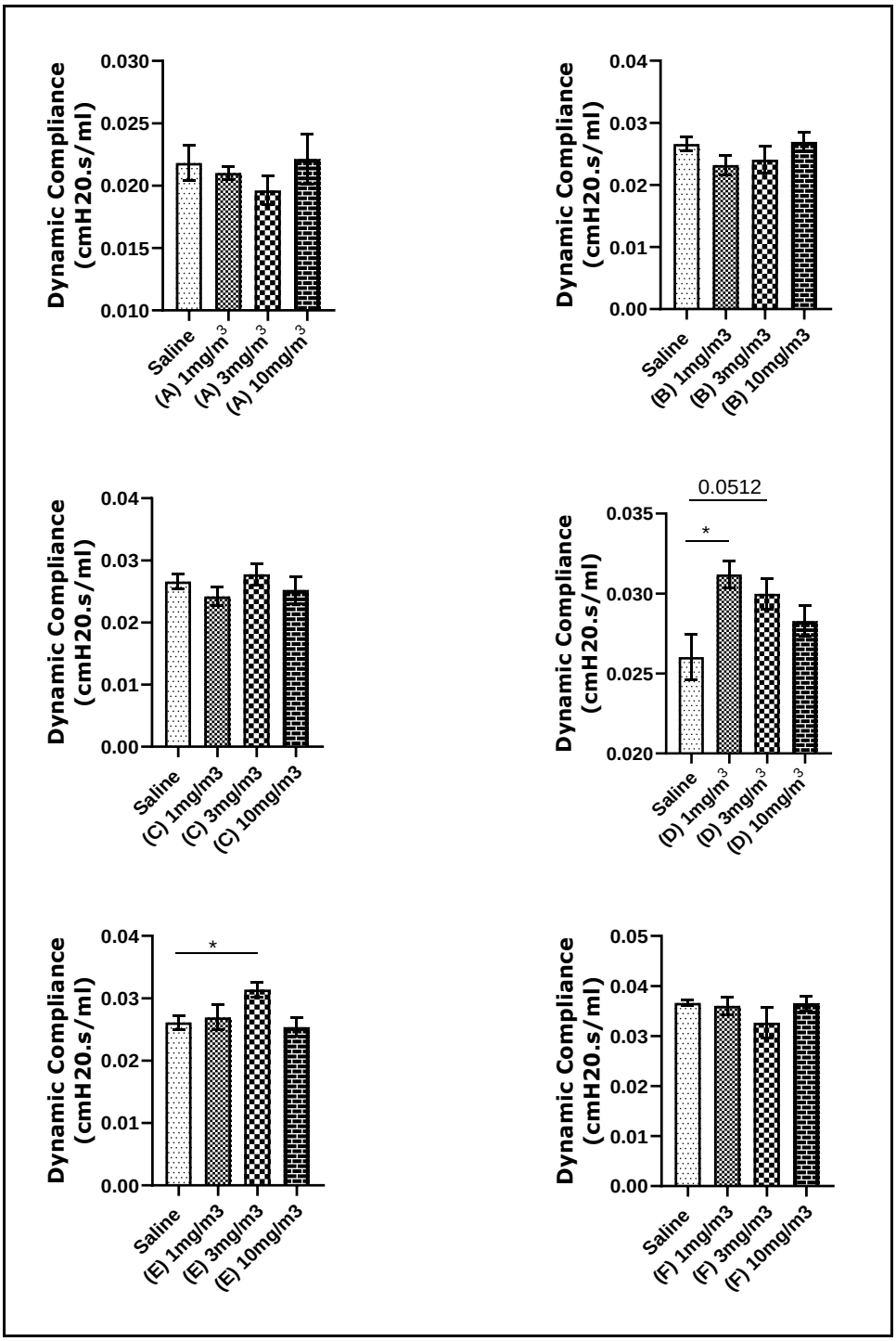


**Figure 14:** Bar graph showing the dynamic compliance of mice exposed to dust (≤ $PM_{10}$) for 2weeks. T-test; n=6; P < 0.05 *; P < 0.01 **; P < 0.001 ***; P < 0.0001 ****

- Dust D showed increased dynamic compliance at lower concentrations compared to a higher dose. An opposite trend was observed with Dust E. Other dust samples did not affect at baseline.

## 2.8 Dynamic elastance (Ers) - Acute model

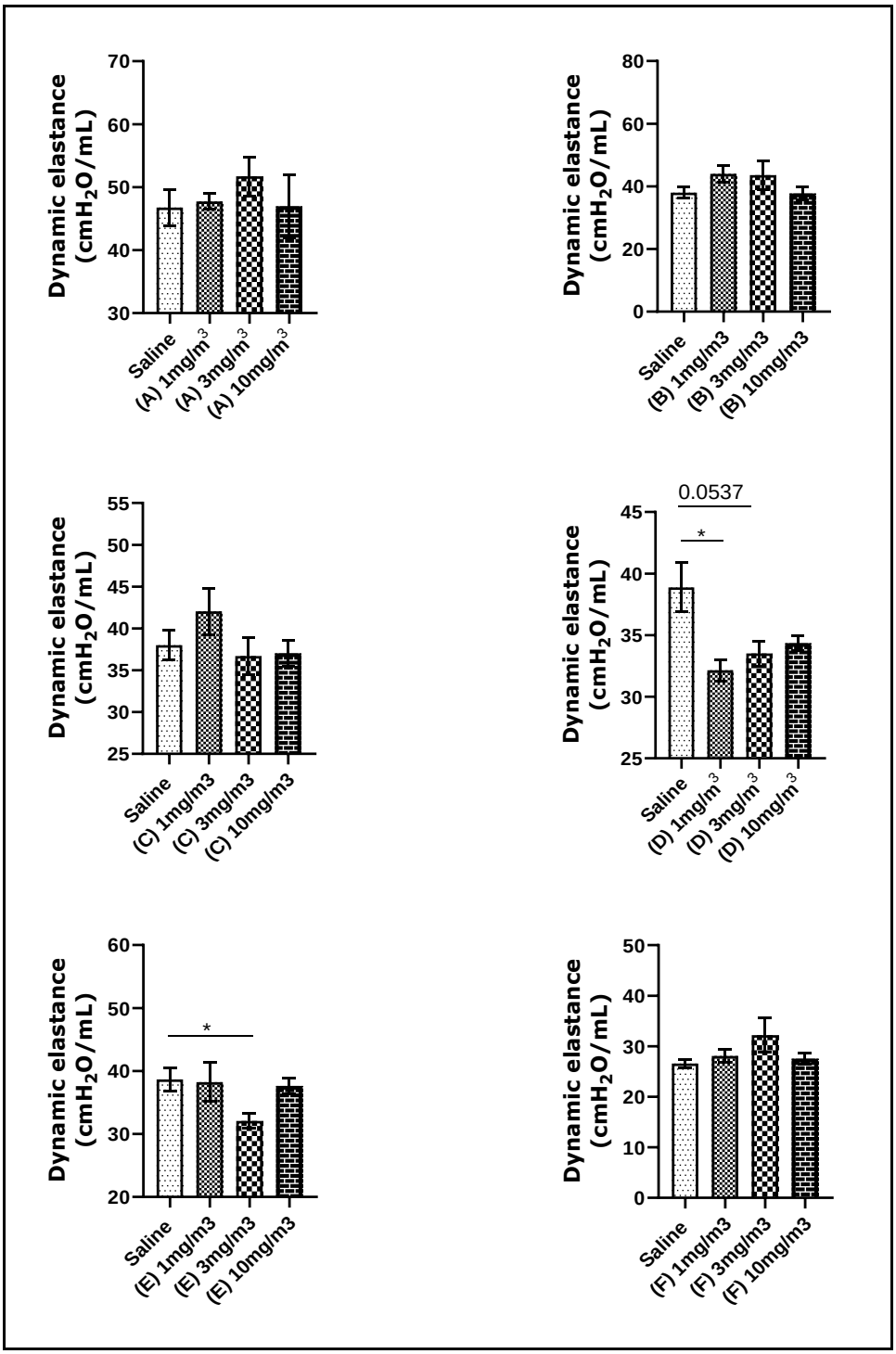


**Figure 15:** Bar graph showing the dynamic elastance of mice exposed to dust (≤ $PM_{10}$) for 2weeks. T-test; n=6; P < 0.05 *; P < 0.01 **; P < 0.001 ***; P < 0.0001 ****

- Dust D showed a decrease in dynamic elastance at lower concentrations compared to a higher dose. However, Dust E 3mg/$m^3$ showed a statistically significant decrease compared to saline and other tested concentrations. Other dust samples did not affect at baseline.

## 2.9 Inspiratory capacity (IC) - Acute model

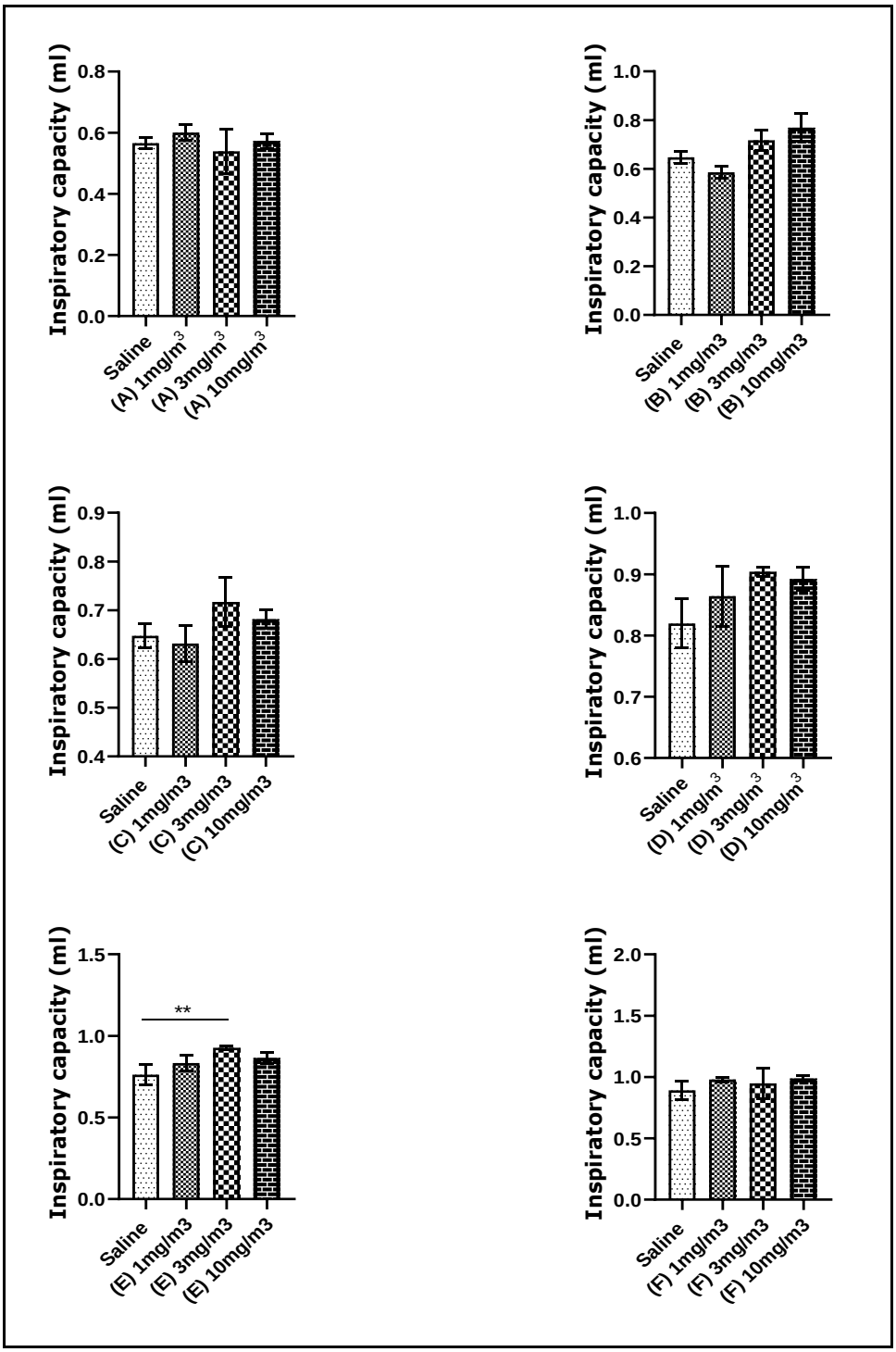


**Figure 16:** Bar graph showing the inspiratory capacity (tidal volume + inspiratory reserve) of mice exposed to dust (≤ $PM_{10}$) for 2weeks. T-test; n=6; P < 0.05 *; P < 0.01 **; P < 0.001 ***; P < 0.0001 ****

- A dose-dependent increase trend was observed across different dust types, however, Dust E 3mg/$m^3$ was found to be statistically significant. Other samples did not affect inspiratory capacity at baseline.

## 2.10 Hysteresis - Acute model

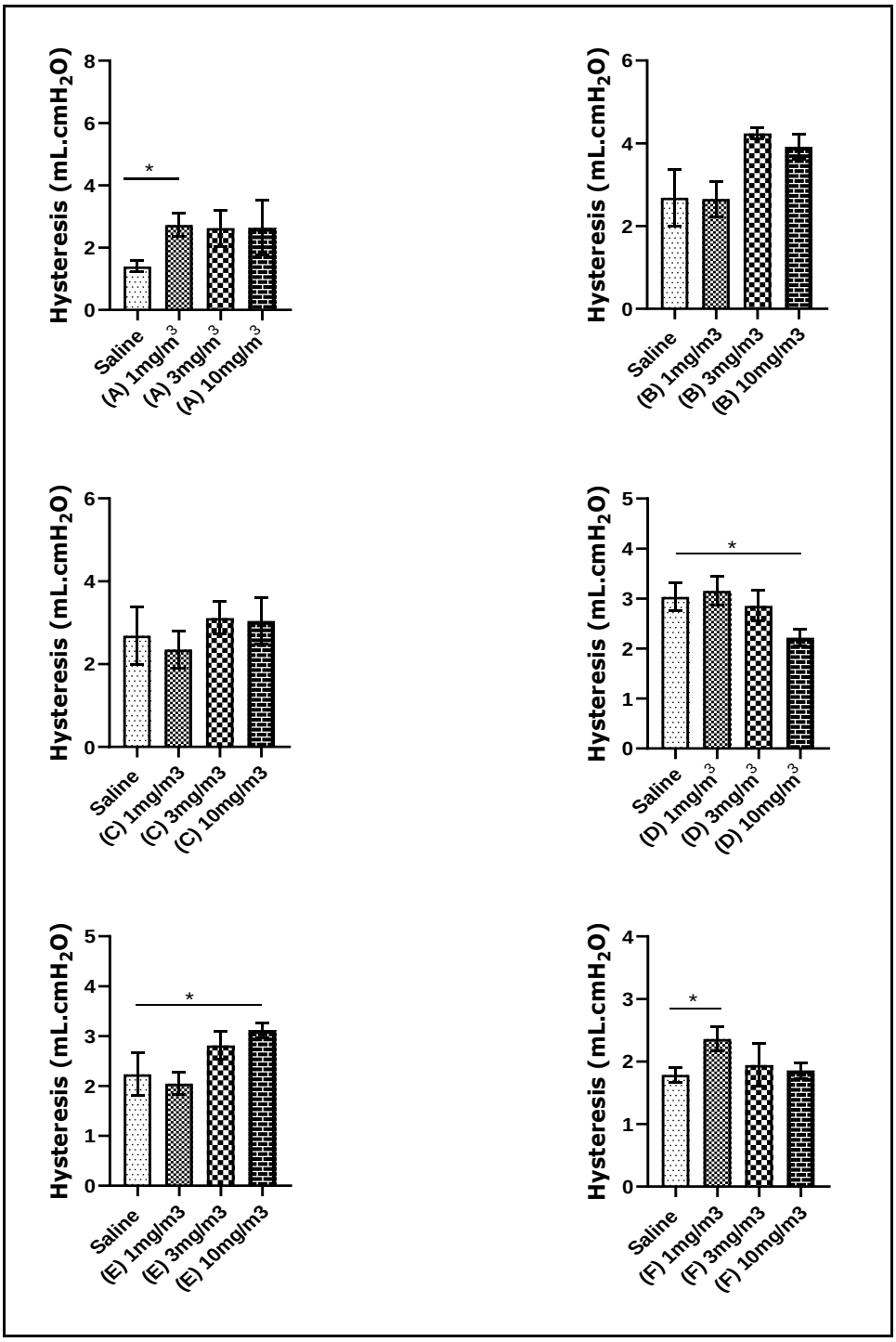


**Figure 17:** Bar graph showing the hysteresis (additional energy required to overcome surface tension) of mice exposed to dust (≤ $PM_{10}$) for 2weeks. T-test; n=6; P < 0.05 *; P < 0.01 **; P < 0.001 ***; P < 0.0001 ****

- Different dust types had different effects on lung hysteresis. However, a dose-dependent response was observed with each sample. Dust A, B, C & E showed increased hysteresis values with increase in dust dose, however, Dust D and F had vice vera effect.

## 2.11 Lung Compliance - Acute model

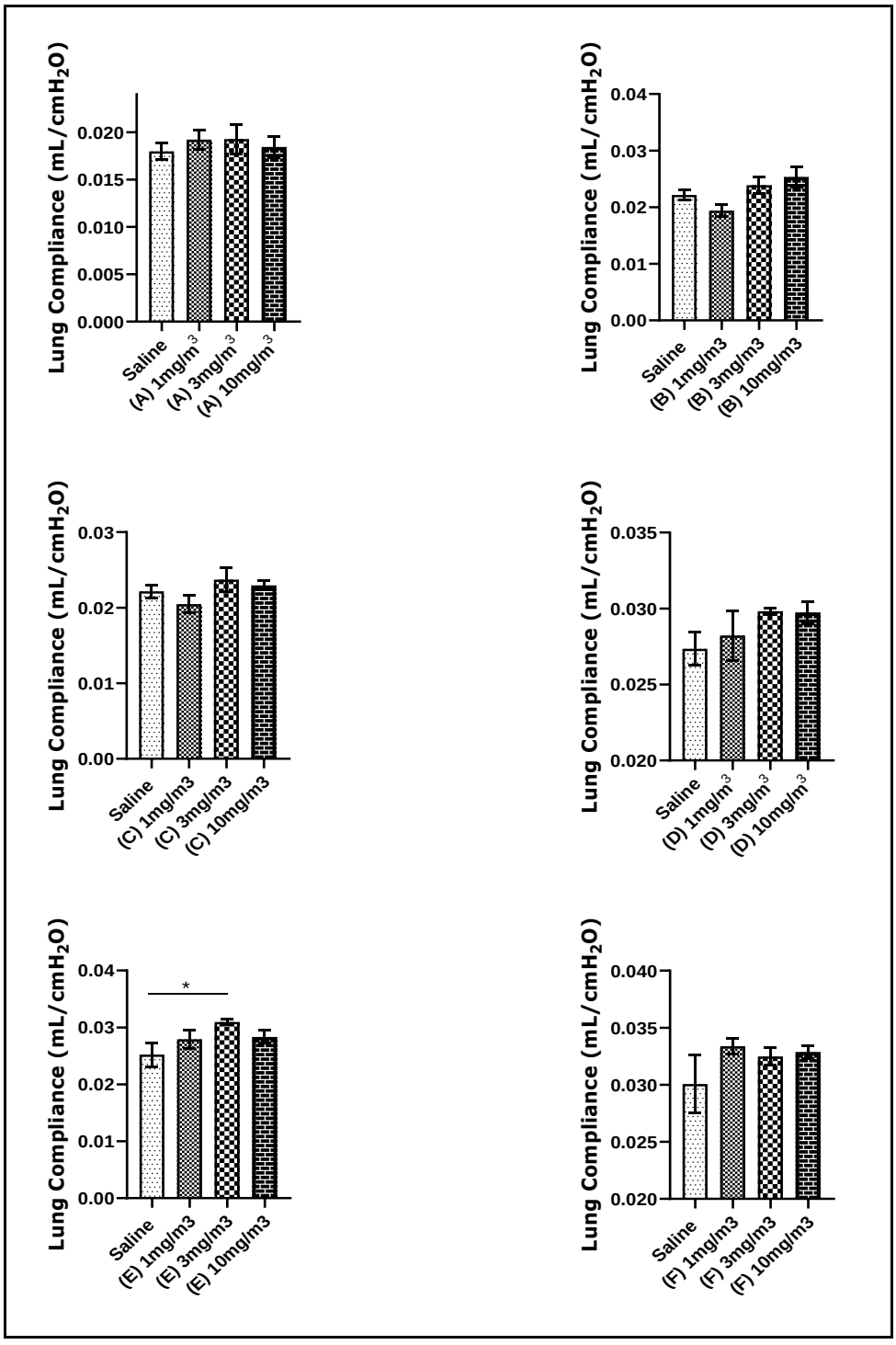


**Figure 18:** Bar graph showing the lung compliance (Δvolume/Δpressure) of mice exposed to dust (≤ $PM_{10}$) for 2weeks. T-test; n=6; P < 0.05 *; P < 0.01 **; P < 0.001 ***; P < 0.0001 ****

- 2-week dust exposure had no significant effect on lung compliance. However, Dust E 3mg showed increased compliance compared to the rest of the doses.

## 2.12 pressure-volume loops - Acute model

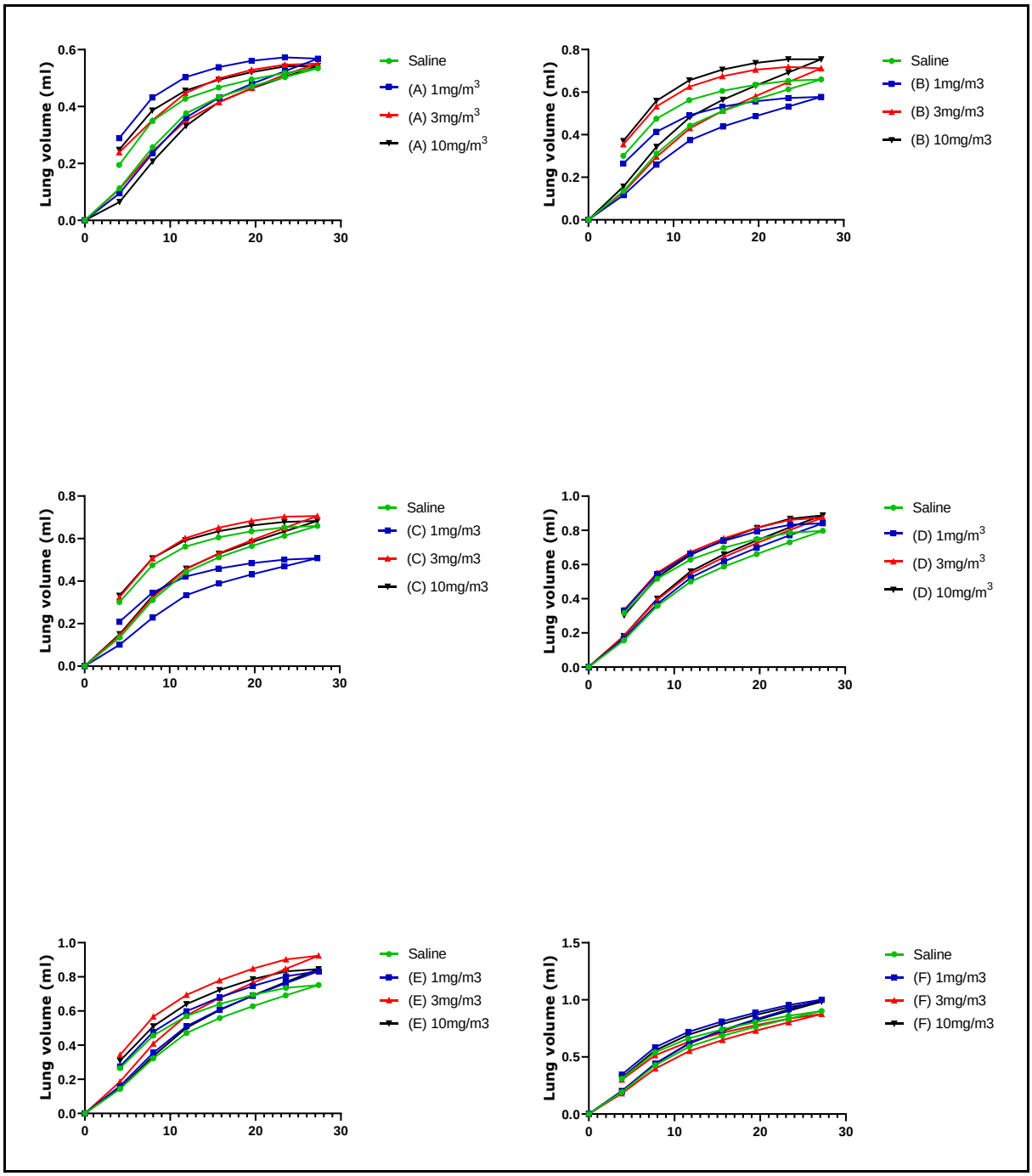


**Figure 19:** Graph showing the Δvolume/Δpressure curves(PV loops) of mice exposed to dust (≤ $PM_{10}$) for 2weeks

- A shift towards upside represents the emphysema; the greater the shift greater the alveoli damage; A shift towards bottom represents the fibrosis; the greater the shift greater the lung fibrosis
- Lower concentration (1mg/$m^3$) of Dust B & C tend to shift towards lower, showing the fibrotic tendency of dust, whereas higher doses tend to show emphysema condition. Irrespective of dose, dust E tend to induce emphysema like conditions. Other dust samples have little or no effect over 2 wk exposure.

## 2.13 Airway-Hyperresponsiveness (AHR) – Central airway resistance (Rn)

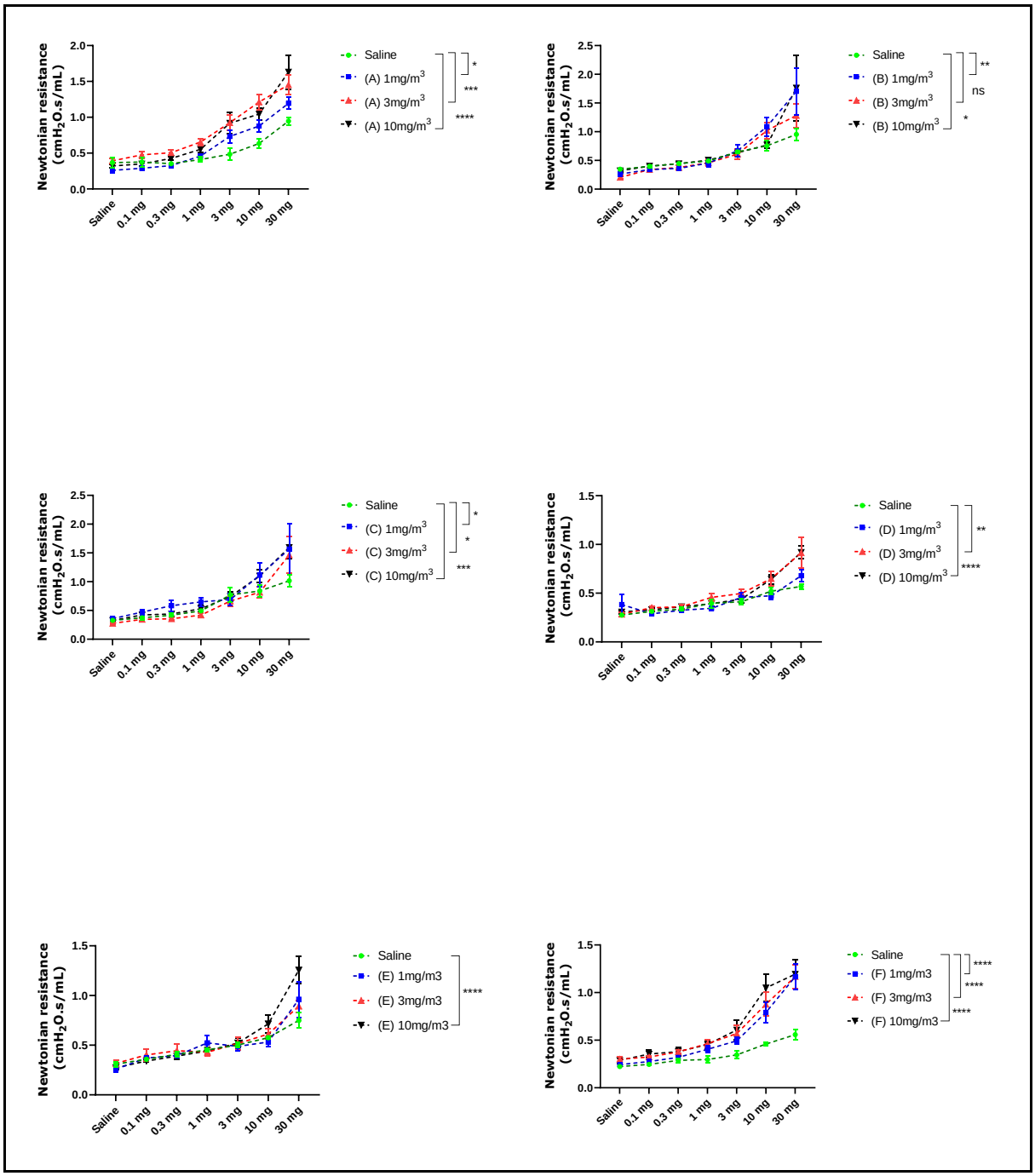


**Figure 20:** Graph showing the dose dependent central airways resistance in response to increasing concentrations of Methacholine for mice exposed to dust (≤ $PM_{10}$) for 2weeks. 2-way anova; n=6; P < 0.05 *; P < 0.01 **; P < 0.001 ***; P < 0.0001 ****

- Irrespective of dust type all the tested doses showed increased central airway resistance compared to saline within 2 weeks of dust exposure. Lowest dose (1mg/$m^3$) was equally effective in inducing the AHR as the highest dose (10mg/$m^3$).

## 2.14 Airway-Hyperresponsiveness (AHR) – Transpulmonary resistance (Rrs)

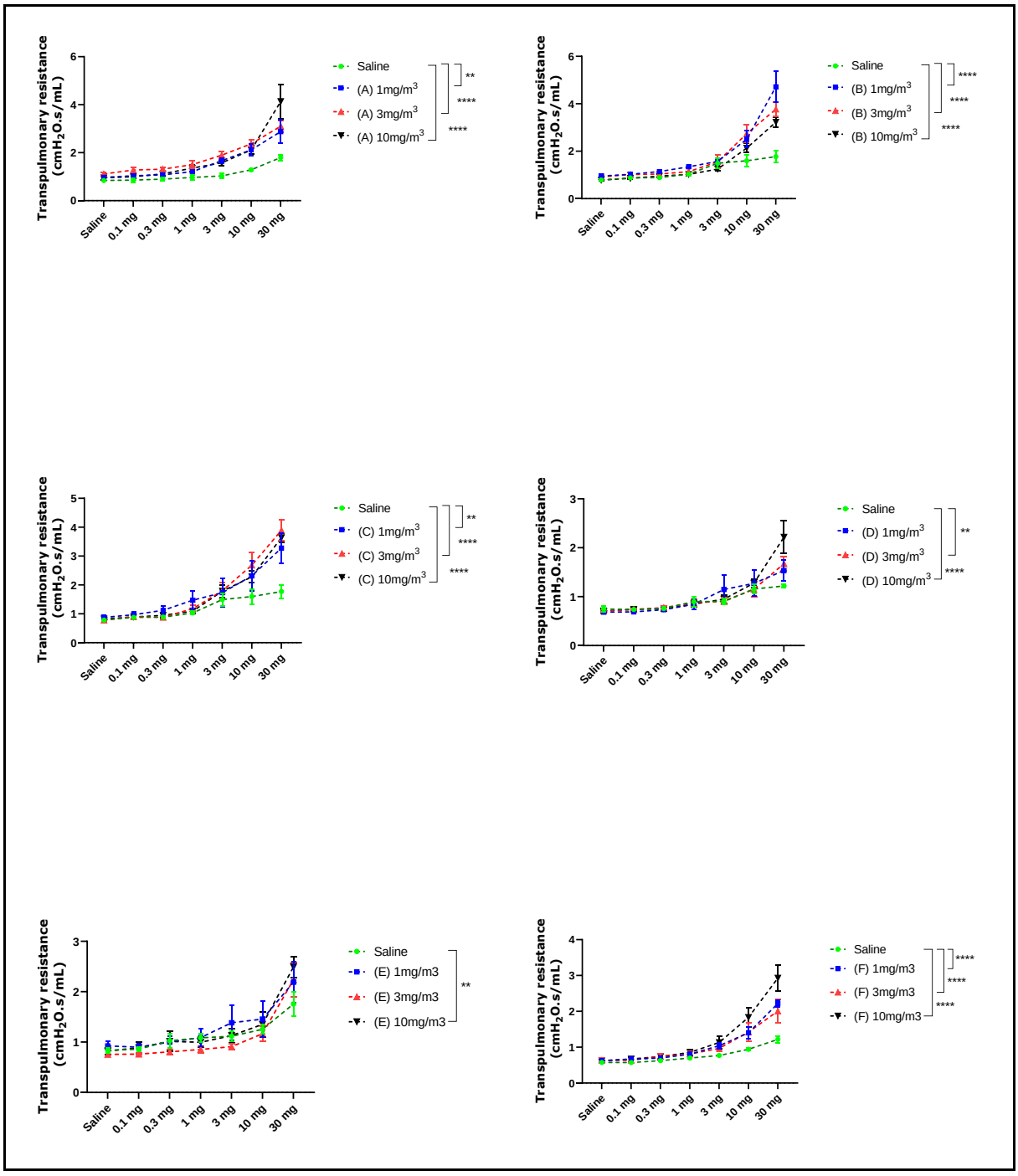


**Figure 21:** Graph showing the dose dependent transpulmonary resistance in response to increasing concentrations of Methacholine for mice exposed to dust (≤ $PM_{10}$) for 2weeks. 2-way anova; n=6; P < 0.05 *; P < 0.01 **; P < 0.001 ***; P < 0.0001 ****

- Irrespective of dust type all the tested doses showed increased Transpulmonary resistance compared to saline within 2 weeks of dust exposure.
- Dust from the final stage of mining (A, B & C) induced higher resistance compared to dust screened from the initial stage (D, E & F).

## 2.15 Airway-Hyperresponsiveness (AHR) – Tissue damping (G)

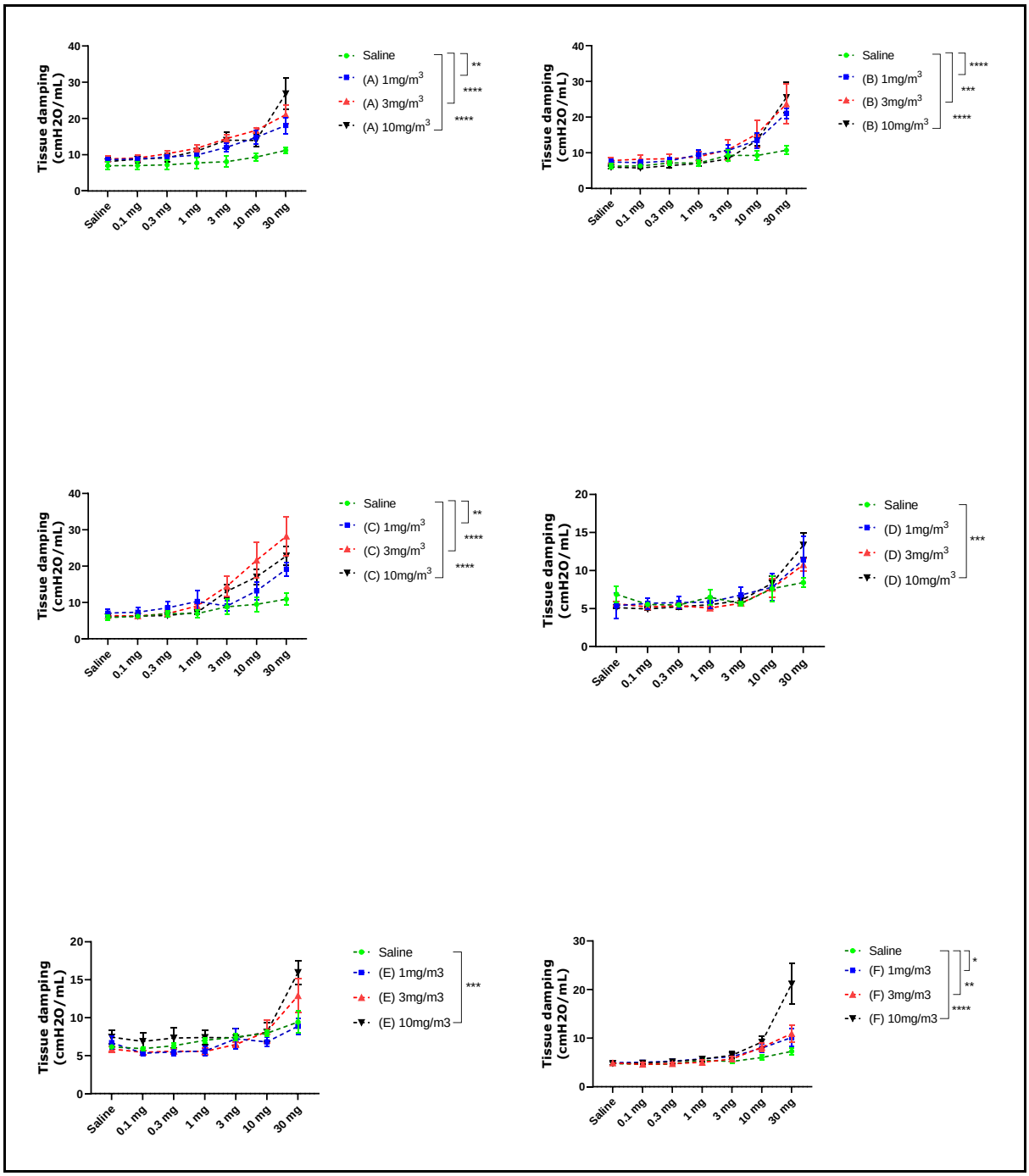


**Figure 22:** Graph showing the dose dependent response of G to increasing concentrations of Methacholine for mice exposed to dust (≤ $PM_{10}$) for 2weeks. 2-way anova; n=6; $P < 0.05$ *; $P < 0.01$ **; $P < 0.001$ ***; $P < 0.0001$ ****

- Irrespective of dust type all the tested doses showed increased Tissue damping compared to saline within 2 weeks of dust exposure.

## 2.16 Airway-Hyperresponsiveness (AHR) – Tissue elastance (H)

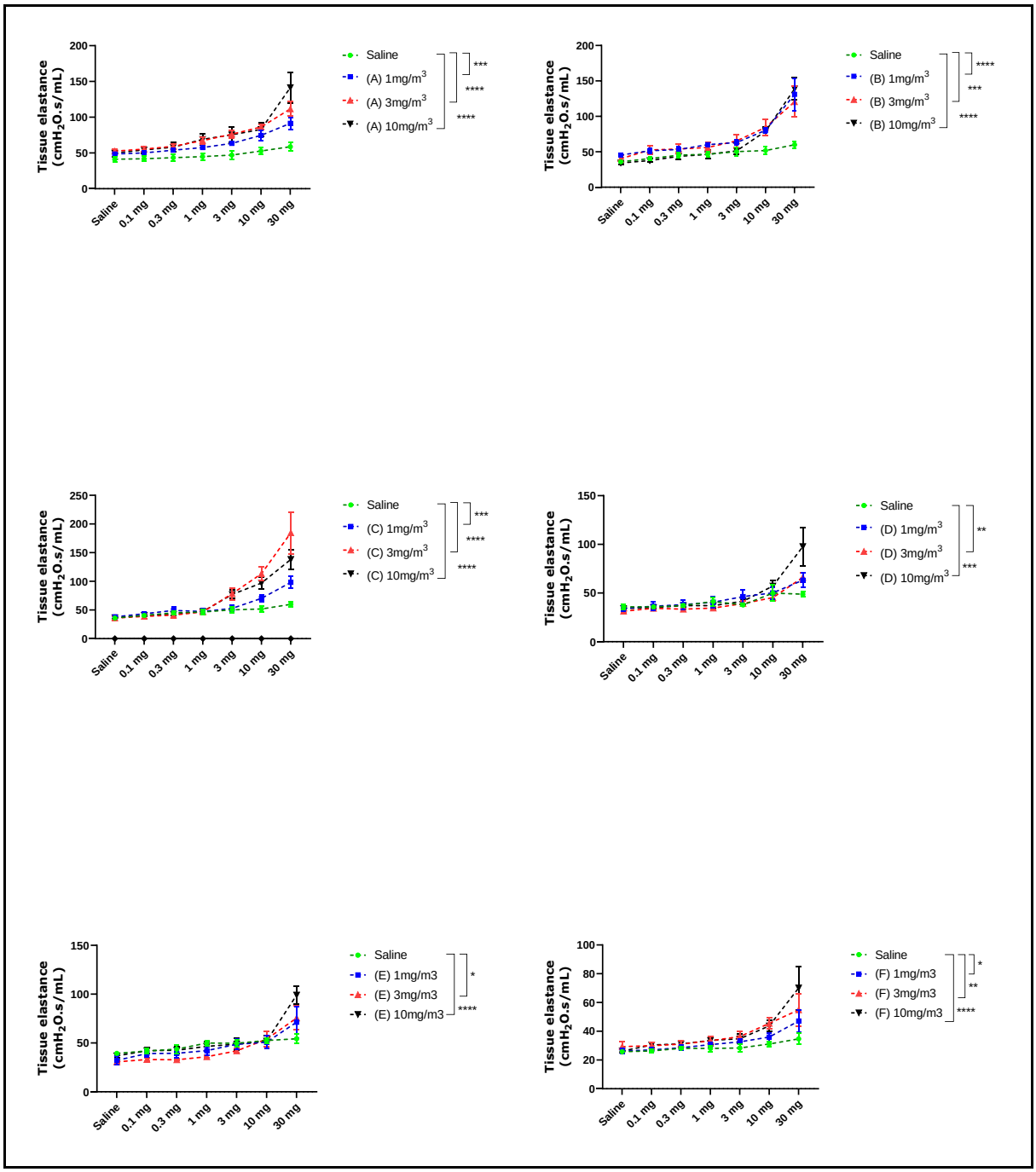


**Figure 23:** Graph showing the dose dependent response of H to increasing concentrations of Methacholine for mice exposed to dust (≤ $PM_{10}$) for 2weeks. 2-way anova; n=6; $P < 0.05$ *; $P < 0.01$ **; $P < 0.001$ ***; $P < 0.0001$ ****

- Irrespective of dust type all the tested doses showed increased Tissue elastance compared to saline within 2 weeks of dust exposure.

## 2.17 Airway-Hyperresponsiveness (AHR) - Dynamic compliance (Crs)

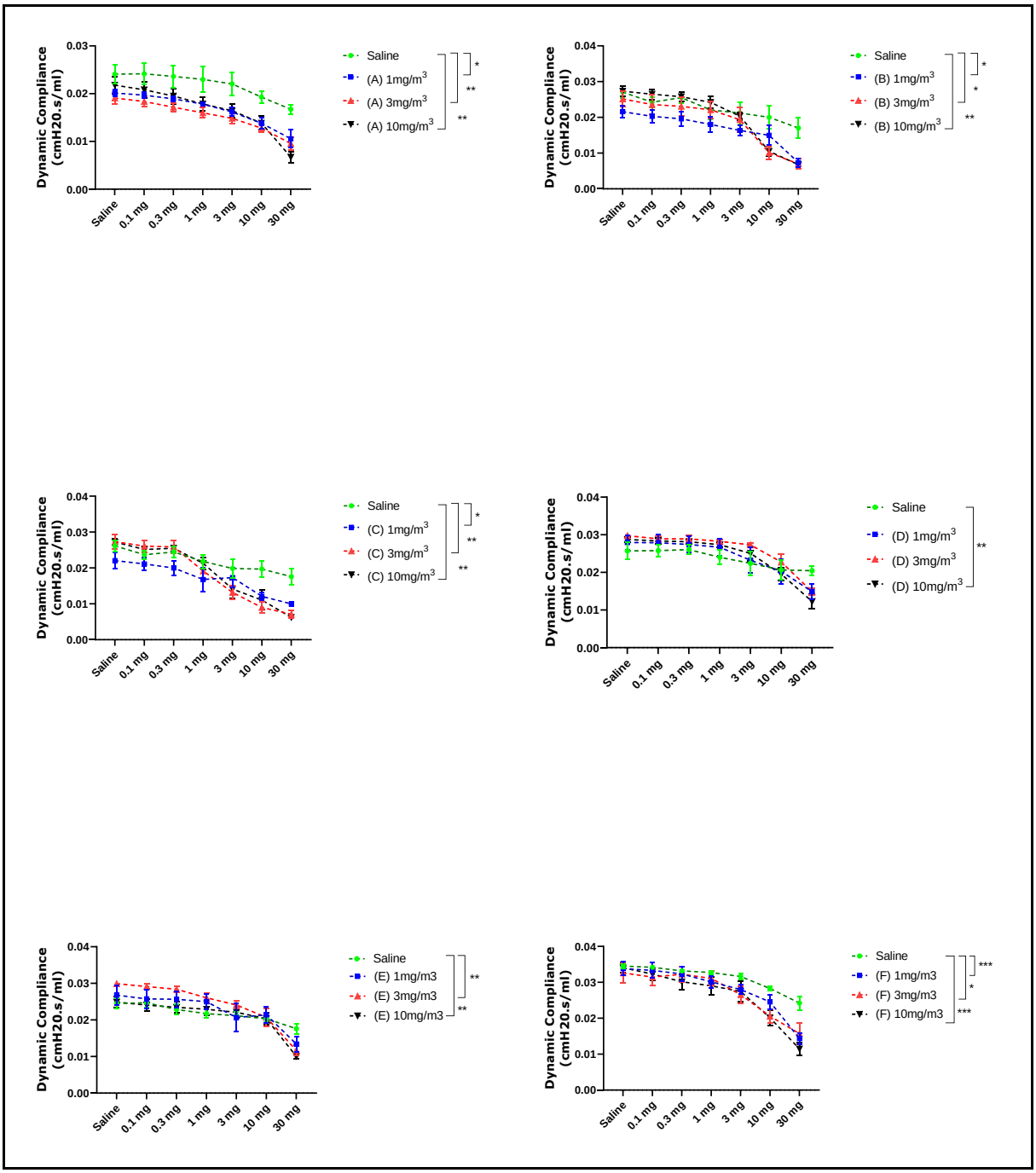


**Figure 24:** Graph showing the dose dependent response of Crs to increasing concentrations of Methacholine for mice exposed to dust (≤ $PM_{10}$) for 2weeks. 2-way anova; n=6; $P < 0.05$ *; $P < 0.01$ **; $P < 0.001$ ***; $P < 0.0001$ ****

- Irrespective of dust type all the tested doses showed decreased Dynamic compliance compared to saline within 2 weeks of dust exposure.

## 2.18 Airway-Hyperresponsiveness (AHR) - Dynamic elastance (Ers)

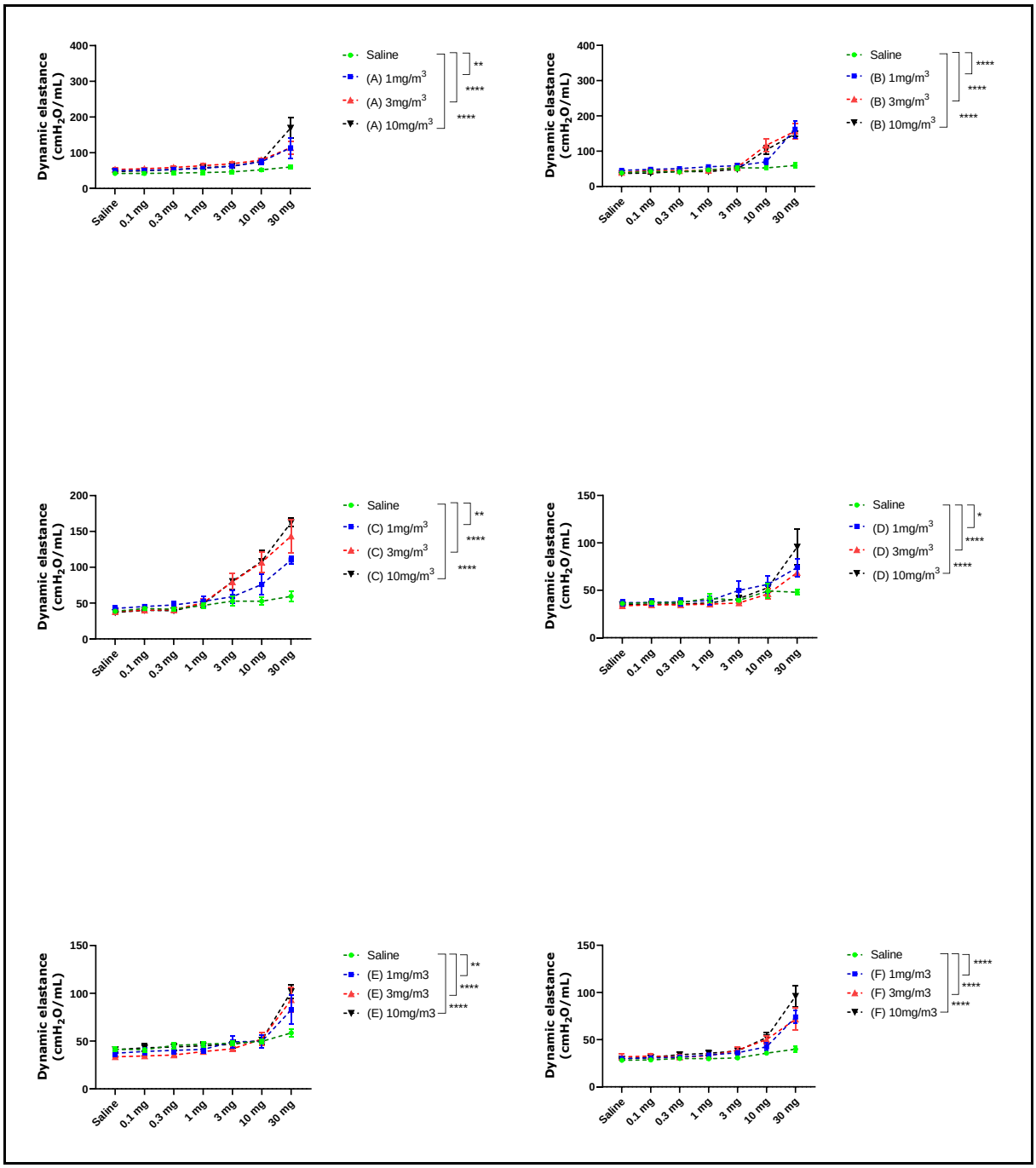


**Figure 25:** Graph showing the dose dependent response of Ers to increasing concentrations of Methacholine for mice exposed to dust (≤ $PM_{10}$) for 2weeks. 2-way anova; n=6; $P < 0.05$ *; $P < 0.01$ **; $P < 0.001$ ***; $P < 0.0001$ ****

- Irrespective of dust type all the tested doses showed increased Dynamic elastance compared to saline within 2 weeks of dust exposure.

## 2.19 Central airways resistance at baseline (Rn) – Chronic model

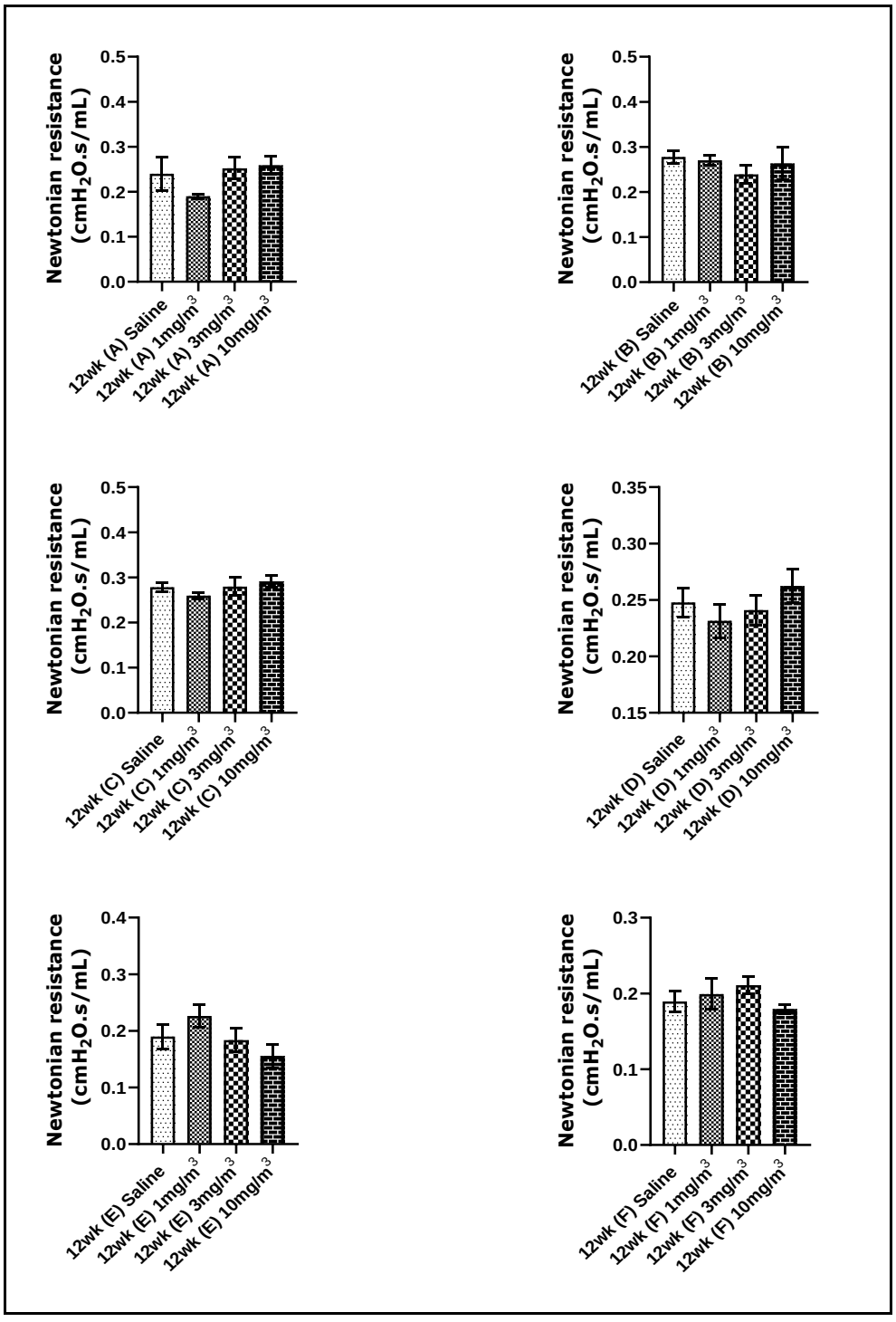


**Figure 26:** Bar graph showing the central airway resistance (baseline) of mice exposed to dust ($\leq PM_{10}$) for 12weeks. T-test; n=8; $P < 0.05$ *; $P < 0.01$ **; $P < 0.001$ ***; $P < 0.0001$ ****

- No statistically significant changes were observed at baseline upon 12 weeks of dust exposure across different dust types and doses.

## 2.20 Transpulmonary resistance at baseline (Rrs) – Chronic model

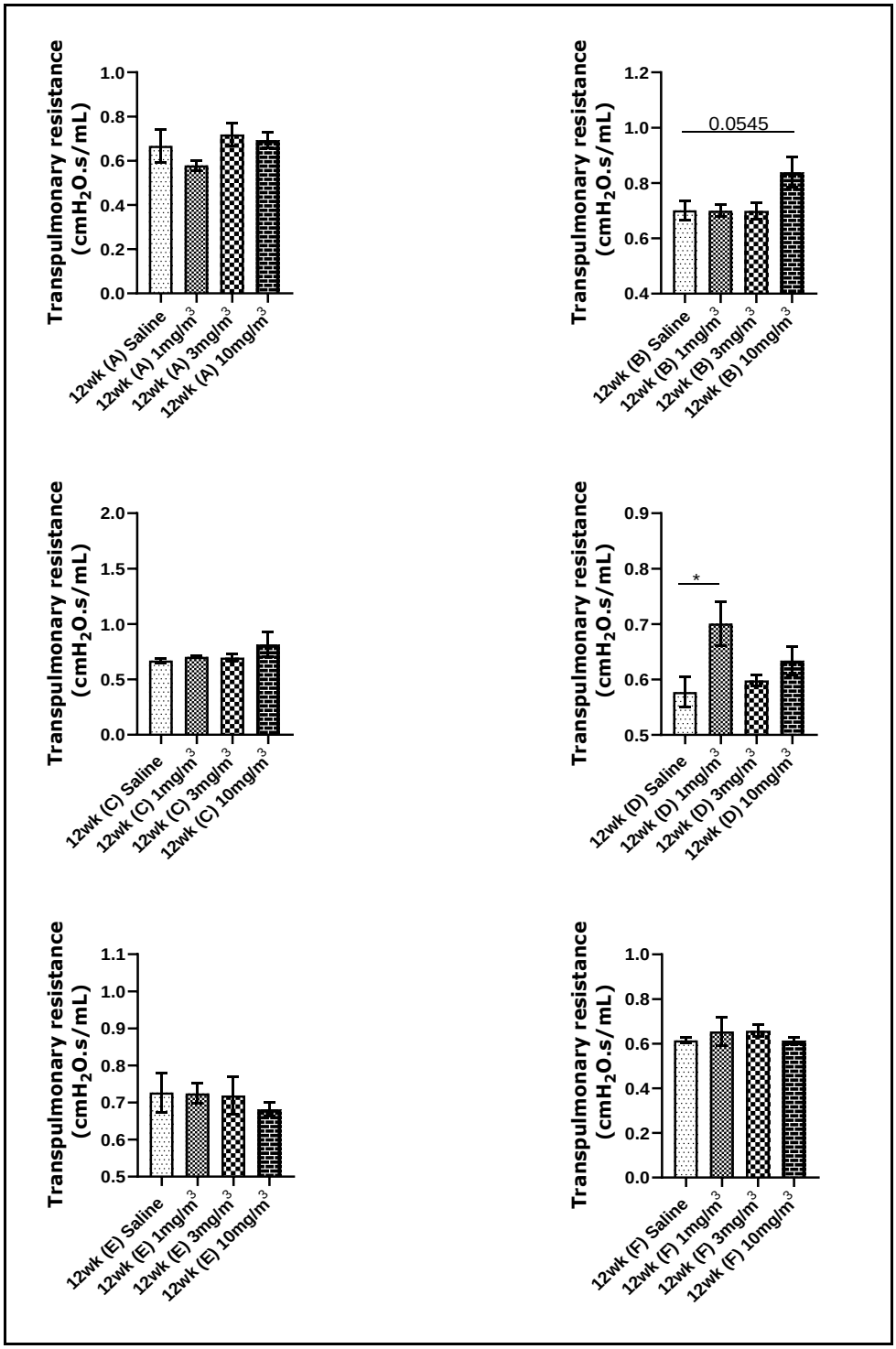


**Figure 27:** Bar graph showing the transpulmonary resistance (baseline) of mice exposed to dust (≤ $PM_{10}$) for 12weeks. T-test; n=8; P < 0.05 *; P < 0.01 **; P < 0.001 ***; P < 0.0001 ****

- Dust B & D showed increased Transpulmonary resistance at 10mg and 1mg/$m^3$. Rest of the samples did not affect the baseline Rrs.

## 2.21 Tissue damping at baseline (G) - Chronic model

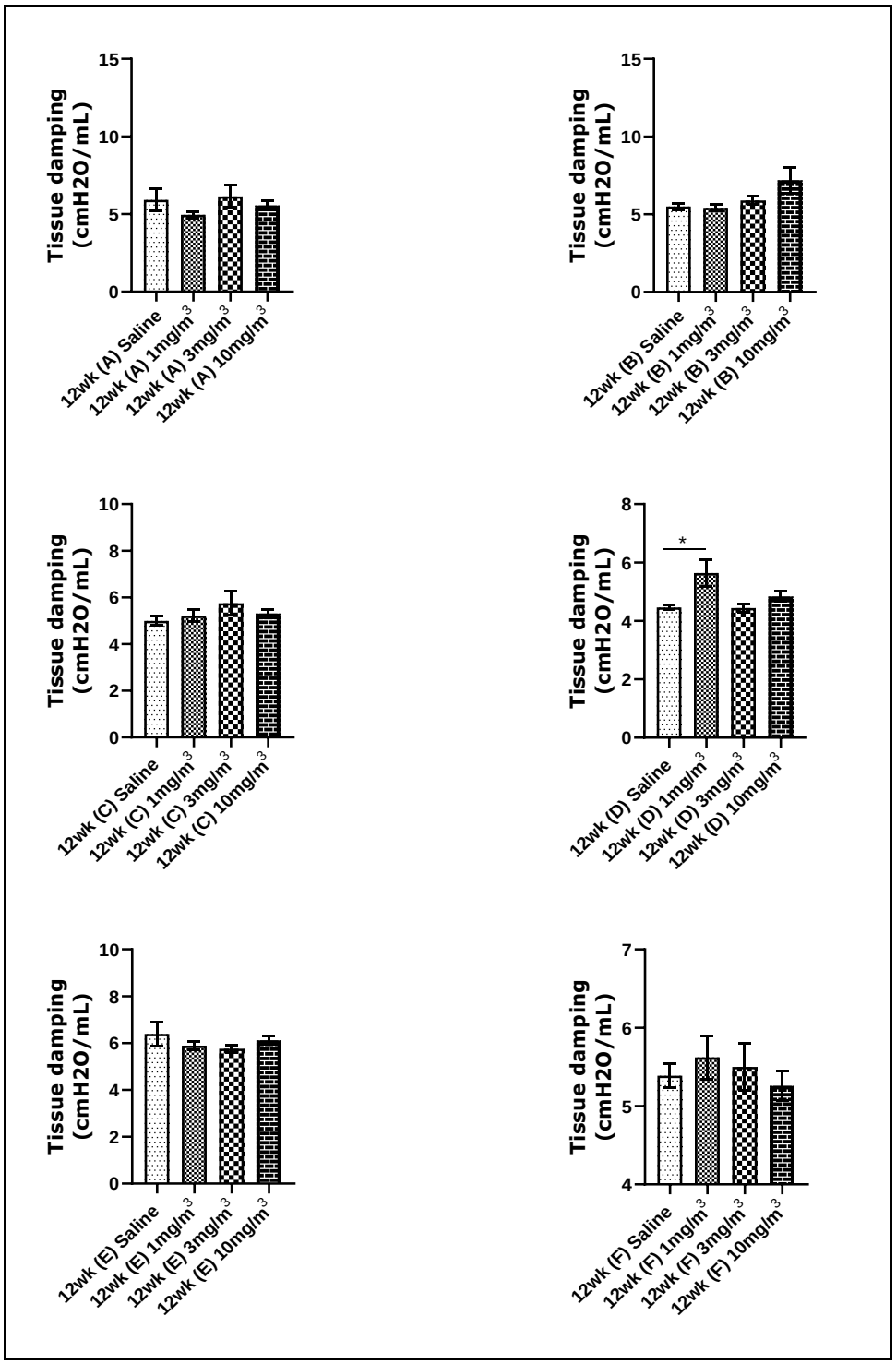


**Figure 28:** Bar graph showing the G (baseline) of mice exposed to dust (≤ $PM_{10}$) for 12weeks. T-test; n=8; P < 0.05 *; P < 0.01 **; P < 0.001 ***; P < 0.0001 ****

- Dust D showed an increase in Tissue damping at a lower dose. Rest of the samples did not affect the baseline G.

## 2.22 Tissue elastance at baseline (H) - Chronic model

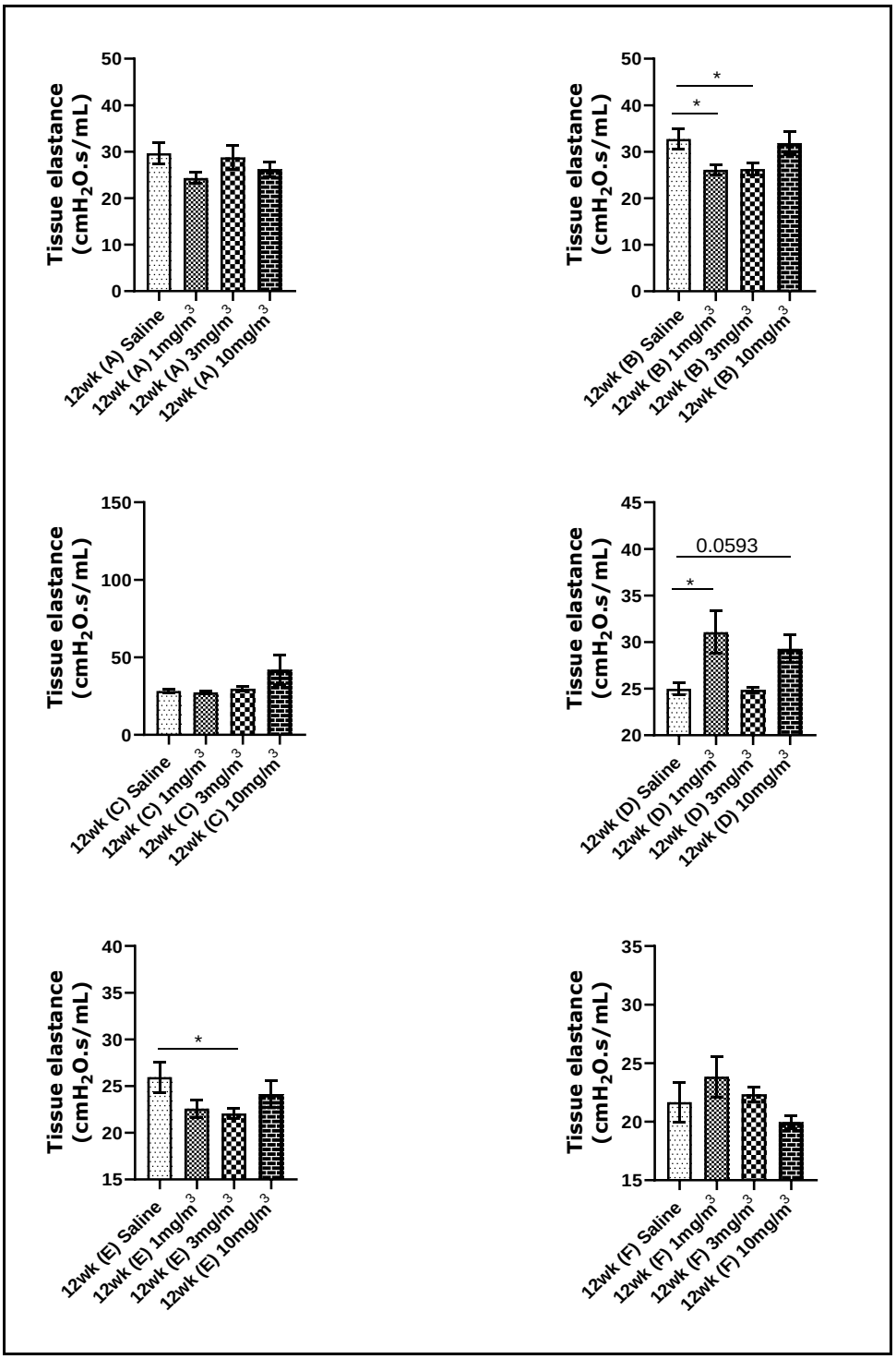


**Figure 29:** Bar graph showing the H (baseline) of mice exposed to dust (≤ $PM_{10}$) for 12weeks. T-test; n=8; P < 0.05 *; P < 0.01 **; P < 0.001 ***; P < 0.0001 ****

- Dust B and Dust D showed a decrease in Tissue elastance at lower doses i.e. 1mg & 3mg/$m^3$. Whereas Dust D was found to increase tissue elastance at lower and a higher dose (1mg & 10mg/$m^3$). Rest of the samples did not affect at baseline H.

## 2.33 Dynamic compliance at baseline (Crs) - Chronic model

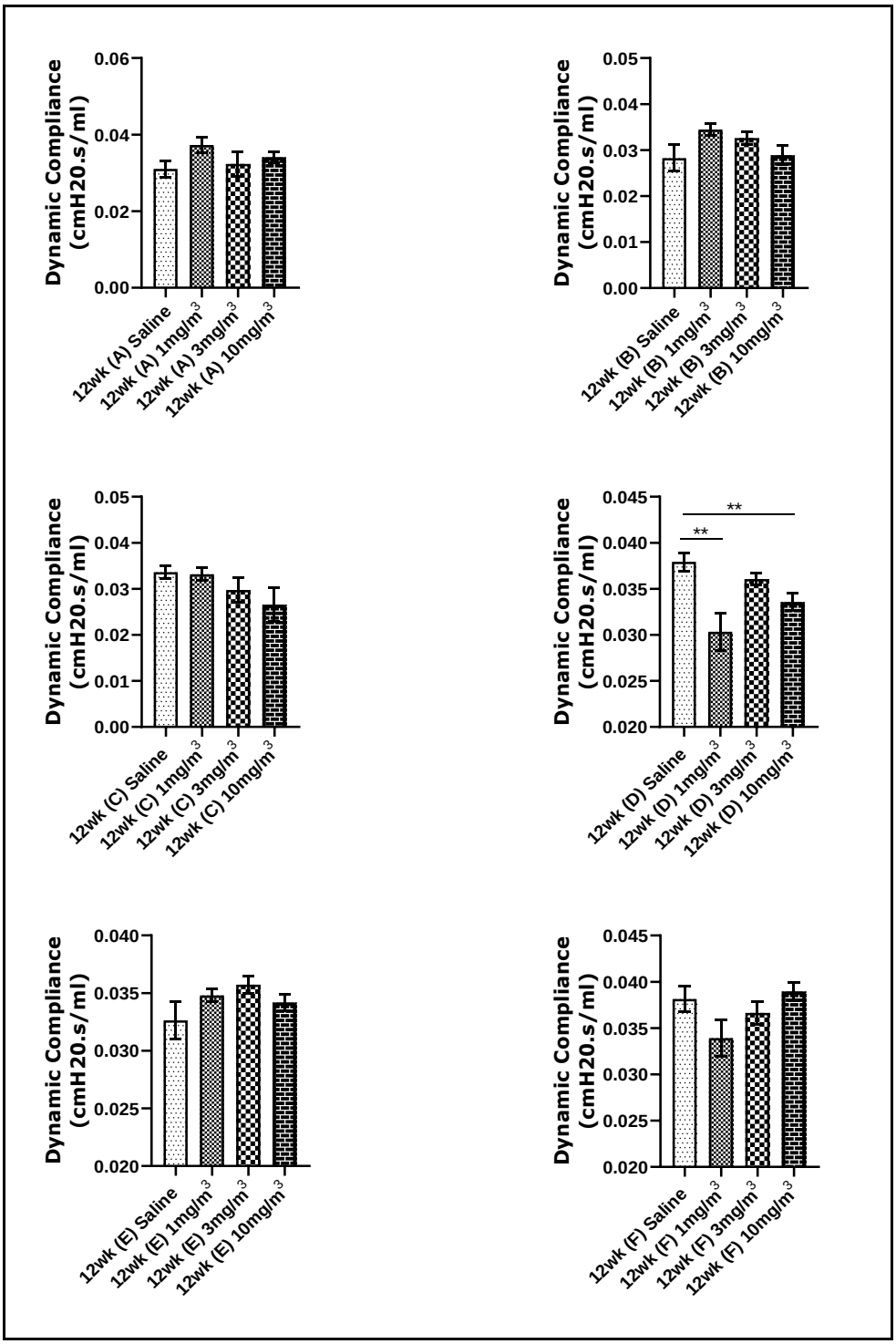


**Figure 30:** Bar graph showing the Crs (baseline) of mice exposed to dust (≤ $PM_{10}$) for 12weeks. T-test; n=8; P < 0.05 *; P < 0.01 **; P < 0.001 ***; P < 0.0001 ****

- Dust D was found to decrease lung compliance in all three tested doses, whereas rest of the samples did not affect the baseline Crs.

## 2.34 Dynamic elastance at baseline (Ers) - Chronic model

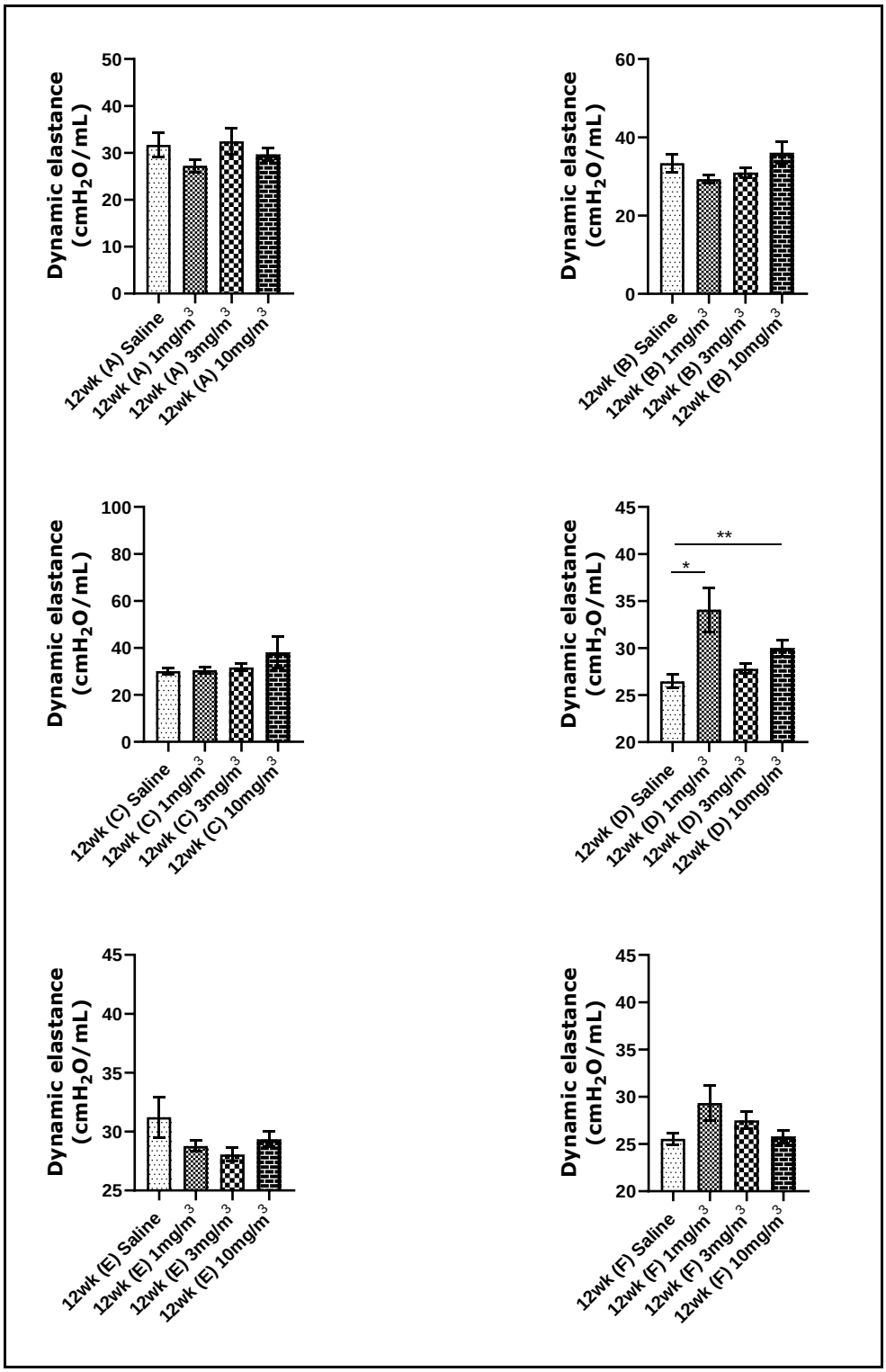


**Figure 31:** Bar graph showing the Ers (baseline) of mice exposed to dust (≤ $PM_{10}$) for 12weeks. T-test; n=8; P < 0.05 *; P < 0.01 **; P < 0.001 ***; P < 0.0001 ****

- Dust D was found to increase the Dynamic elastance, however other samples did not affect baseline Ers.

## 2.35 Inspiratory capacity (IC) - Chronic model

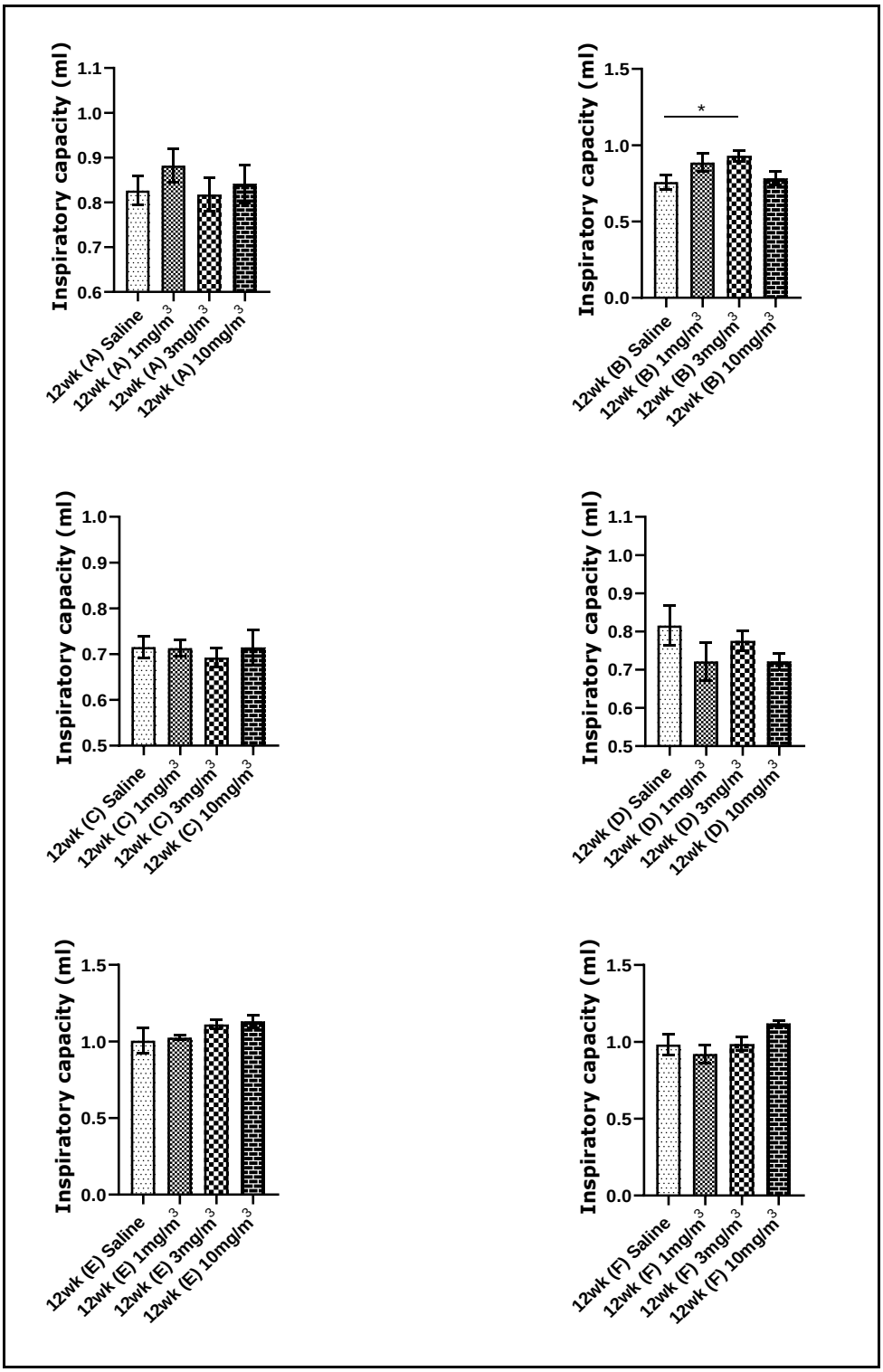


**Figure 32:** Bar graph showing the inspiratory capacity of mice exposed to dust (≤ $PM_{10}$) for 12weeks. T-test; n=8; $P < 0.05$ *; $P < 0.01$ **; $P < 0.001$ ***; $P < 0.0001$ ****

- Dust B induced an increase in Inspiratory capacity at lower doses (1mg & 3mg/$m^3$), however other samples did not affect IC.

## 2.36 Hysteresis - Chronic model

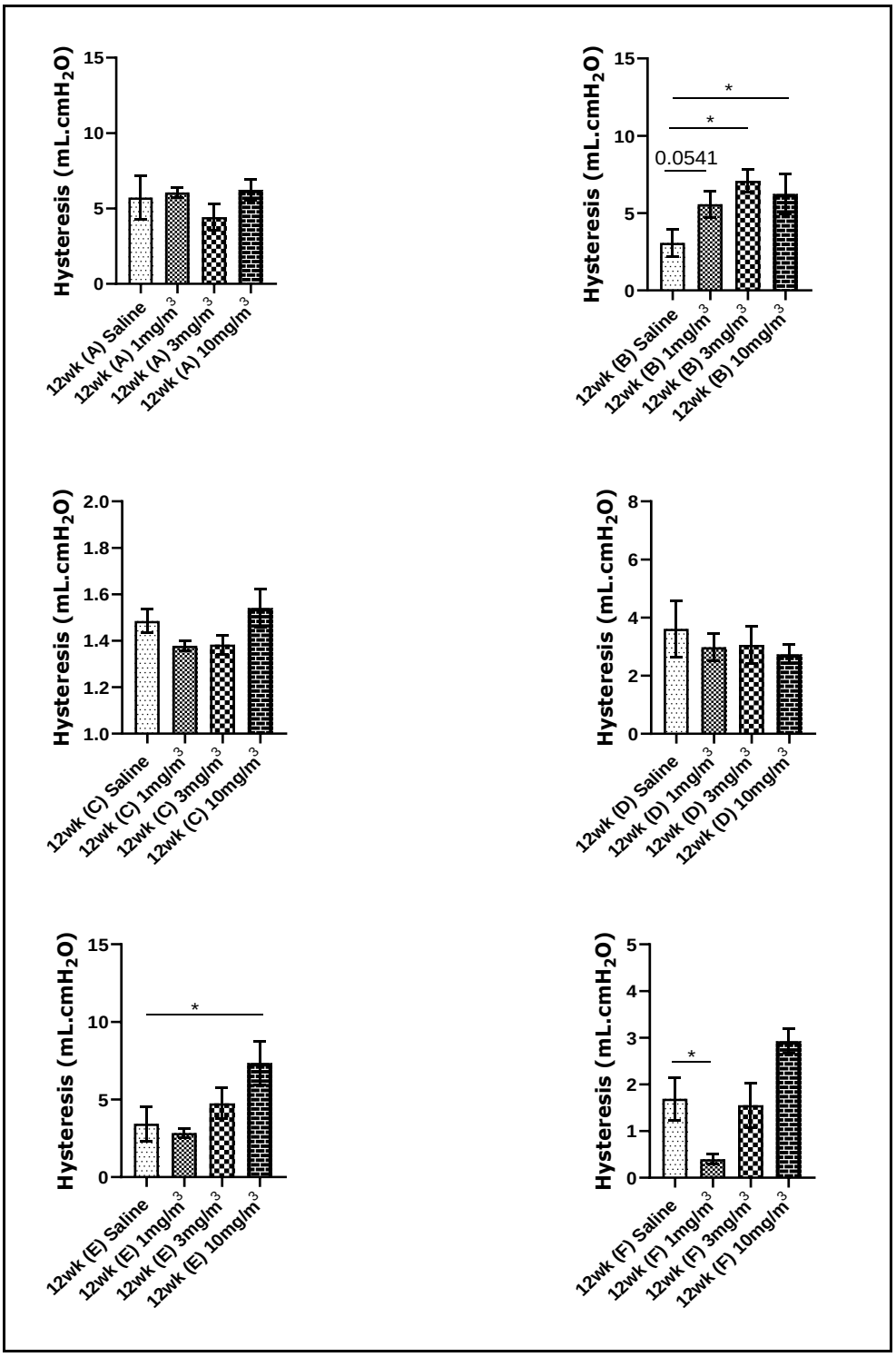


**Figure 33:** Bar graph showing the hysteresis of mice exposed to dust ($\leq PM_{10}$) for 12weeks. T-test; n=8; P < 0.05 *; P < 0.01 **; P < 0.001 ***; P < 0.0001 ****

- A dose-dependent increase in lung hysteresis was observed with Dust B, E & F. Other samples had no effect.

## 2.37 Lung compliance - Chronic model

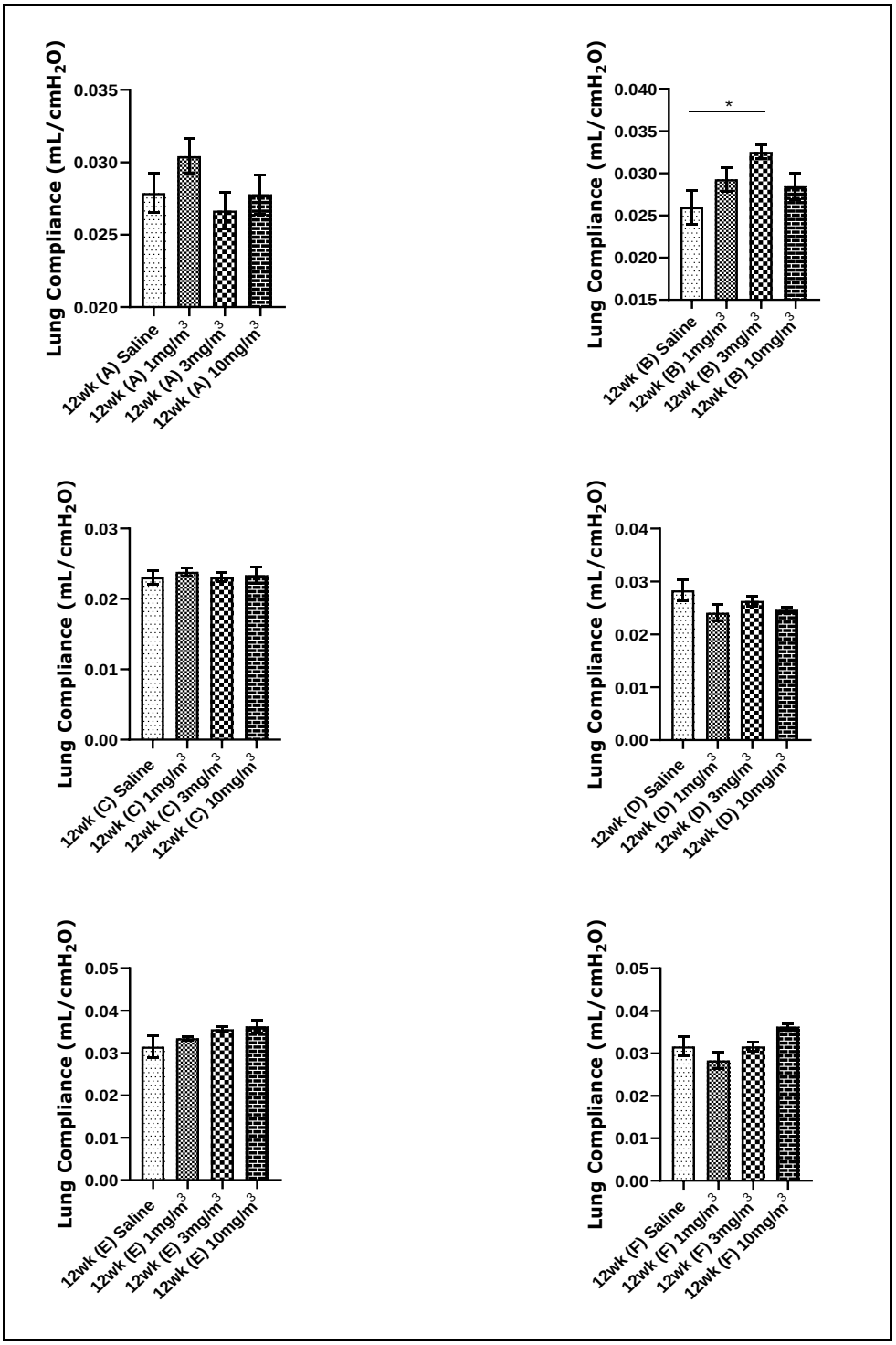


**Figure 34:** Bar graph showing the lung compliance of mice exposed to dust (≤ $PM_{10}$) for 12weeks. T-test; n=8; P < 0.05 *; P < 0.01 **; P < 0.001 ***; P < 0.0001 ****

- 12 weeks of dust exposure had no effect on lung compliance.

## 2.38 Pressure-volume loops (PV loops) – Chronic model

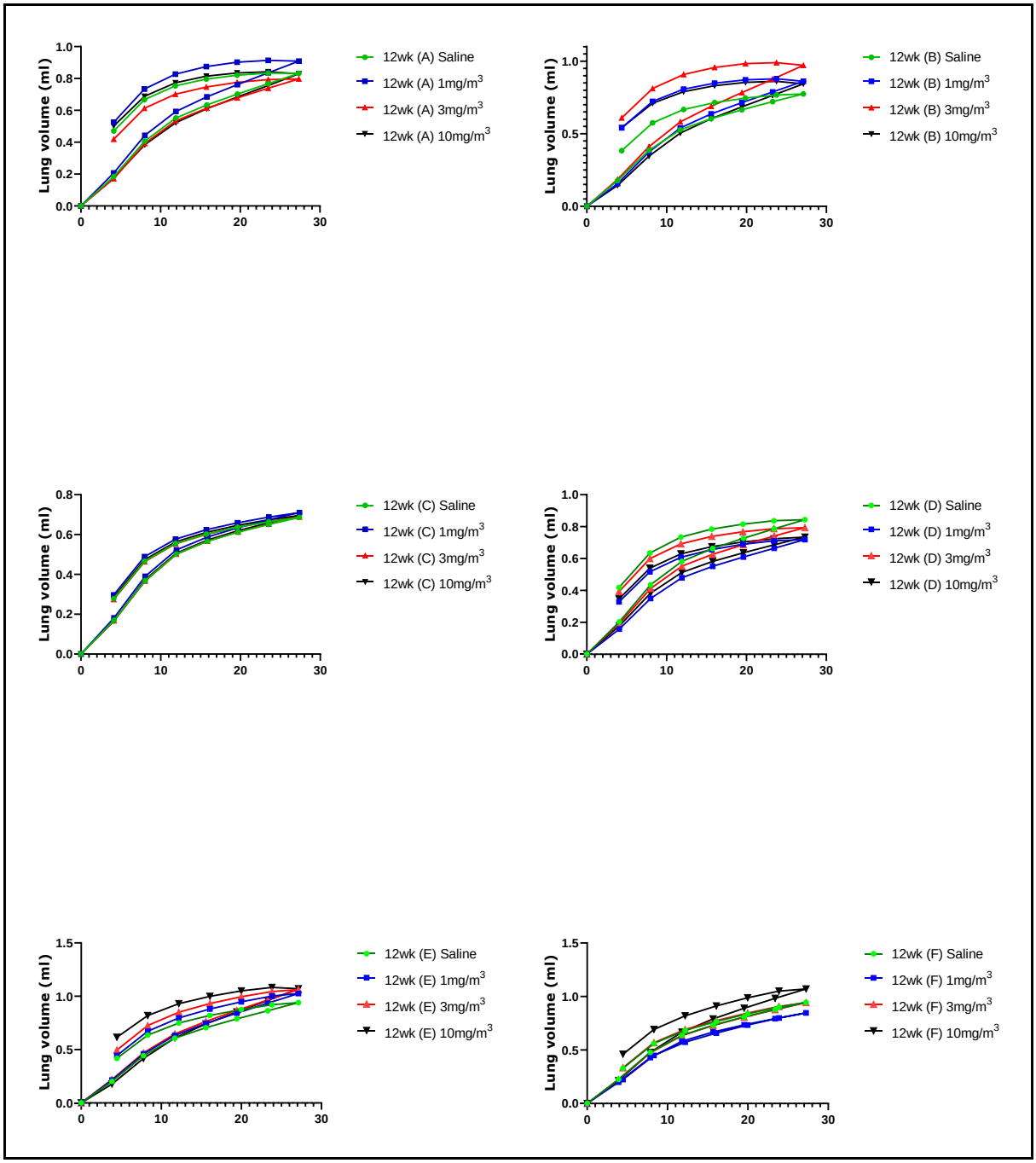


**Figure 35:** Graph showing the pressure volume curves of mice exposed to dust (≤ $PM_{10}$) for 12weeks. T-test; n=8; P < 0.05 *; P < 0.01 **; P < 0.001 ***; P < 0.0001 ****

- A shift towards upside represents the emphysema; the greater the shift greater the alveoli damage; A shift towards the bottom represents the fibrosis; the greater the shift greater the lung fibrosis
- Interestingly, all the three tested doses of Dust B & E showed PV loop shift above the saline, whereas sample D induced a shift towards the bottom.

## 2.39 Airway-Hyperresponsiveness (AHR) – Central airways resistance (Rn)

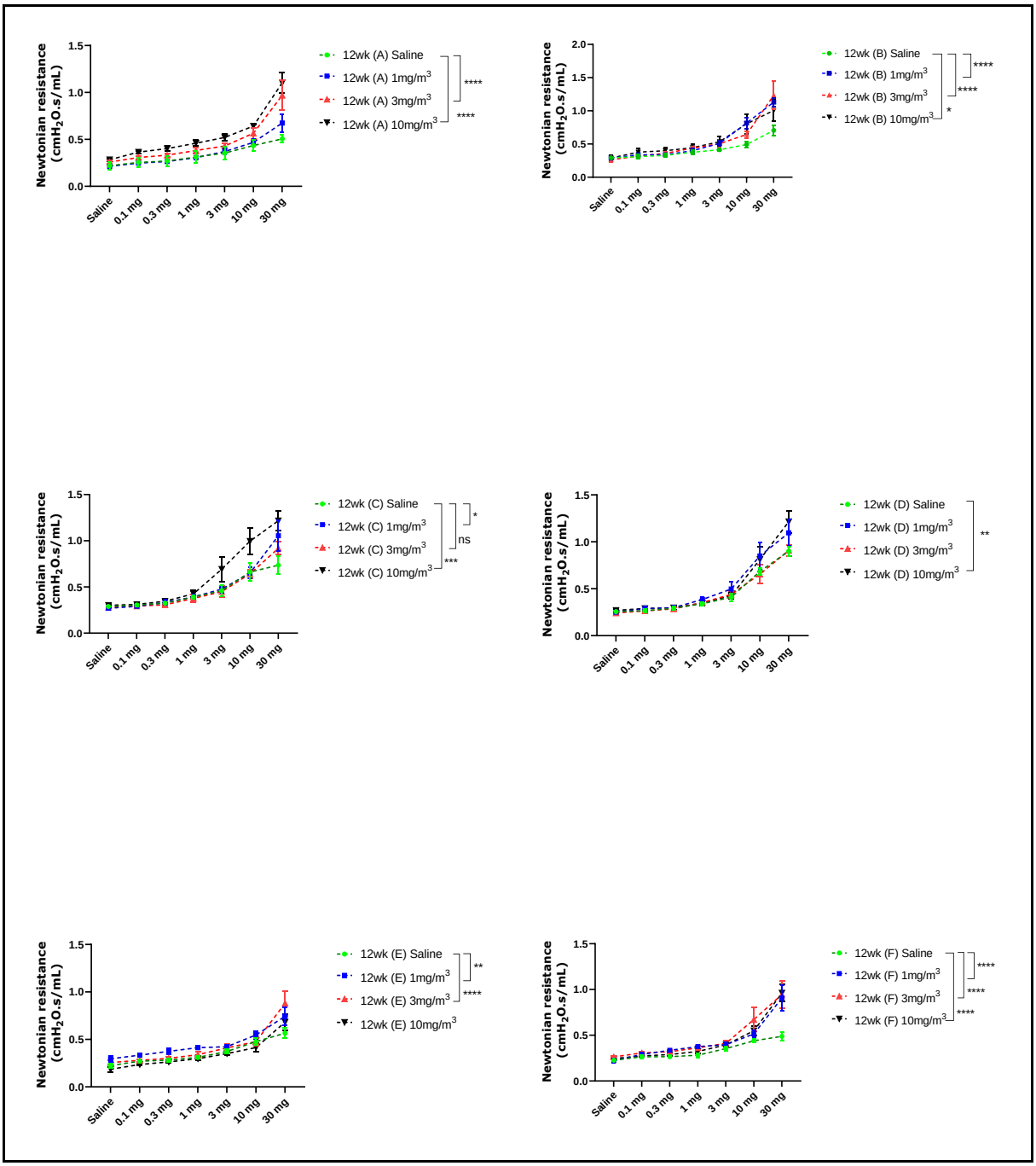


**Figure 36:** Graph showing the dose dependent central airways resistance in response to increasing concentrations of Methacholine for mice exposed to dust (≤ $PM_{10}$) for 12weeks. 2-way anova; n=8; $P < 0.05$ *; $P < 0.01$ **; $P < 0.001$ ***; $P < 0.0001$ ****

- Irrespective of dust type all the tested doses showed increased central airway resistance compared to saline within 12 weeks of dust exposure.
- Compared to 2wk, 12wk models showed lesser central airways resistance upon challenging with increasing concentration of Methacholine.

## 2.40 Airway-Hyperresponsiveness (AHR) - Transplumonary resistance (Rrs)

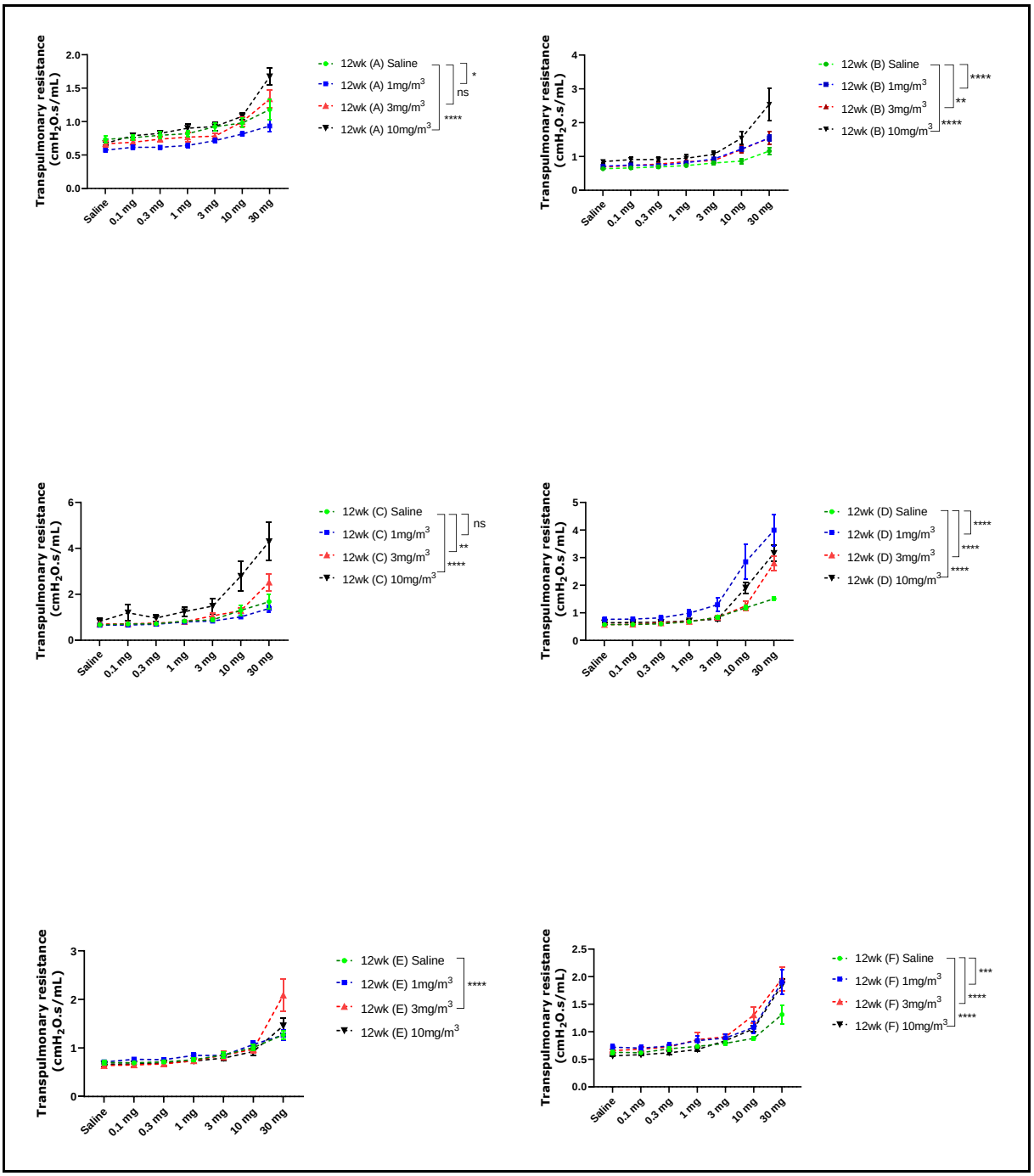


**Figure 37:** Graph showing the dose dependent transpulmonary resistance in response to increasing concentrations of Methacholine for mice exposed to dust (≤ $PM_{10}$) for 12weeks. 2-way anova; n=8; P < 0.05 *; P < 0.01 **; P < 0.001 ***; P < 0.0001 ****

- Dust A, B & C showed a dose-dependent increase in Transplumonary resistance, however Dust D, E, and F shown higher resistance values for lower doses compared to 10mg/$m^3$

## 2.41 Airway-Hyperresponsiveness (AHR) – Tissue damping (G)

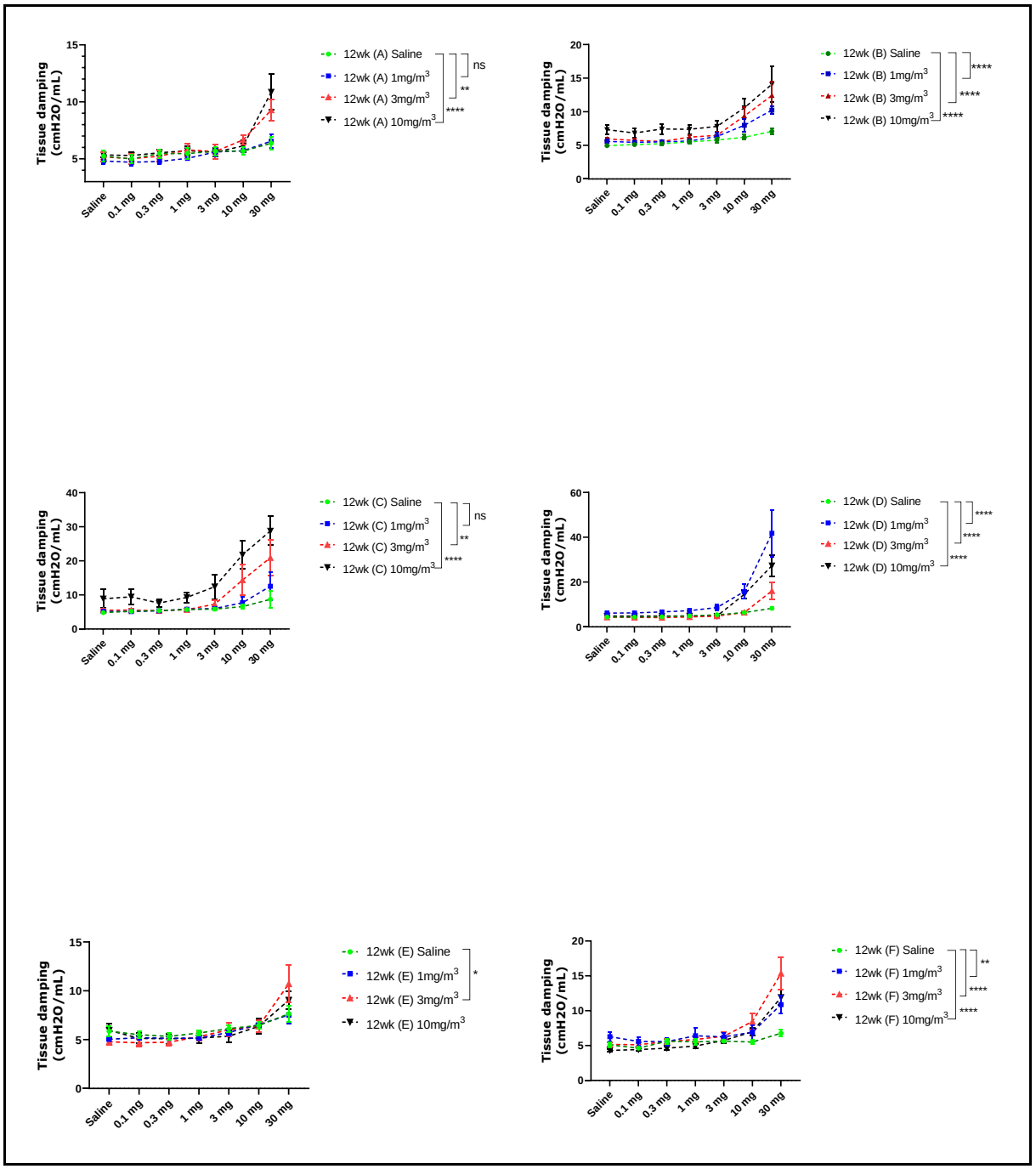


**Figure 38:** Graph showing the dose dependent response of G to increasing concentrations of Methacholine for mice exposed to dust (≤ $PM_{10}$) for 12weeks. 2-way anova; n=8; P < 0.05 *; P < 0.01 **; P < 0.001 ***; P < 0.0001 ****

- Dust A, B & C showed a dose-dependent increase in Tissue damping, however Dust D, E, and F shown higher response to lower doses compared to 10mg/$m^3$

## 2.42 Airway-Hyperresponsiveness (AHR) – Tissue elastance (H)

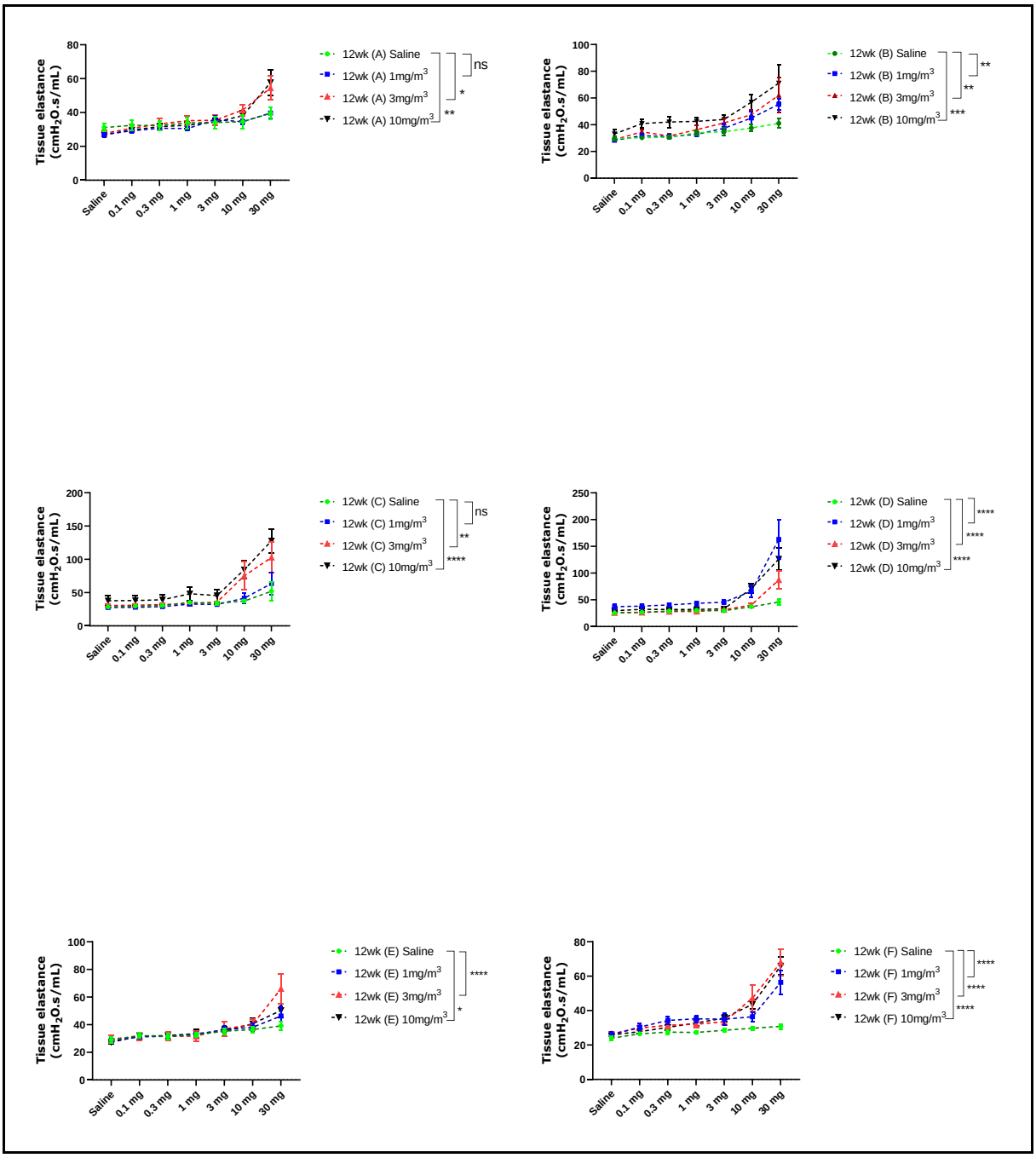


**Figure 39:** Graph showing the dose dependent response of H to increasing concentrations of Methacholine for mice exposed to dust (≤ $PM_{10}$) for 12weeks. 2-way anova; n=8; P < 0.05 *; P < 0.01 **; P < 0.001 ***; P < 0.0001 ****

- All six samples showed an increase in Tissue elastance in all tested doses.

## 2.43 Airway-Hyperresponsiveness (AHR) – Dynamic compliance (Crs)

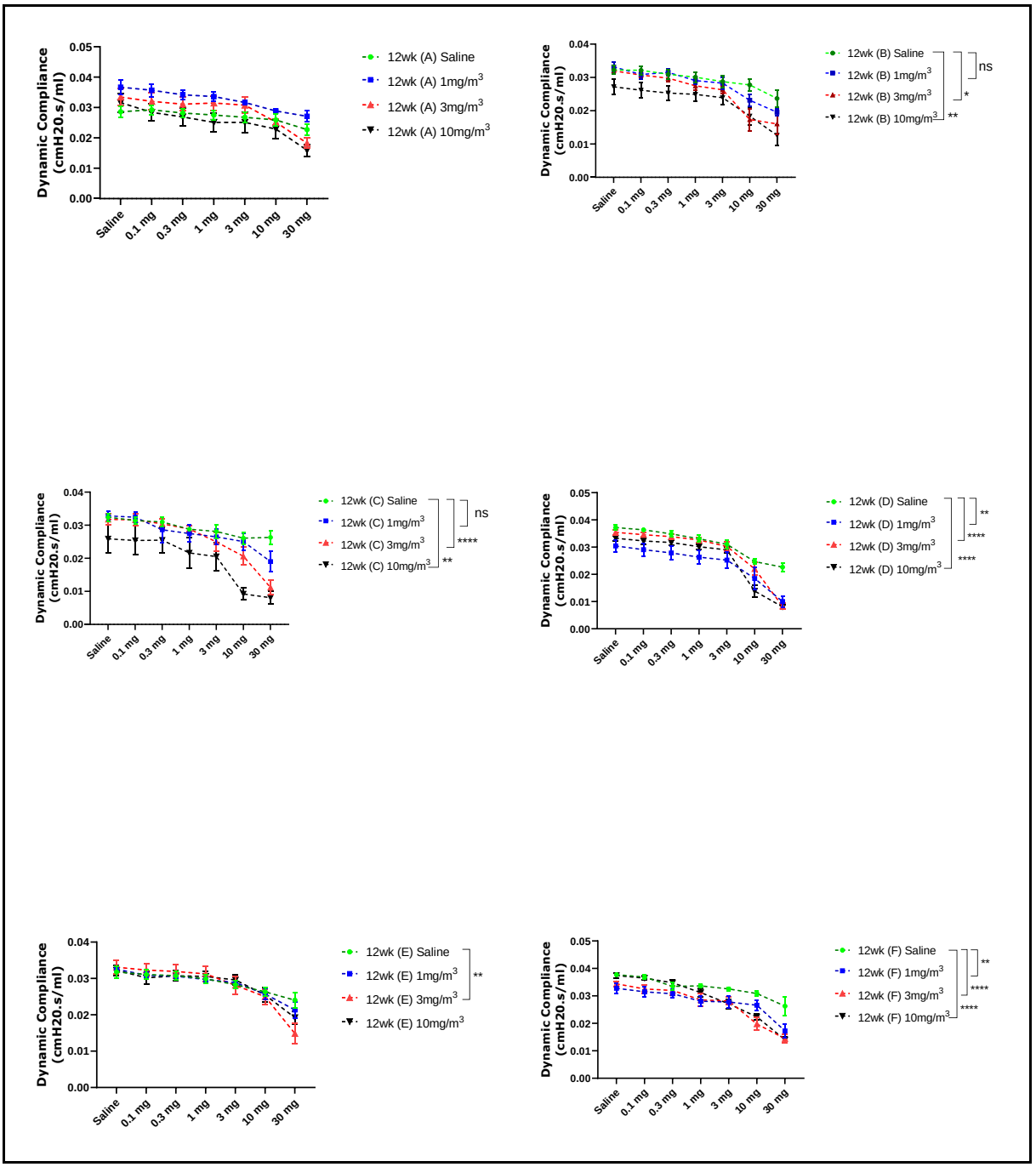


**Figure 40:** Graph showing the dose dependent response of Crs to increasing concentrations of Methacholine for mice exposed to dust (≤ PM10) for 12weeks. 2-way anova; n=8; $P < 0.05$ *; $P < 0.01$ **; $P < 0.001$ ***; $P < 0.0001$ ****

- All dust samples, except Dust A showed a decrease in Dynamic compliance compared to saline in all three tested doses.

## 2.44 Airway-Hyperresponsiveness (AHR) – Dynamic elastance (Ers)

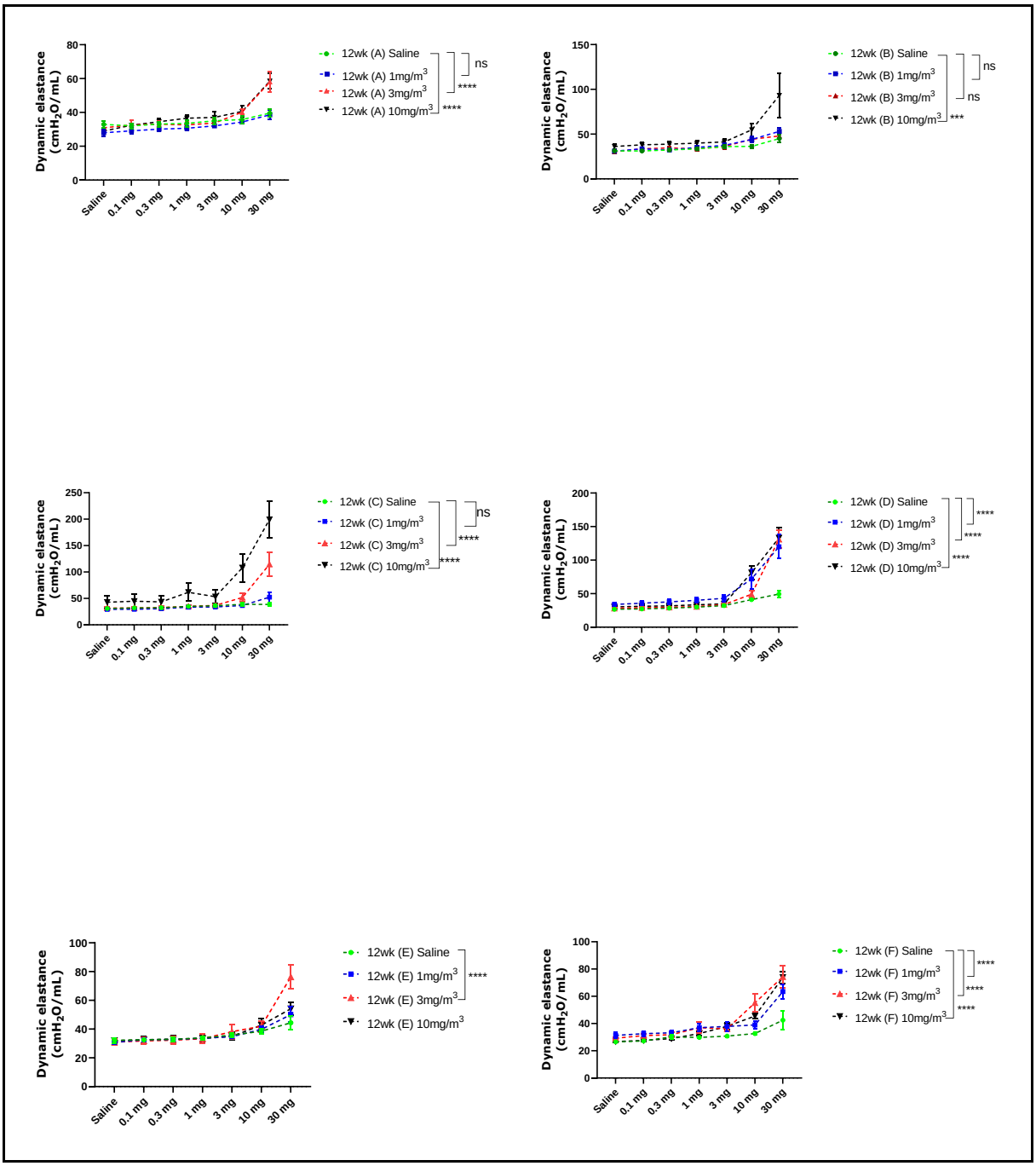


**Figure 41:** Graph showing the dose dependent response of Ers to increasing concentrations of Methacholine for mice exposed to dust (≤ $PM_{10}$) for 12weeks. 2-way anova; n=8; $P < 0.05$ *; $P < 0.01$ **; $P < 0.001$ ***; $P < 0.0001$ ****

- All the tested samples have shown increased Dyanamic elastance compared to saline.

## 2.45 Lung inflammation – Acute mode

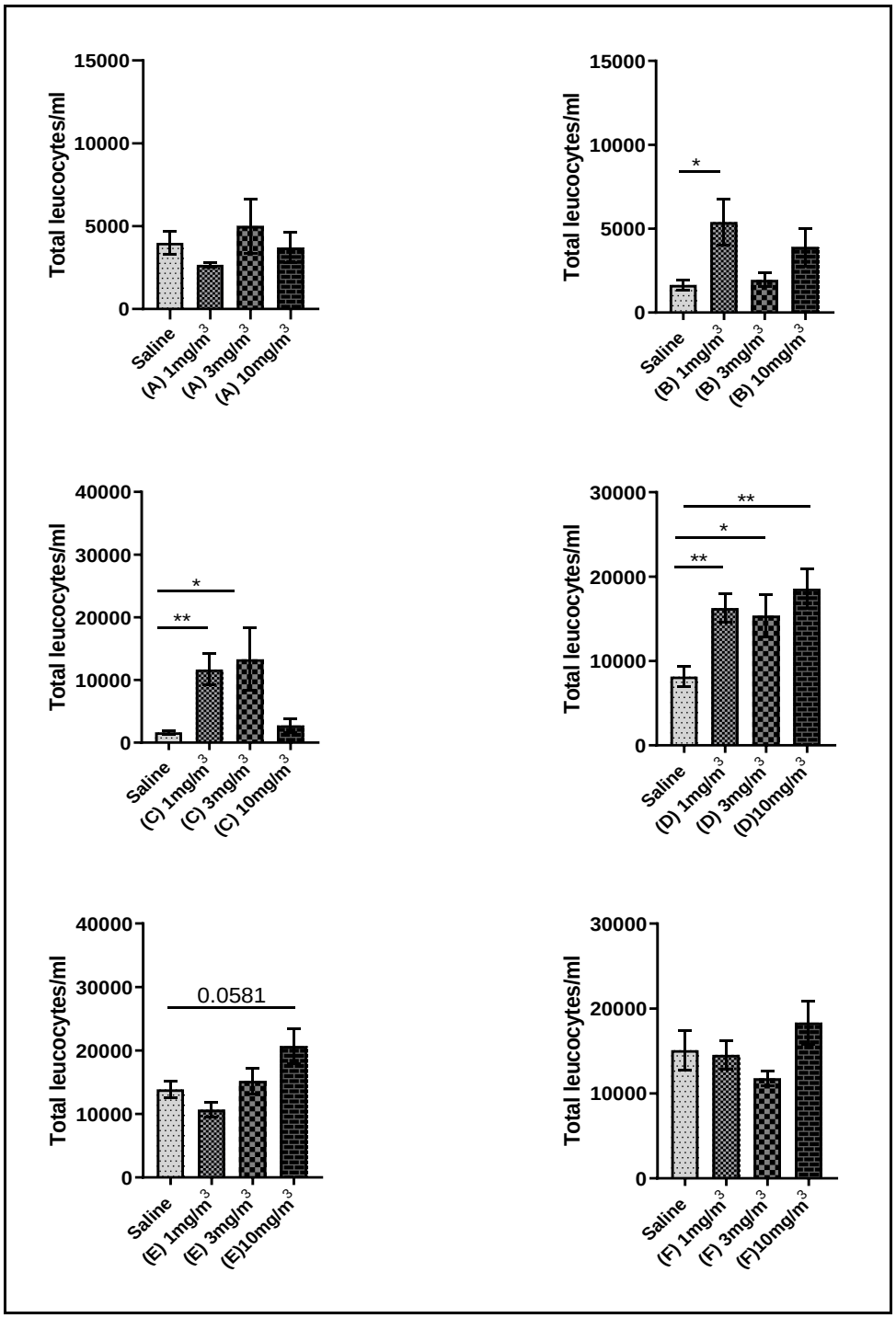


**Figure 42:** Bar graph showing the total inflammatory cells in BALF collected from mice exposed to 2wk of **dust** (≤ $PM_{10}$). T-test; n=6; P < 0.05 *; P < 0.01 **; P < 0.001 ***; P < 0.0001 ****

- Increased WBC counts in BALF was observed with 1mg/m$^3$ of Dust B and C compared to 10mg/m$^3$
- Further, a dose-dependent increase was observed in the mice treated with Dust D & E.
- Dust A and F had no statistically significant increase in total inflammatory cells

## 2.46 Total macrophages – 2wk model

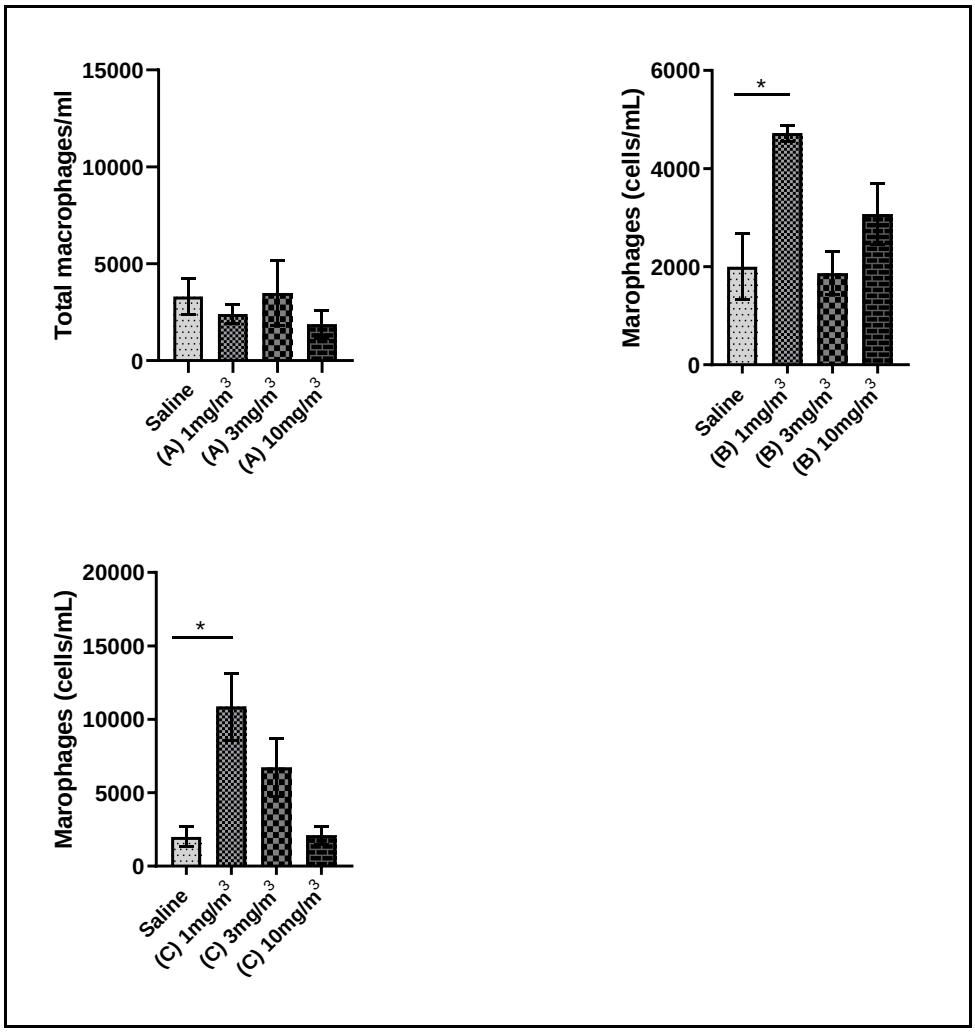


**Figure 43:** Bar graph showing the total macrophages in BALF collected from mice exposed to 2wk of **dust** ($\leq PM_{10}$). T-test; n=6; $P < 0.05$ *; $P < 0.01$ **; $P < 0.001$ ***; $P < 0.0001$ ****

- The microscopic observations showed dust-laden macrophages as a major type of cells associated with dust.
- Interestingly, microscopic counts have shown that the mice exposed to lower concentrations of dust i.e. $1mg/m^3$ to recruit a higher macrophage population compared to higher doses.

## 2.47 Total lymphocytes - Acute model

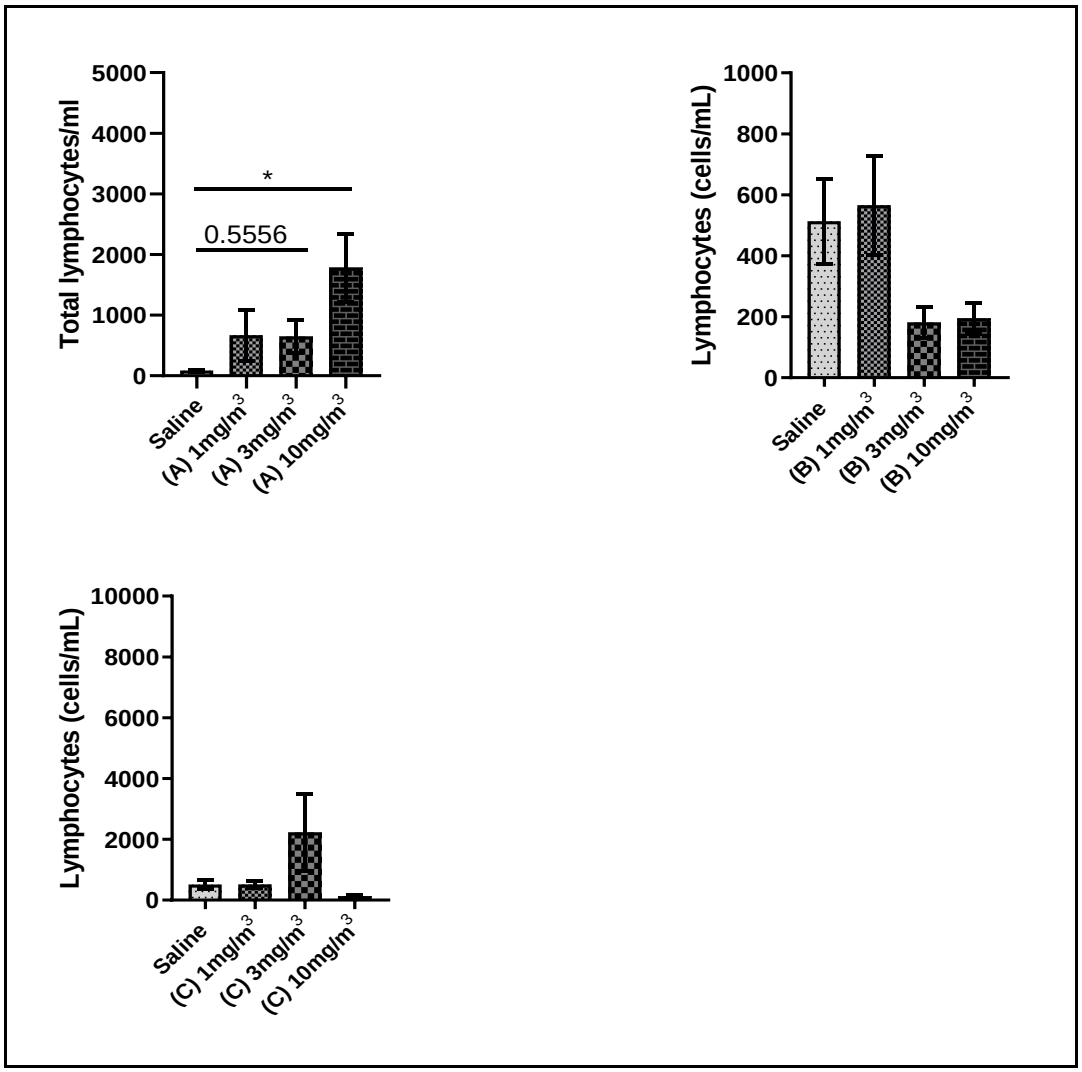


**Figure 44:** Bar graph showing the total lymphocytes in BALF collected from mice exposed to 2wk of **dust** (≤ $PM^{10}$). T-test; n=6; P < 0.05 *; P < 0.01 **; P < 0.001 ***; P < 0.0001 ****

- Mice exposed to Dust A shown a dose-dependent increase in the influx of lymphocytes into the lungs. Where Dust B and C showed a vice vesa effect.

**2.48 Total neutrophils – Acute model**

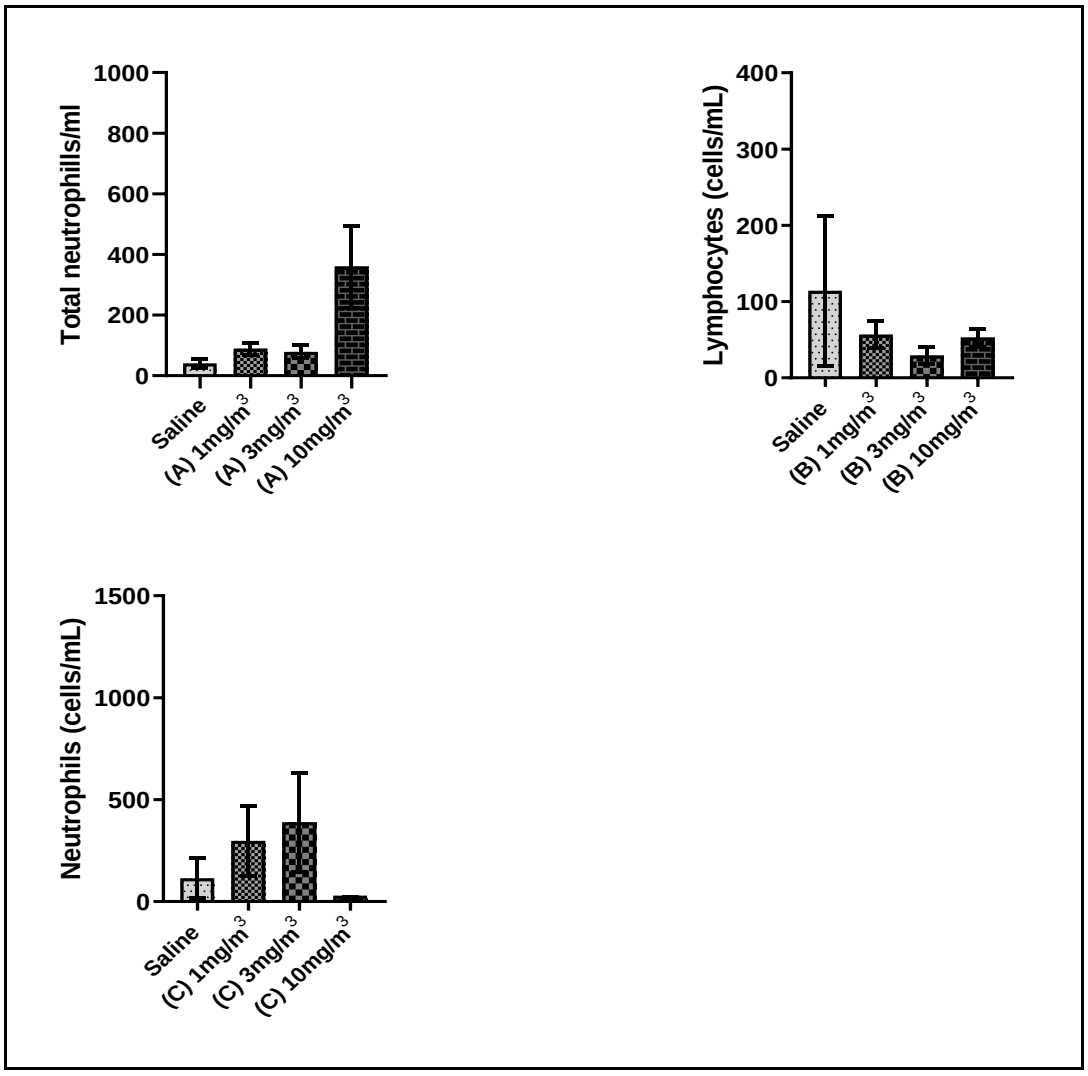


**Figure 45:** Bar graph showing the total neutrophils in BALF collected from mice exposed to 2wk of **dust** (≤ $PM_{10}$). T-test; n=6; P < 0.05 *; P < 0.01 **; P < 0.001 ***; P < 0.0001 ****

## 2.49 Lung inflammation – Chronic exposure (12wk)

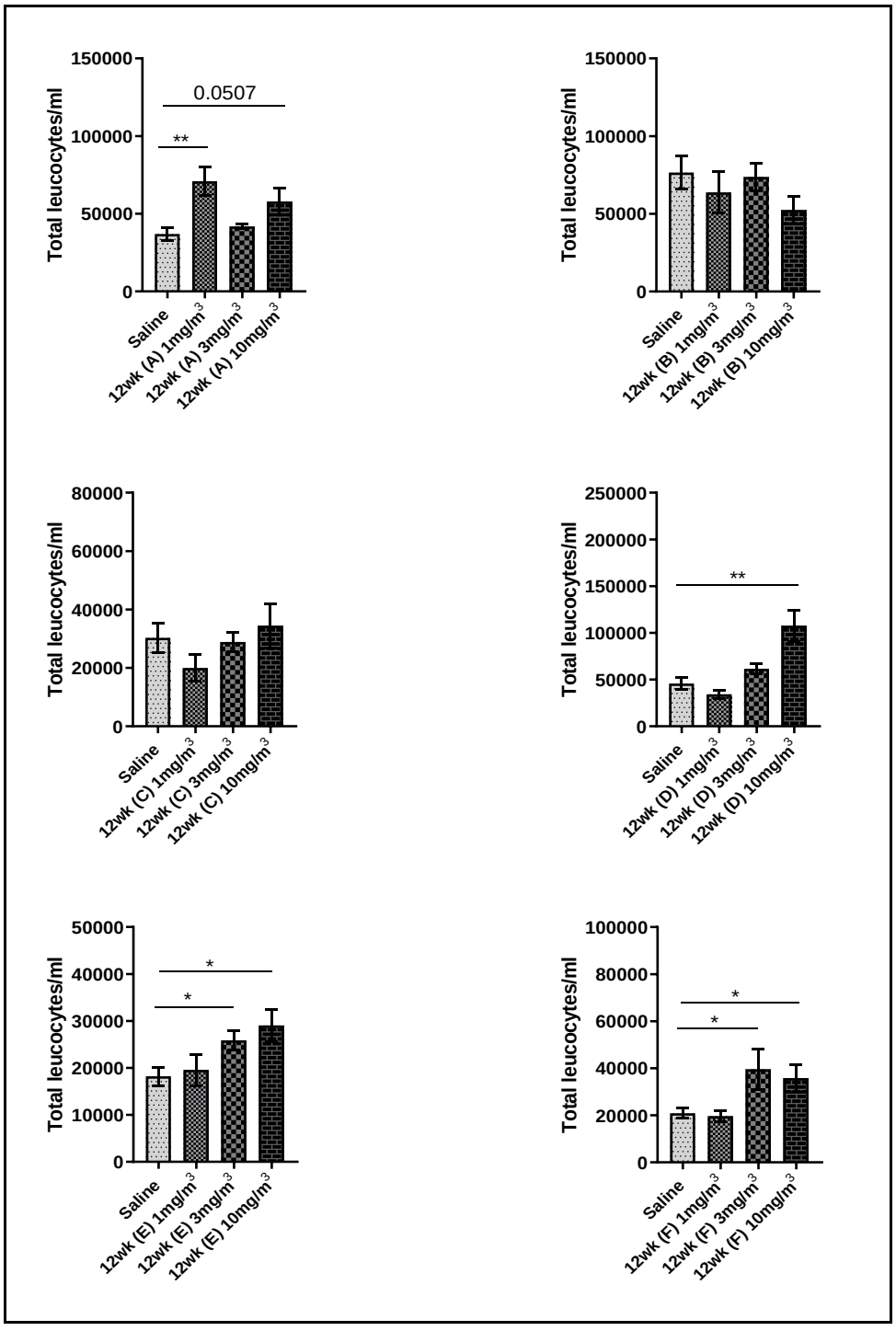


**Figure 46:** Bar graph showing the total inflammatory cells in BALF collected from mice exposed to 12wk of **dust** (≤ $PM_{10}$). T-test; n=8; P < 0.05 *; P < 0.01 **; P < 0.001 ***; P < 0.0001 ****

- Increased leucoyte population in BALF was observed in mice exposed to higher concentrations of Dust A, D, E, and F. No statistically significant numbers were observed in mice exposed to Dust B and C.

## 2.50 Total Macrophages - Chronic model

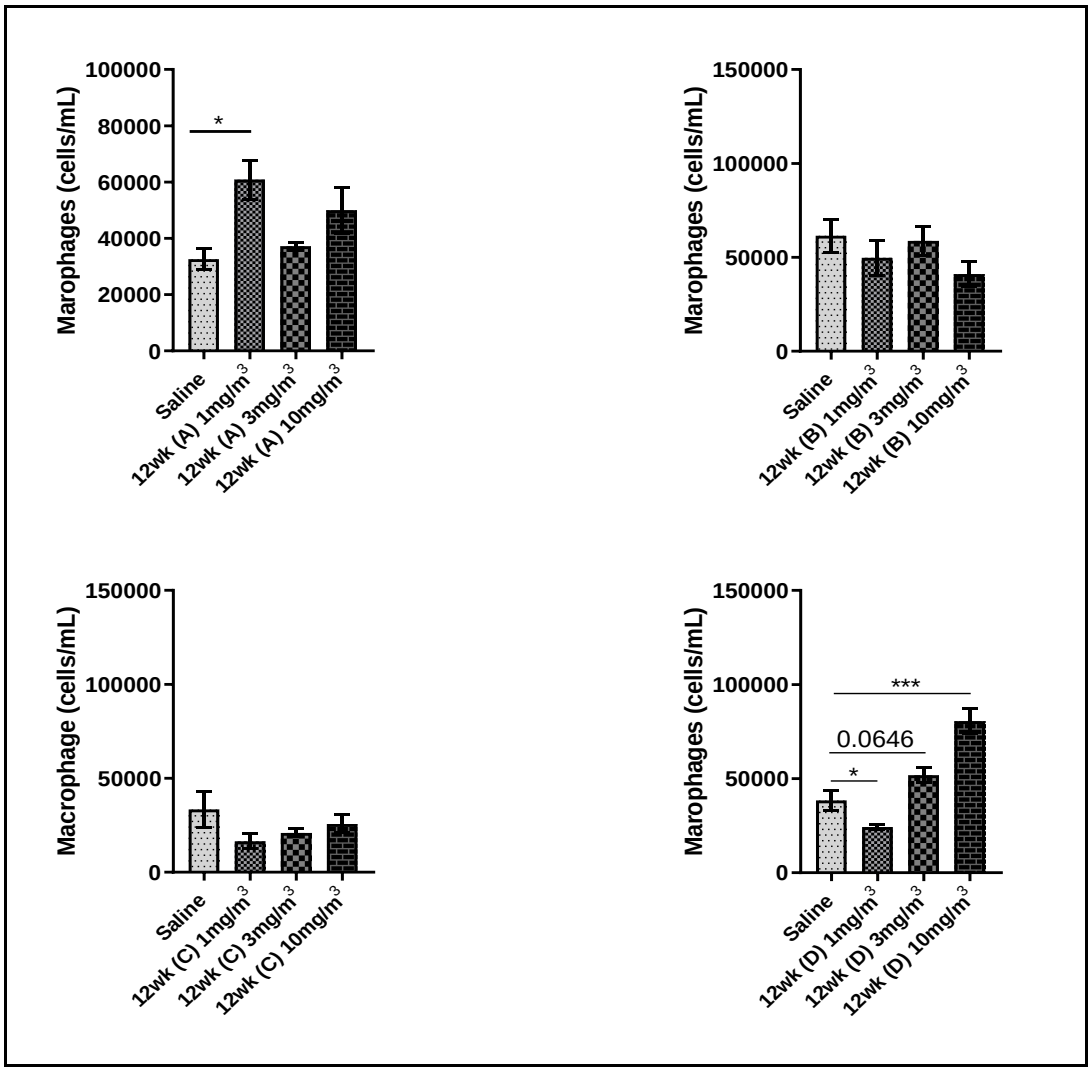


**Figure 47:** Bar graph showing the total macrophages in BALF collected from mice exposed to 12wk of **dust** (≤ $PM_{10}$). T-test; n=8; P < 0.05 *; P < 0.01 **; P < 0.001 ***; P < 0.0001 ****

- Similar to the 2wk model, macrophages were the major cell type observed in chronic exposure in all dust samples.
- Dust D showed an increased influx of macrophages at higher concentrations, however, the B and C showed a decreased trend of macrophage number compared to saline.

## 2.51 Total lymphocytes – Chronic model

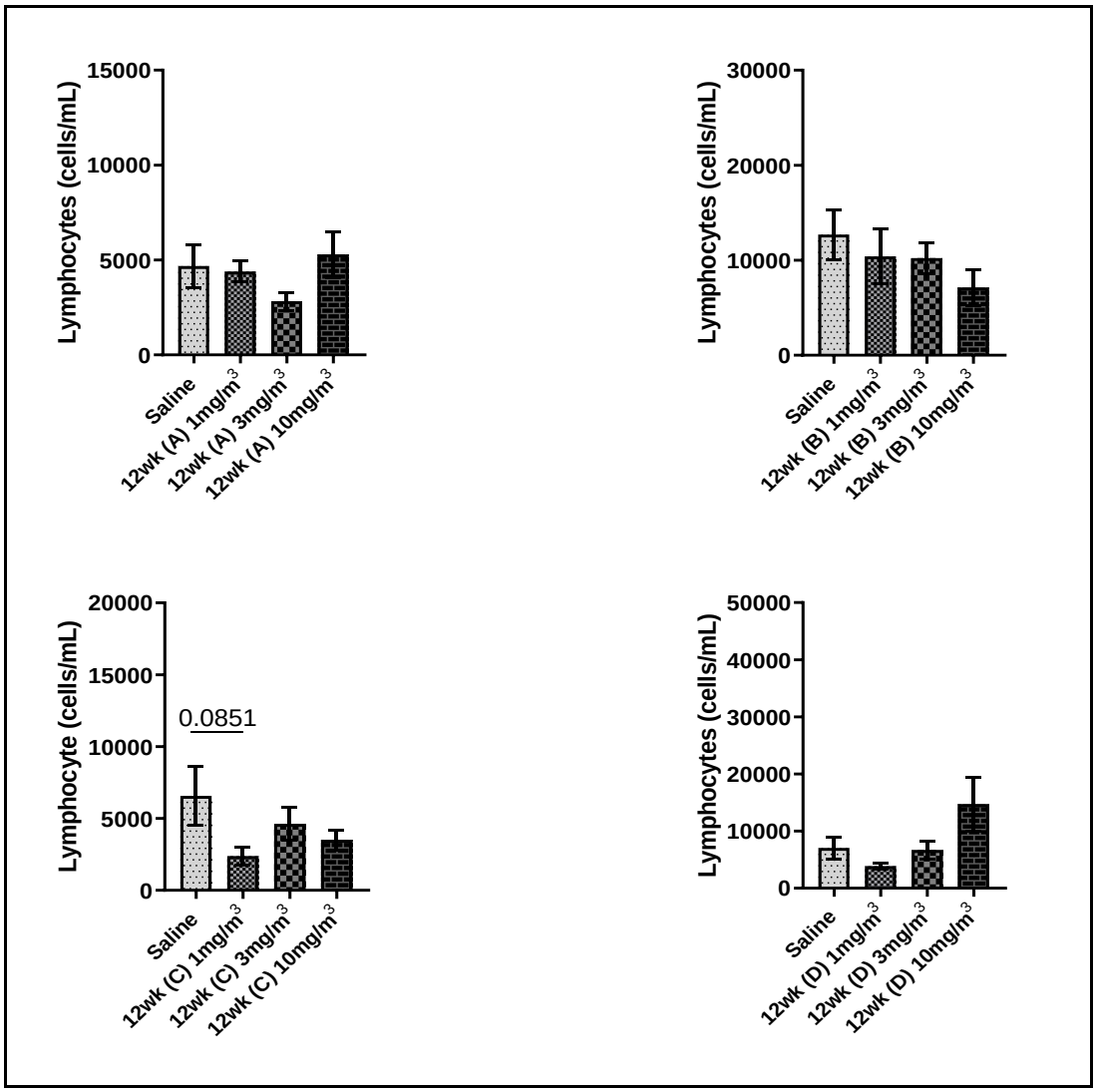


**Figure 49:** Bar graph showing the total lymphocytes in BALF collected from mice exposed to 12wk of **dust** (≤ $PM_{10}$). T-test; n=8; P < 0.05 *; P < 0.01 **; P < 0.001 ***; P < 0.0001 ****

## 2.52 Total neutrophils

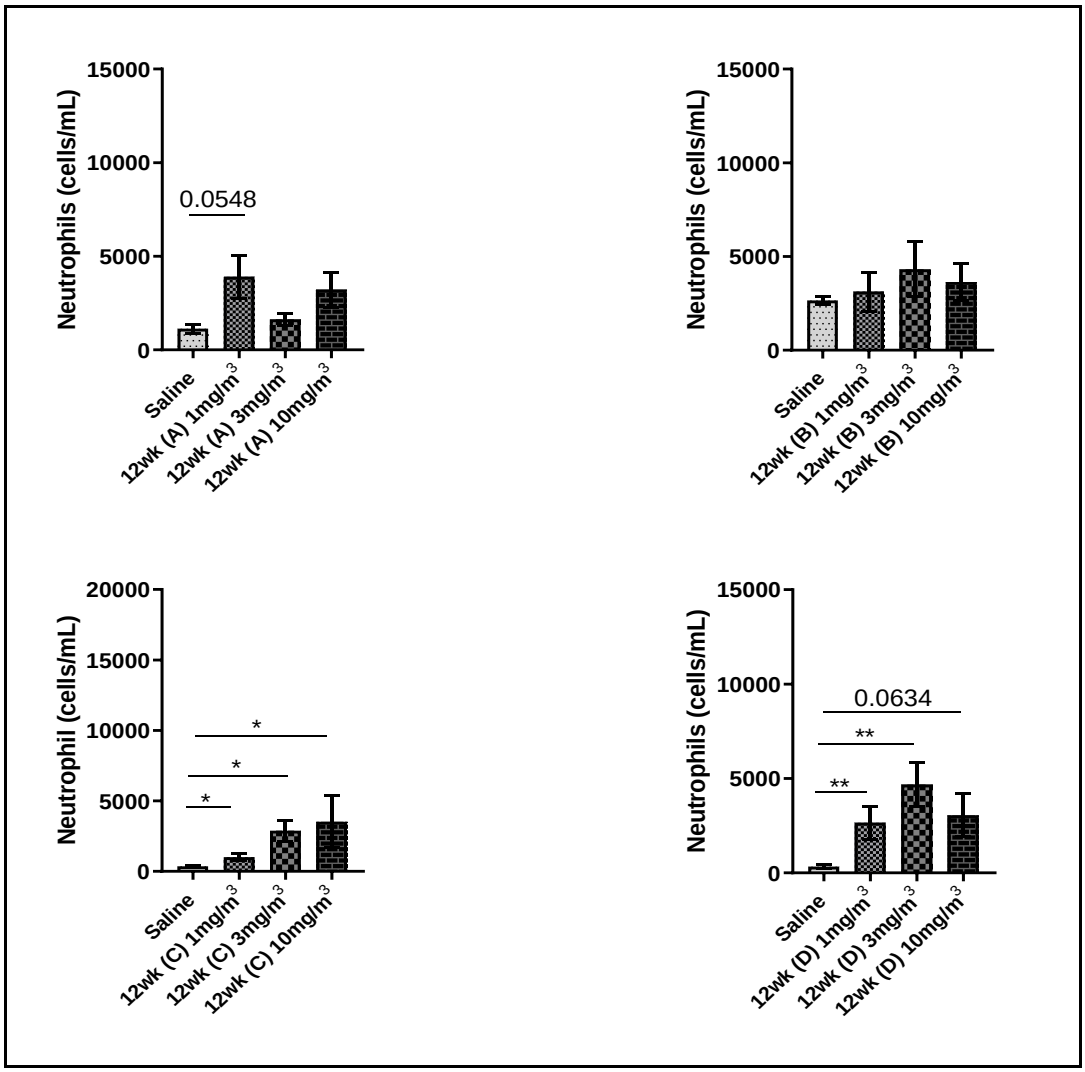


**Figure 50:** Bar graph showing the total neutrophils in BALF collected from mice exposed to 12wk of **dust** (≤ $PM_{10}$). T-test; n=8; P < 0.05 *; P < 0.01 **; P < 0.001 ***; P < 0.0001 ****

- Dust C and D showed an increased influx of neutrophils with increased concentrations of dust.

## 2.53 Lung histology – Chronic exposure

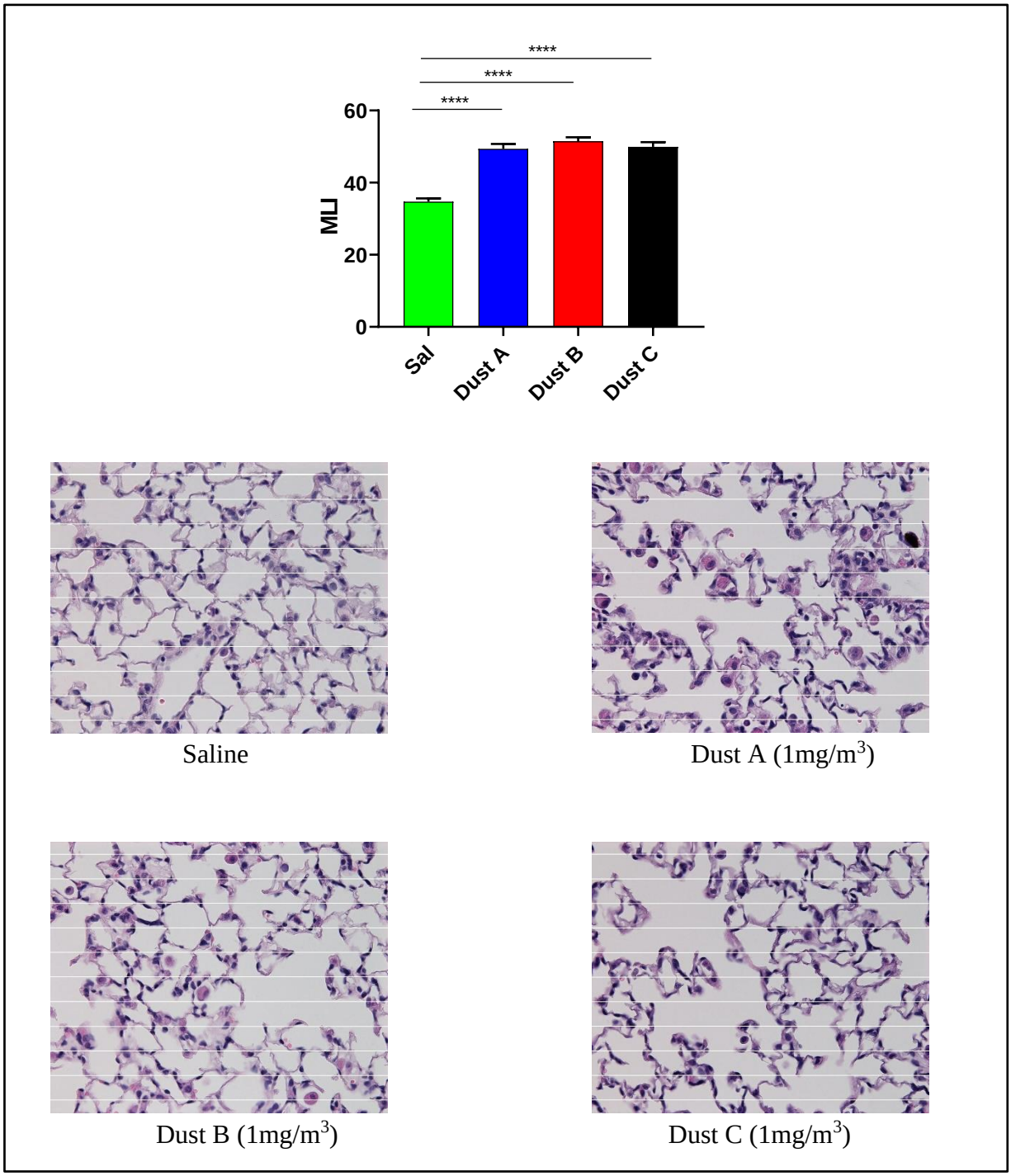


**Figure 51:** Bar graph showing the alveolar destruction (MLI) from mice exposed to 12wk of **dust** ($\leq PM_{10}$) at 1mg/m$^3$ concentration. One way-anova; n=4; P < 0.05 *; P < 0.01 **; P < 0.001 ***; P < 0.0001 ****

- Mice exposed to Dust A, B and C at lower concentration i.e. 1mg/m$^3$ have shown enlarged alveoli with increased alveolar destruction leading to emphysema like condition.
- The 1mg/m$^3$ is below the current safe level standards i.e. 2.5mg/m$^3$

**2.54 Coal macules**

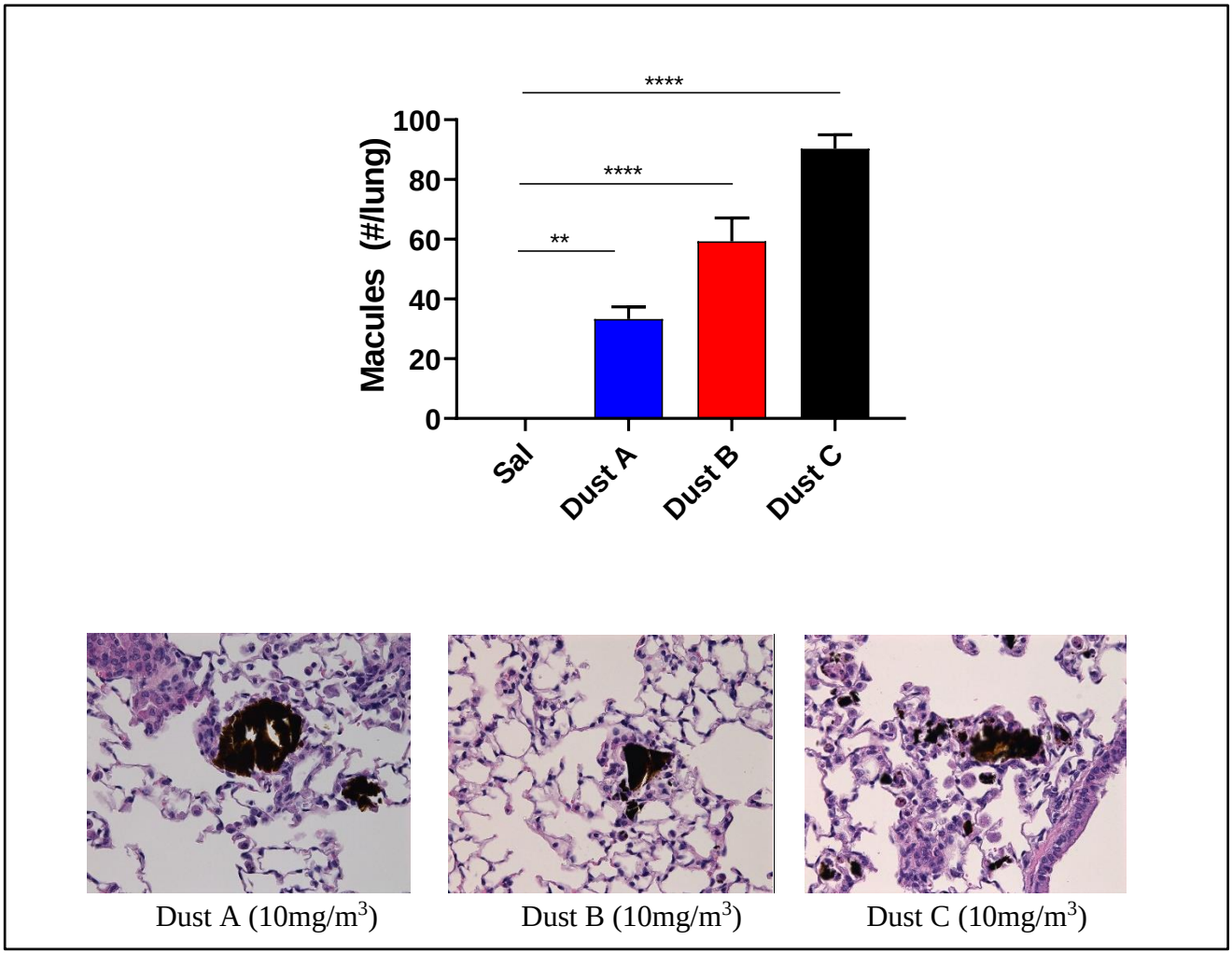


**Figure 52:** Bar graph showing the alveolar destruction and formation of coal macules from mice exposed to 12wk of **dust** (≤ $PM_{10}$) at 10mg/$m^3$ concentration. One way-anova; n=4; P < 0.05 *; P < 0.01 **; P < 0.001 ***; P < 0.0001 ****

- Mice exposed to Dust A, B & C at 10mg/$m^3$ for 12 weeks exposure period showed the development of coal macules similar to macules observed in humans suffering with coal worker pneumoconiosis (CWP).
- The number of macules produced by Dust C is greater in number compared to Dust B and Dust A (Dust C > Dust B > Dust A).

## 3 Inflammatory gene markers (qPCR) - Acute model

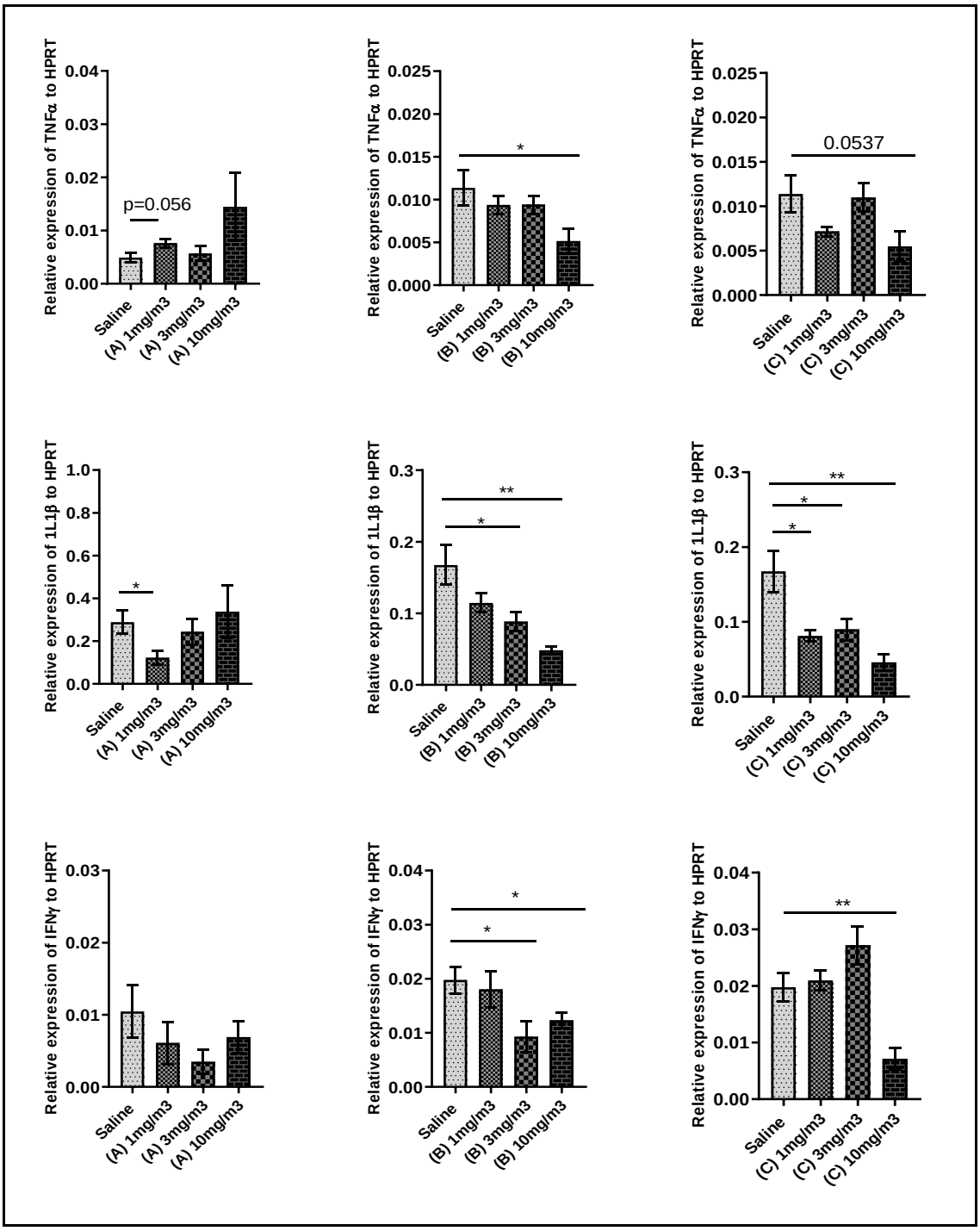


**Figure 53:** Bar graph showing expression of inflammatory & pro inflammatory gene markers in response to 2wk dust exposure. T-test; n=6; P < 0.05 *; P < 0.01 **; P < 0.001 ***; P < 0.0001 ****

**Acute exposure (2wk)**

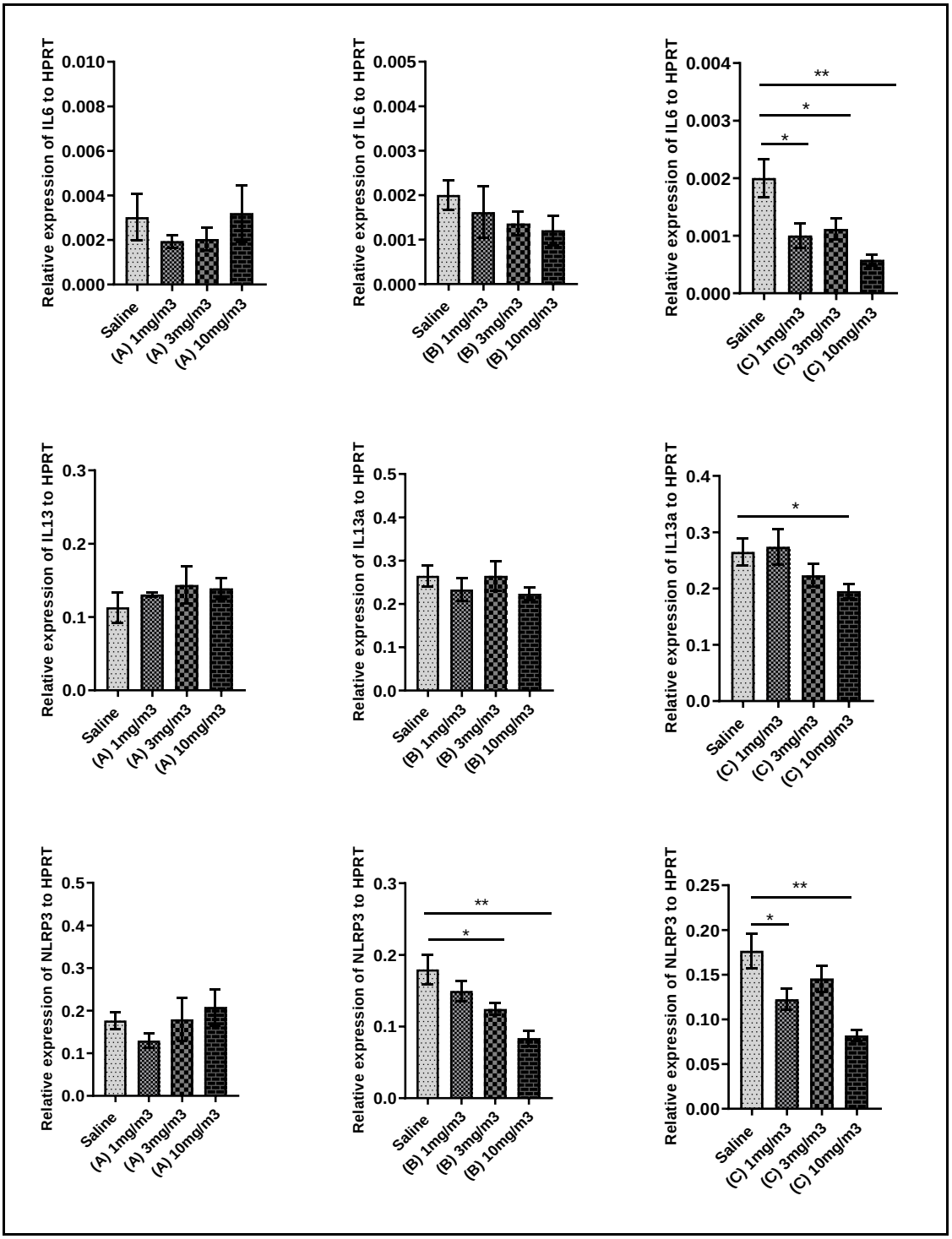


**Figure 54:** Bar graph showing expression of inflammatory & pro inflammatory gene markers in response to 2wk dust exposure. T-test; n=6; $P < 0.05$ *; $P < 0.01$ **; $P < 0.001$ ***; $P < 0.0001$ ****

**Acute exposure (2wk)**

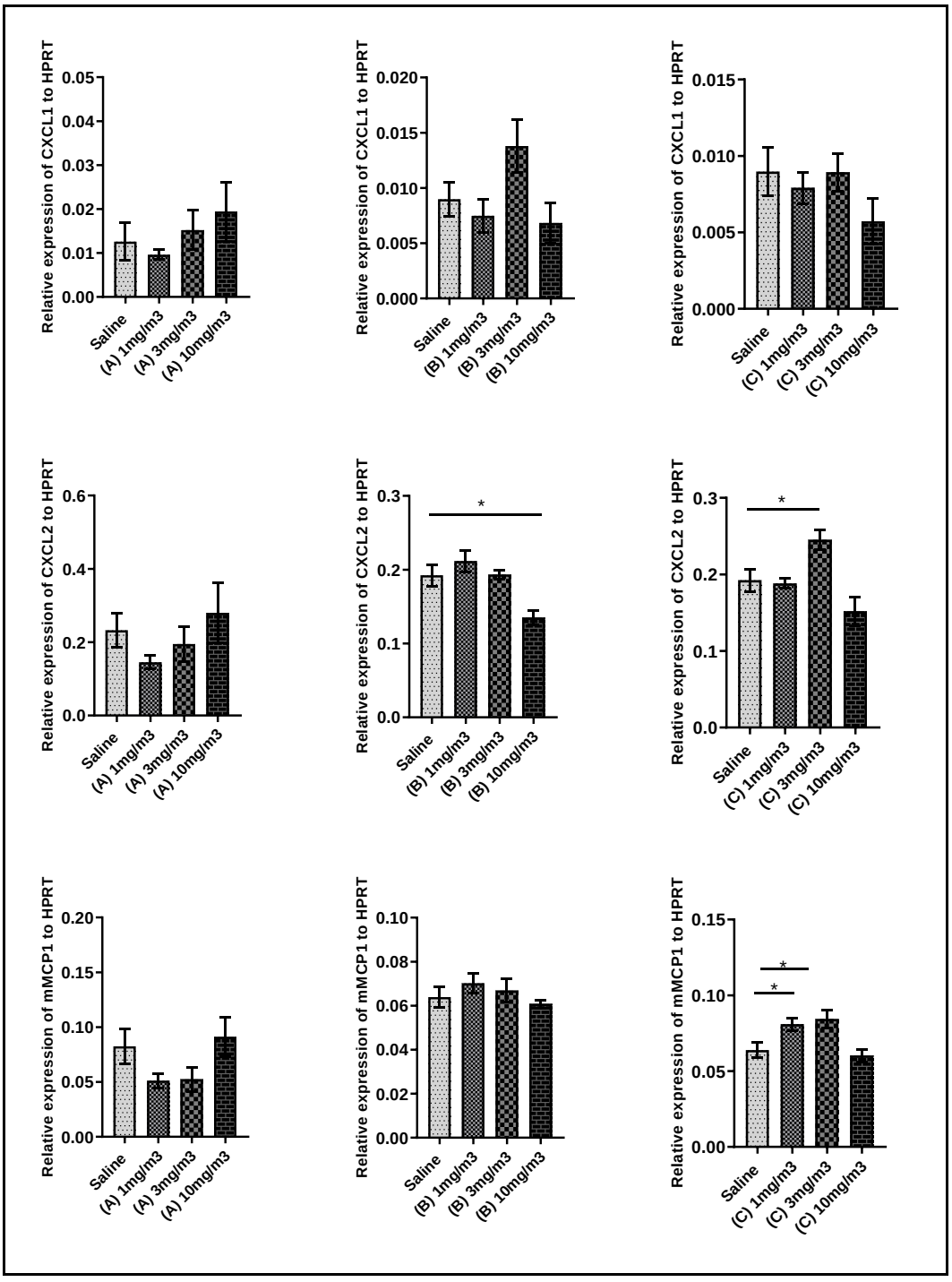


**Figure 55:** Bar graph showing expression of inflammatory & pro inflammatory gene markers in response to 2wk dust exposure. T-test; n=6; $P < 0.05$ *; $P < 0.01$ **; $P < 0.001$ ***; $P < 0.0001$ ****

- Interestingly, an inverse relationship was observed between the expression of major inflammatory and pro-inflammatory gene markers with dust concentrations in mice exposed to Dust B and C. However, the Dust A showed a positive trend.
- Declined expression of inflammatory genes can be linked to reduced inflammatory cells at higher dust doses compared to increased cell count in lower dust doses.

**Chronic exposure – 12wk**

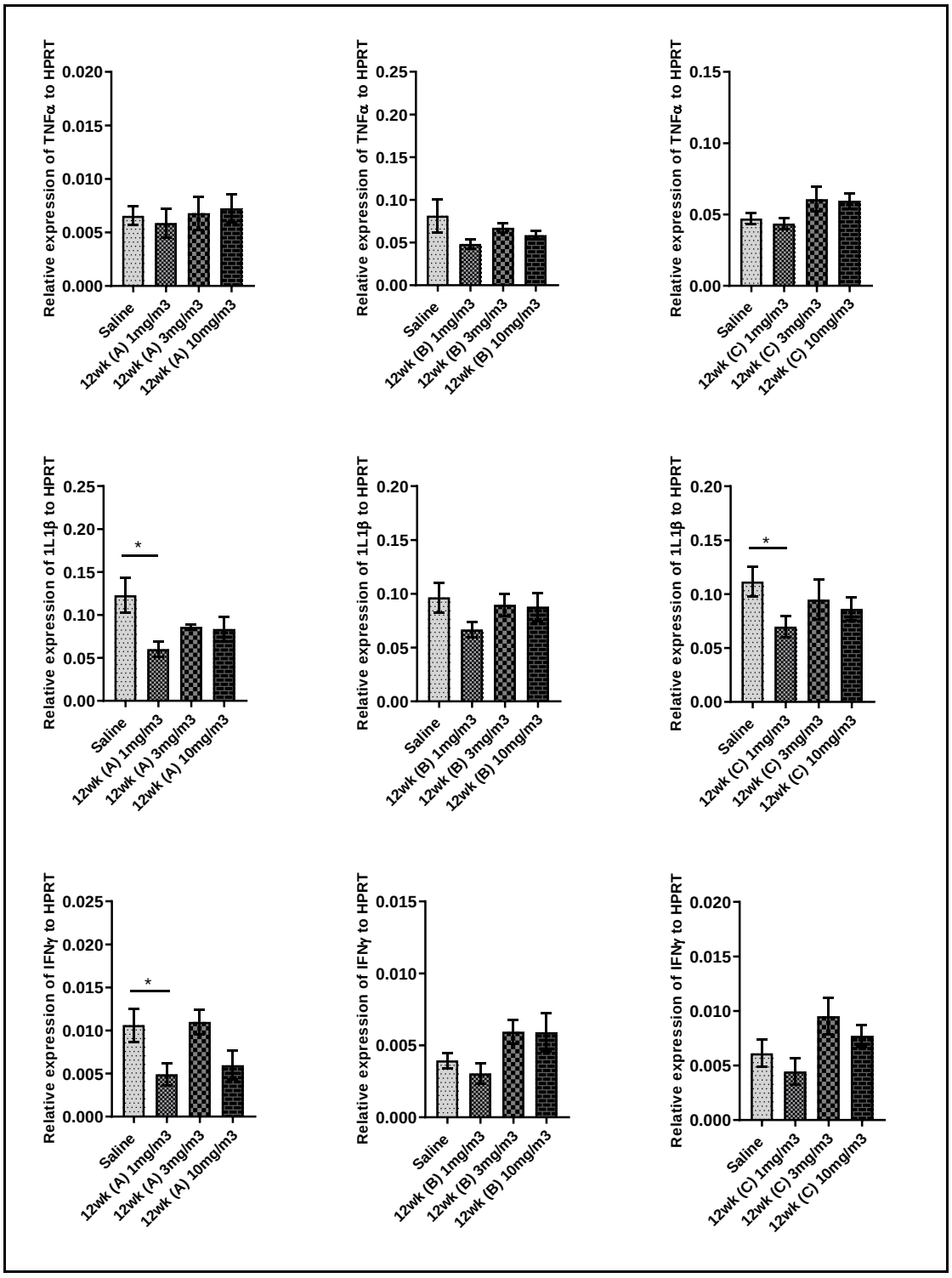


**Figure 56:** Bar graph showing expression of inflammatory & pro inflammatory gene markers in response to 12wk dust exposure. T-test; n=8; $P < 0.05$ *; $P < 0.01$ **; $P < 0.001$ ***; $P < 0.0001$ ****

**Chronic exposure – 12wk**

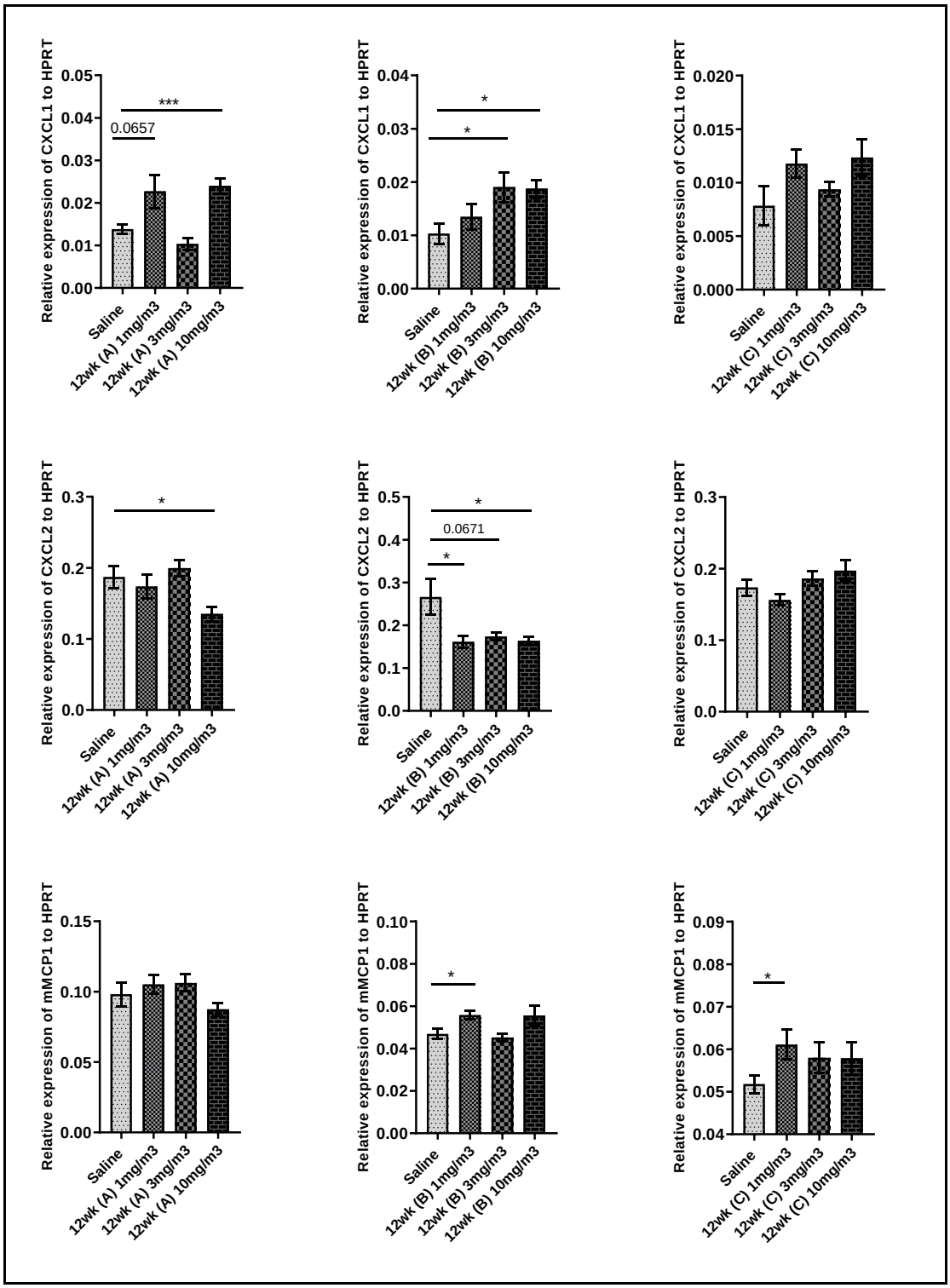


**Figure 57:** Bar graph showing expression of inflammatory & pro inflammatory gene markers in response to 12wk dust exposure. T-test; n=8; P < 0.05 *; P < 0.01 **; P < 0.001 ***; P < 0.0001 ****

- Unlike 2wk exposure model, the 12wk dust exposure did not affect major inflammatory gene markers. However, an increasing trend with increasing doses was observed.

# 4 Infection models

## 4.1 *Influenza A* virus model

The dust *influenza* model was developed to understand how the dust exposed lungs react to flu infection. Similar to the acute model, the mice were exposed to different dust types at the lowest dose i.e. 1mg/m$^3$ for 2 weeks. At the end of the exposure period, the mice were infected with *Influenza A* virus through the intranasal route and left for 3 days (3dpi). Post incubation, mice were euthanized and lung function, inflammation and gene markers were analysed.

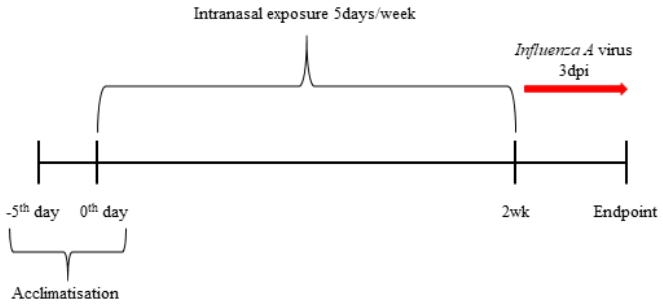


**Figure 58:** Schematic representation of dust *influenza A* virus model (3dpi)

## 4.2 *Non-typeable Haemophilus influenza* (NTHi) model

The dust NTHi model was designed to study how dust exposed lungs respond to bacterial infection and the phagocytic ability of macrophages. Similar to the acute model, the mice were exposed to different dust types at the lowest dose i.e. 1mg/m$^3$ for 2 weeks. At the end of the exposure period, the mice were infected with NTHi through intranasal exposure and left for 24h. Post incubation mice were euthanized and lung macrophages ability were assessed.

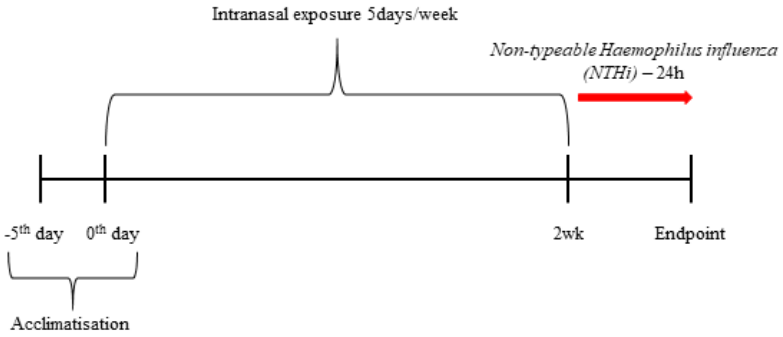


**Figure 59:** Schematic representation of dust NTHi model

### 4.1.1 Central airway resistance, Tissue damping, Tissue elastance at baseline

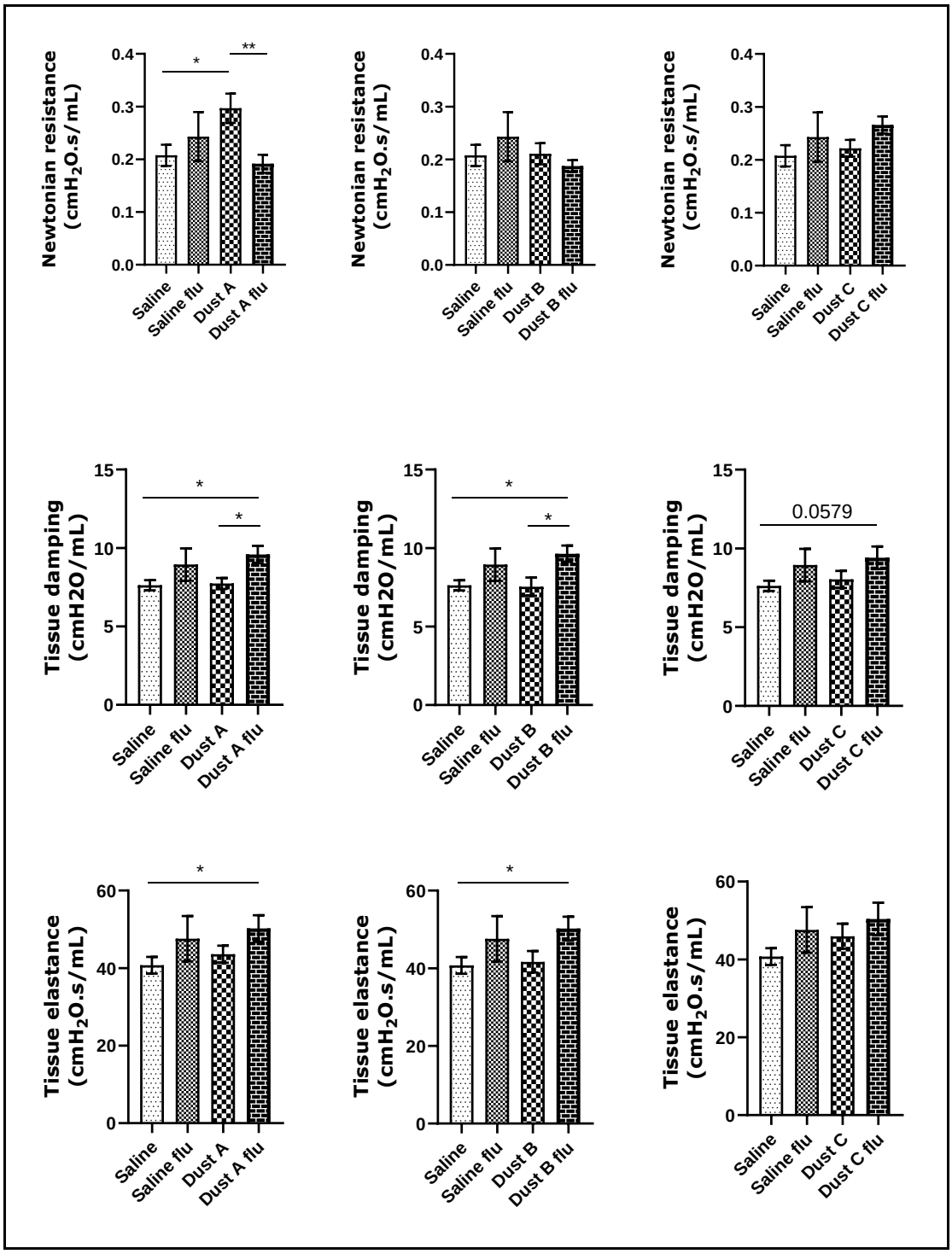


**Figure 60:** Bar graph showing FOT analysis of mice exposed to 2wk dust exposure and infected with flu (3dpi) T-test; n=6-8; $P < 0.05$ *; $P < 0.01$ **; $P < 0.001$ ***; $P < 0.0001$ ****

### 4.1.2 Transpulmonary resistance, Dynamic compliance, Dynamic elastance at baseline

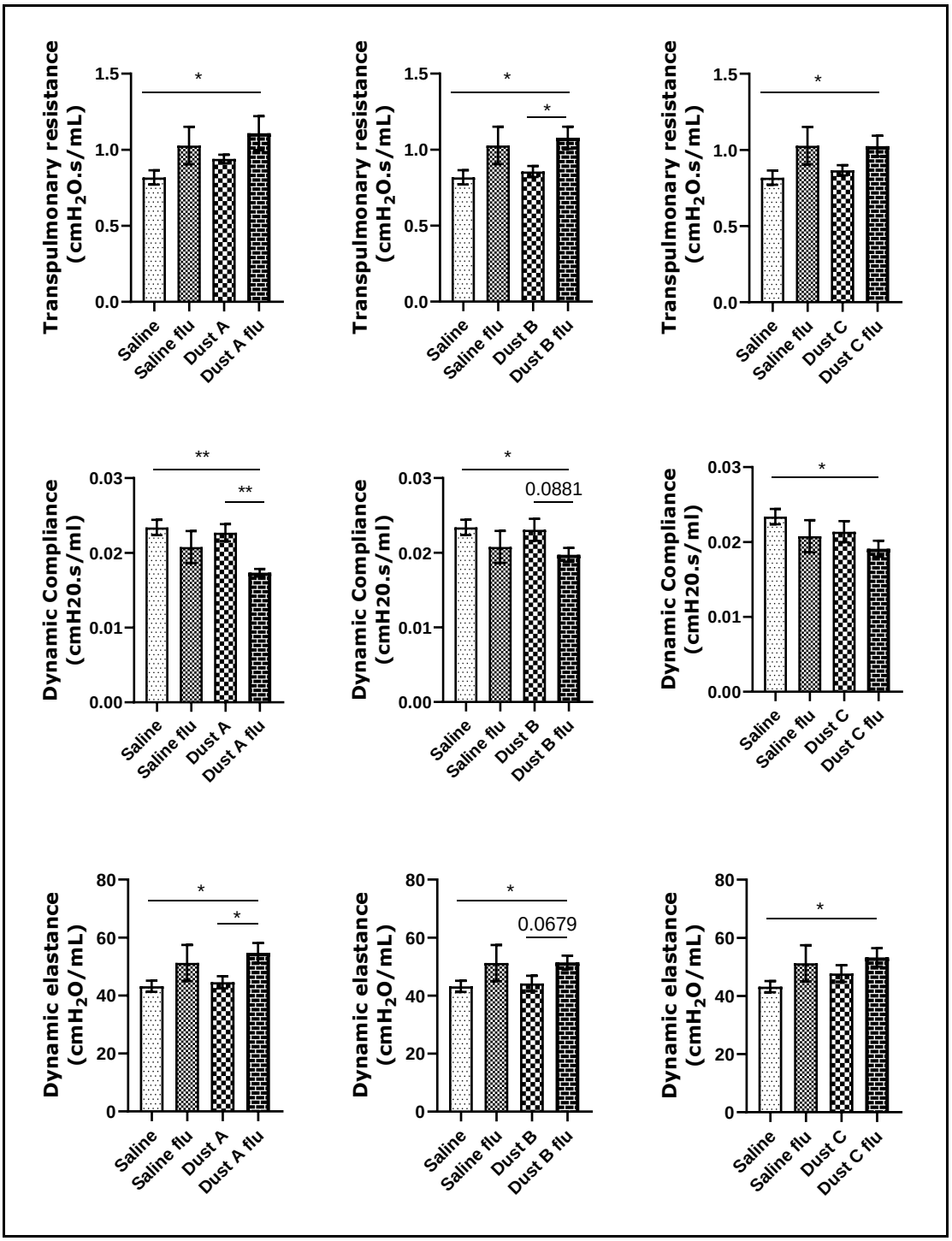


**Figure 61:** Bar graph showing FOT analysis of mice exposed to 2wk dust exposure and infected with flu (3dpi) T-test; n=6-8; P < 0.05 *; P < 0.01 **; P < 0.001 ***; P < 0.0001 ****

### 4.1.3 Inspiratory capacity, Hysteresis, Lung compliance

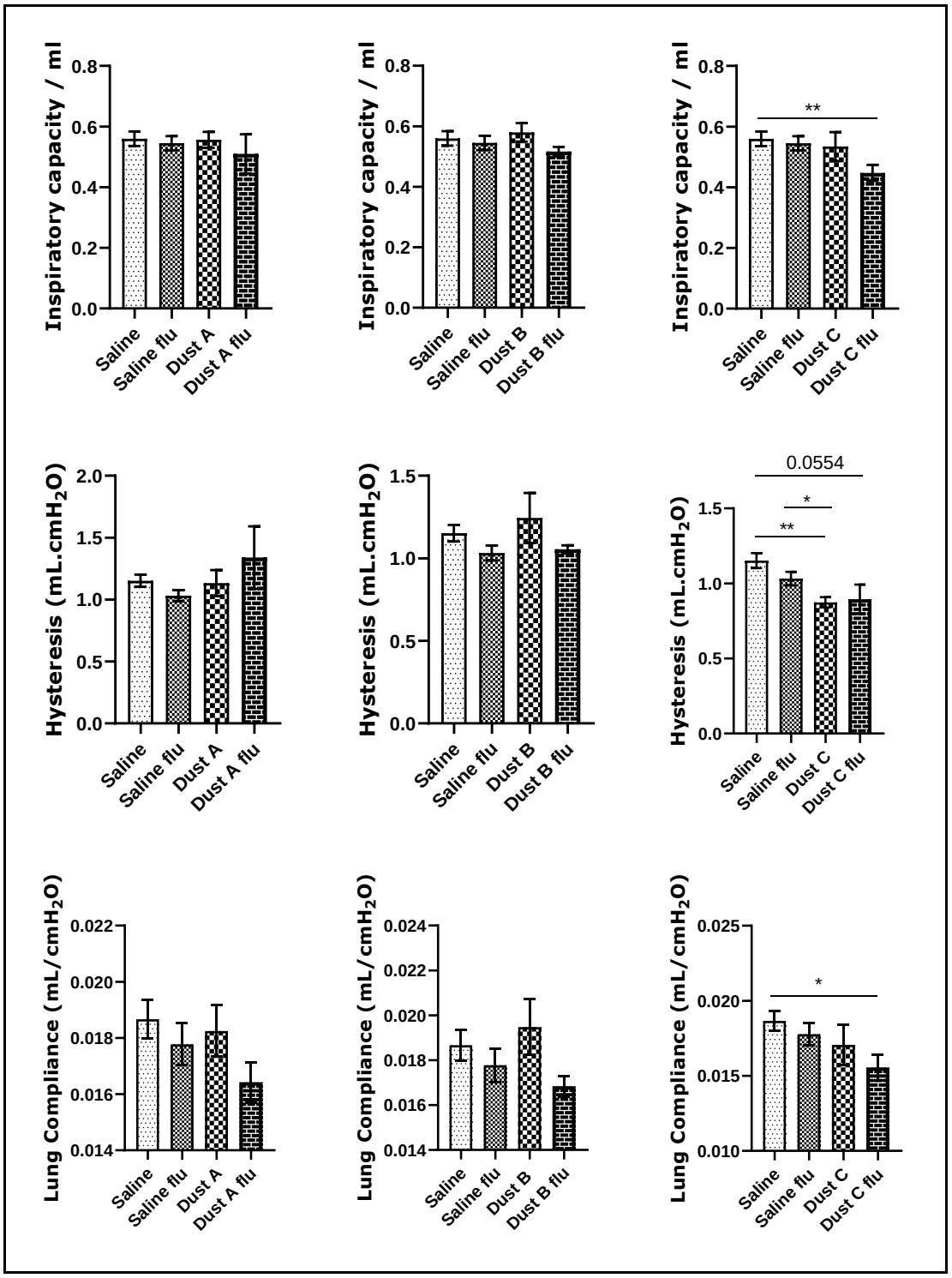


**Figure 62:** Bar graph showing FOT analysis of mice exposed to 2wk dust exposure and infected with flu (3dpi) T-test; n=6-8; $P < 0.05$ *; $P < 0.01$ **; $P < 0.001$ ***; $P < 0.0001$ ****

### 4.1.4 Pressure volume loops

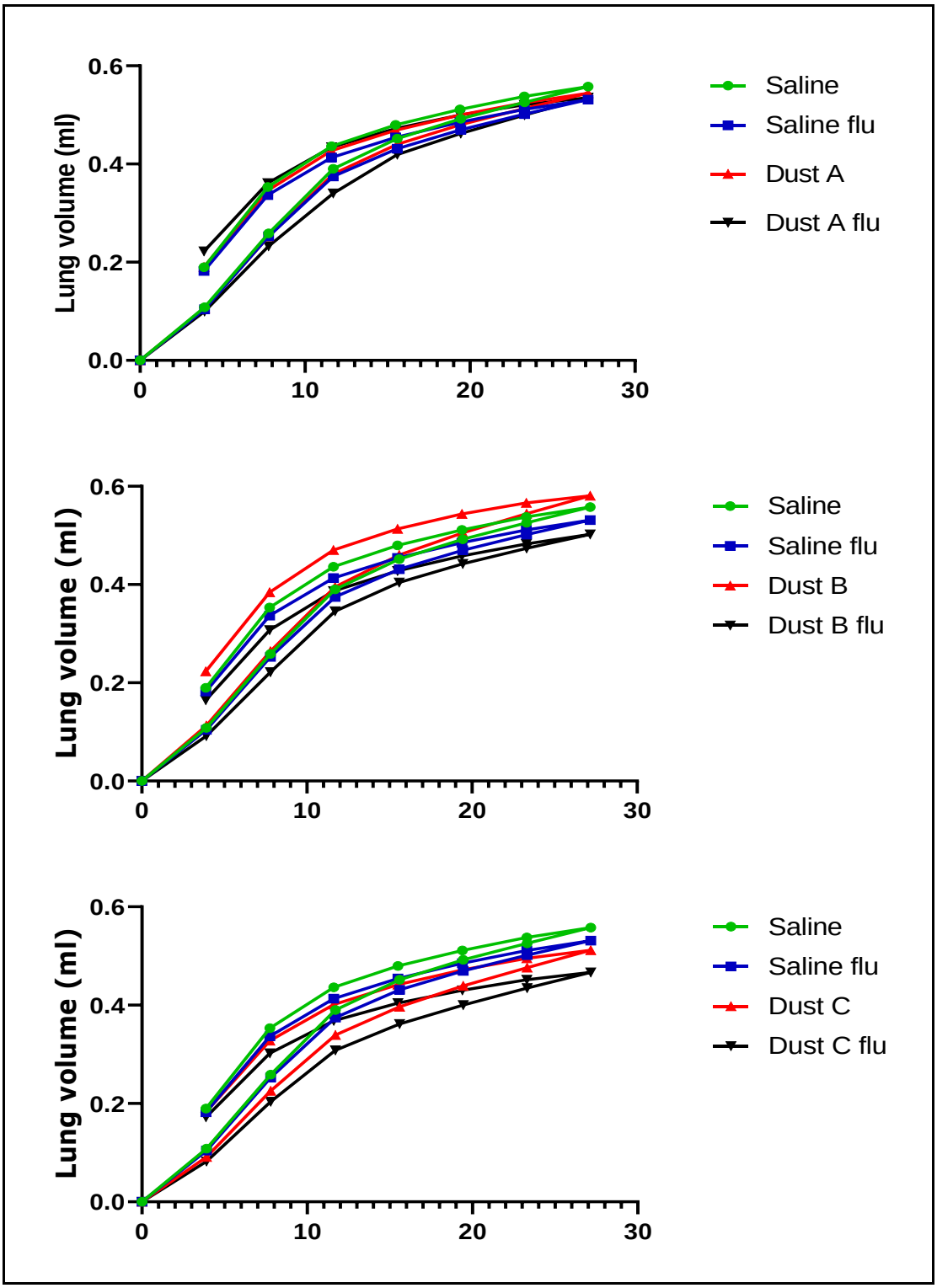


**Figure 63:** Bar graph showing PV loops analysis of mice exposed to 2wk dust exposure and infected with flu (3dpi)

### 4.1.5 Airway Hyperresponsiveness (AHR) – Transpulmonary resistance (Rrs)

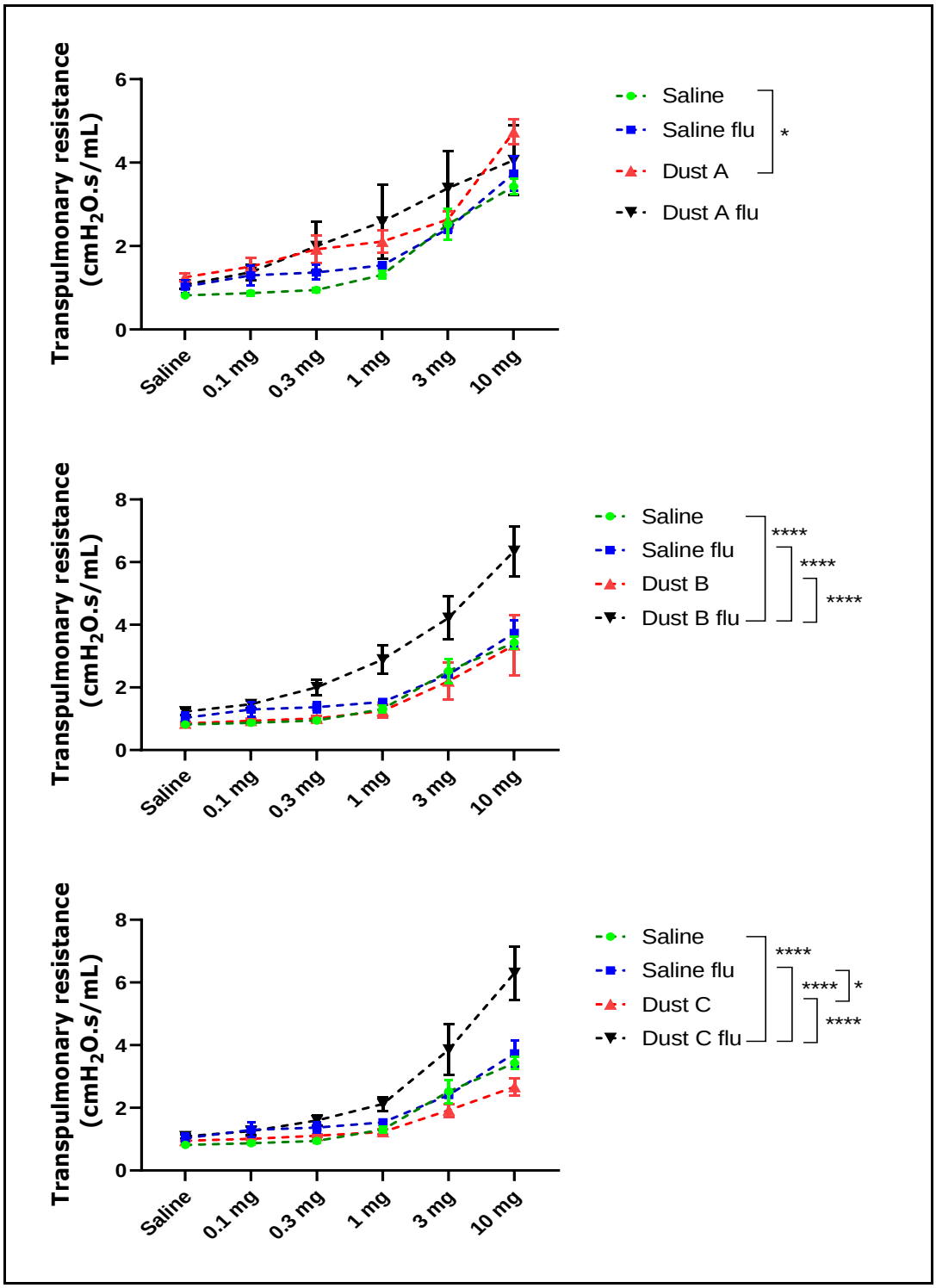


**Figure 64:** Graph showing the dose dependent transpulmonary resistance in response to increasing concentrations of Methacholine after 3dpi. 2-way anova; n=6; $P < 0.05$ *; $P < 0.01$ **; $P < 0.001$ ***; $P < 0.0001$ ****

- Mice exposed to all 3 dust samples showed increased Transpulmonary resistance, however, mice exposed to dust and infected with flu had several fold increase in resistance compared to only flu or only dust.

### 4.1.6 Airway Hyperresponsiveness (AHR) – Dynamic elastance (Ers)

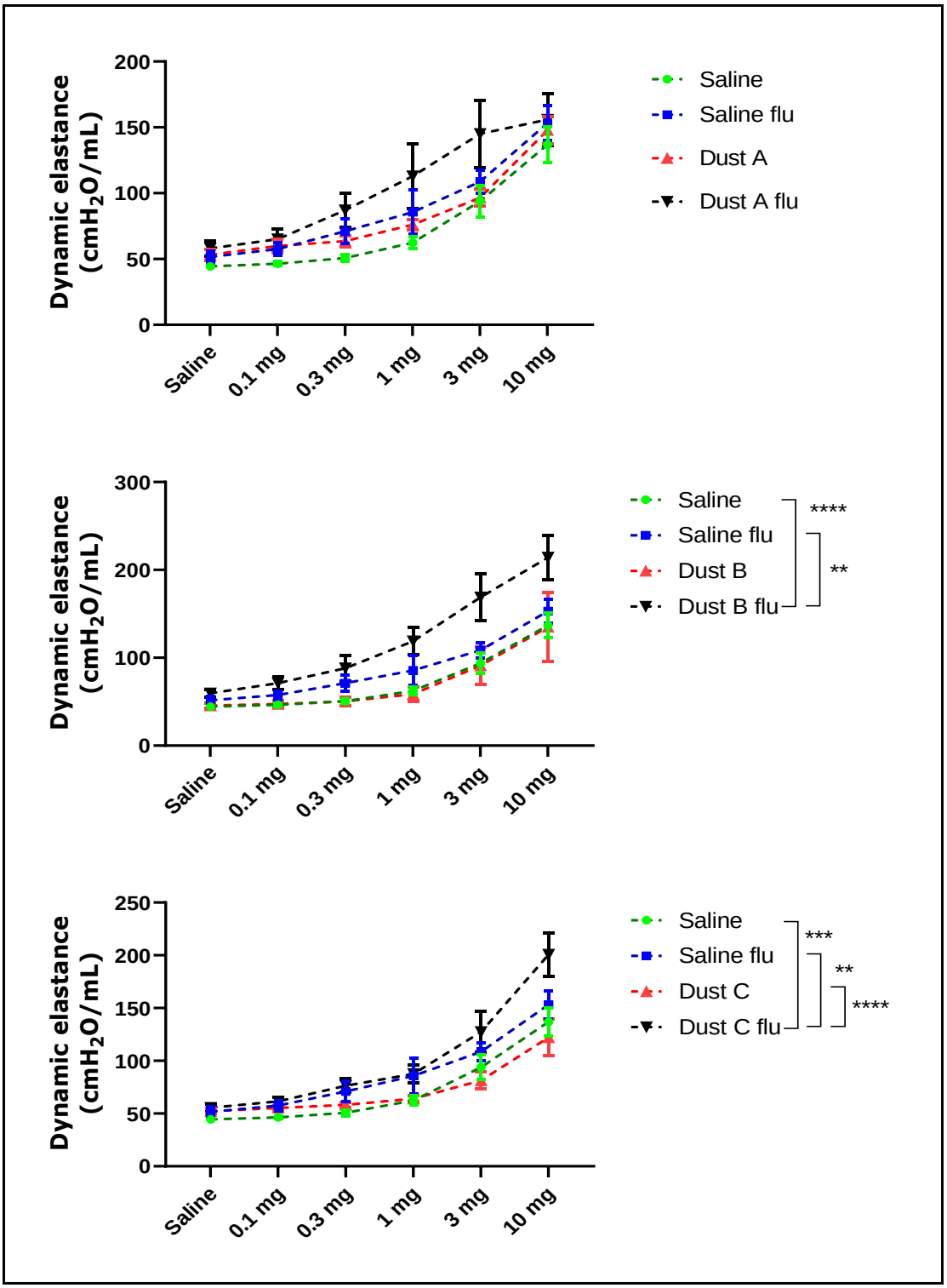


**Figure 65:** Graph showing the dose dependent response of Ers to increasing concentrations of Methacholine after 3dpi. 2-way anova; n=6; P < 0.05 *; P < 0.01 **; P < 0.001 ***; P < 0.0001 ****

- Mice exposed to all 3 dust samples showed increased Dynamic elastance, however, mice exposed to dust and infected with flu had a several-fold increase in elastance compared to only flu or only dust.

### 4.1.7 Inflammation

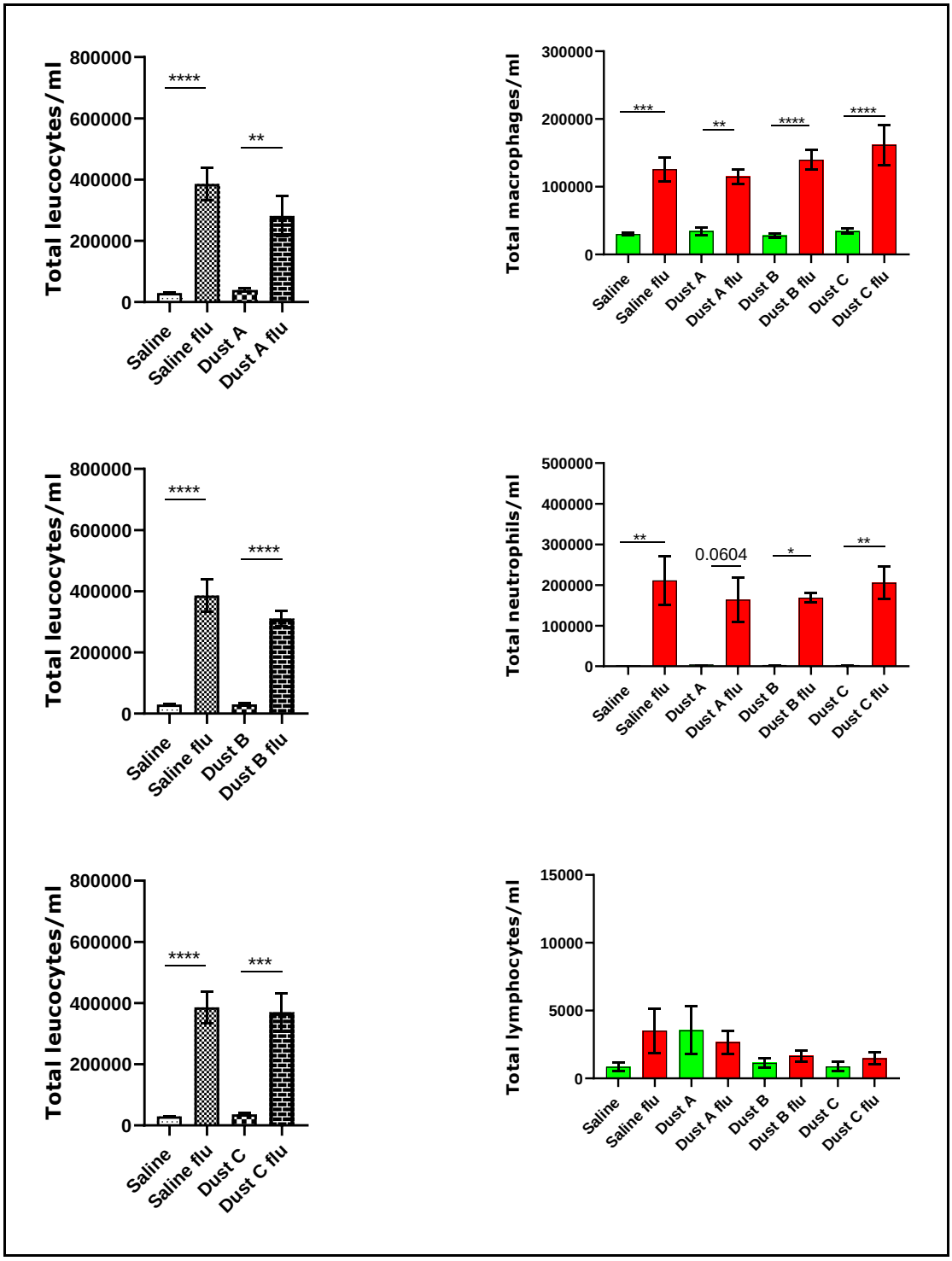


**Figure 66:** Graph showing the inflammatory cells in BALF of mice exposed to 2wk dust and infected with flu (3dpi). One way anova; n=6; $P < 0.05$ *; $P < 0.01$ **; $P < 0.001$ ***; $P < 0.0001$ ****

### 4.2 *Non-typeable Haemophilus influenza* (NTHi) - Phagocytic assay

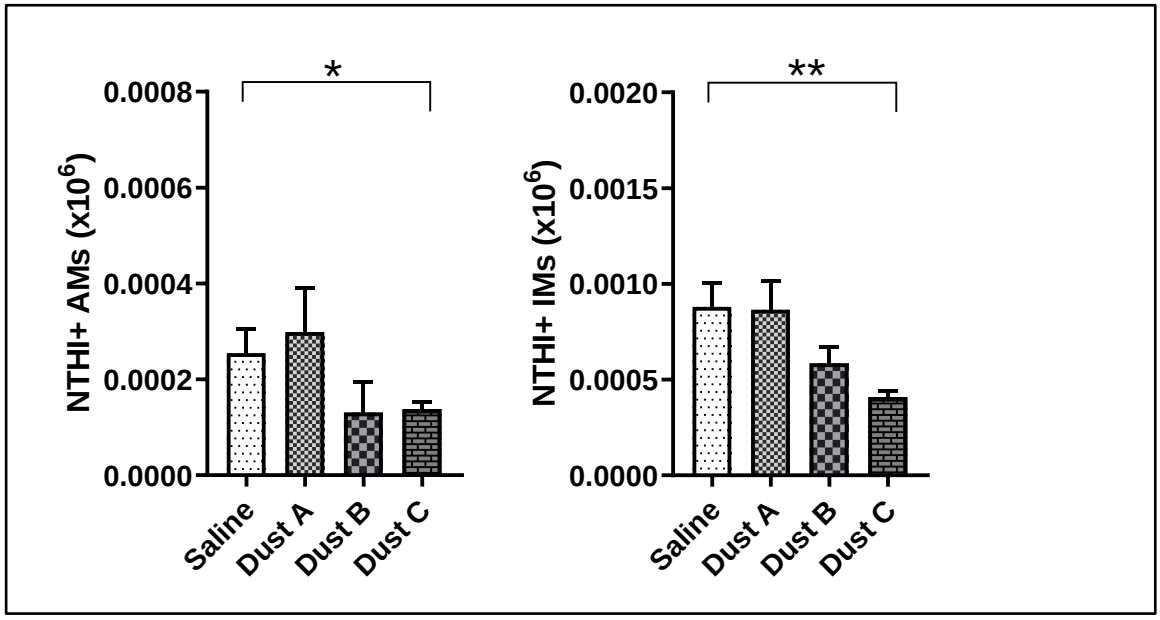


**Figure 67:** Graph showing the phagocytosis ability of dust exposed macrophages in up taking labelled HI using flow cytometry. One way anova; n=6; P < 0.05 *; P < 0.01 **; P < 0.001 ***; P < 0.0001 ****

- The primary dust-laden macrophages (alveolar and interstitial) isolated from the mice exposed to Dust B and C have shown decreased phagocytic ability compared to non-dust-laden macrophages.
- Dust A did not affect the phagocytic ability of the macrophages.

## 5 *In vitro* analysis (ALI's) - qPCR analysis

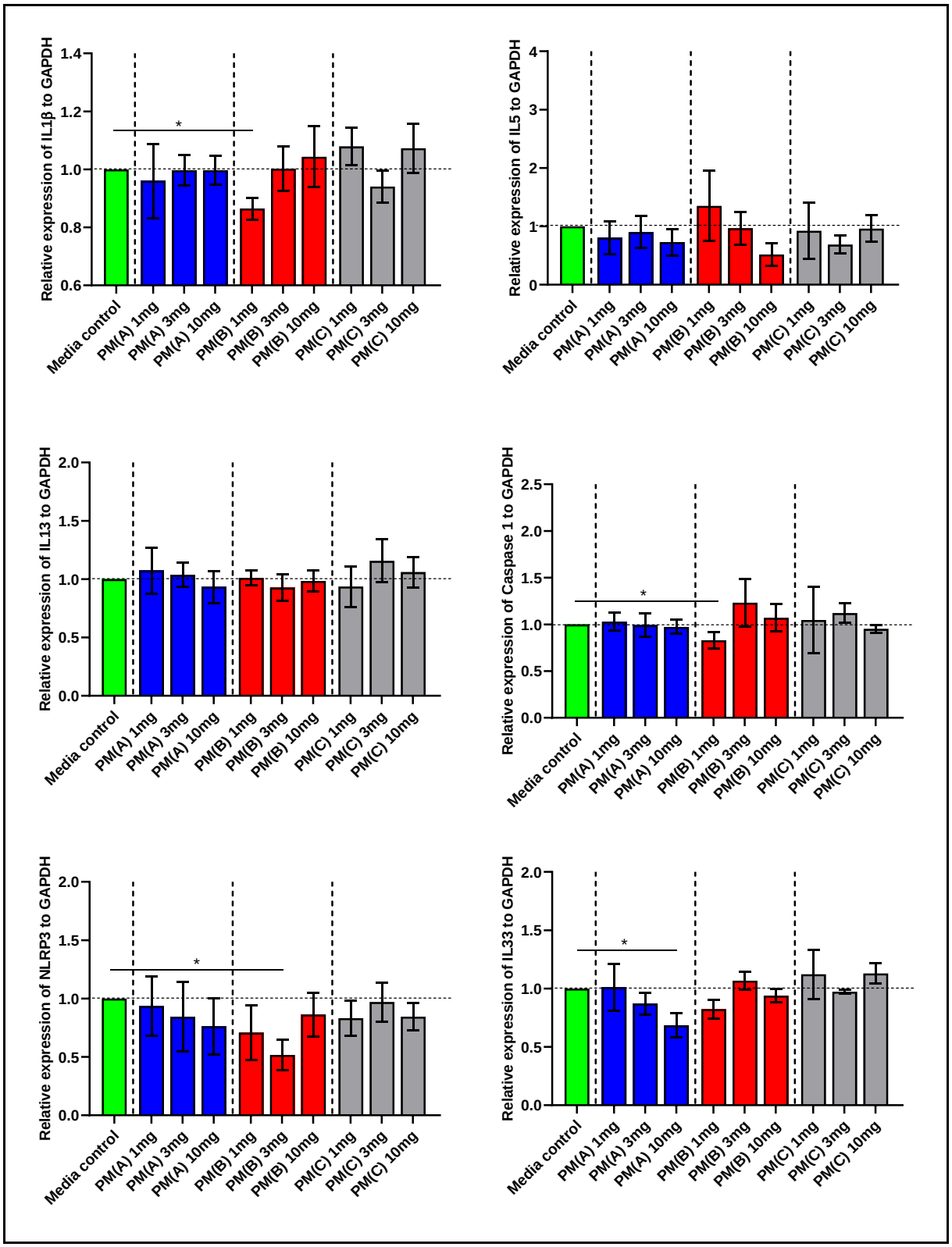


**Figure 68:** Graph showing the expression of key immune regulator genes in primary bronchial epithelial cells exposed to dust for 8h. T-test; n=4; P < 0.05 *; P < 0.01 **; P < 0.001 ***; P < 0.0001 ****

- Exposure of primary bronchial epithelial cells (ALI's) collected from healthy donars to dust at 1mg/$m^3$ for 8h had no significant effect on the expression of inflammatory regulator genes.